2010

Depositional Environment, Diagenetic History and Chemostratigraphy of the Mid-Cretaceous Sarvak Carbonates in Southern Iran

Elham Hajikazemi
University of Windsor

Depositional Environment, Diagenetic History and Chemostratigraphy of the Mid-Cretaceous Sarvak Carbonates in Southern Iran

by
Elham Hajikazemi

A Dissertation
Submitted to the Faculty of Graduate Studies
through the Department of Earth and Environmental Sciences
in Partial Fulfillment of the Requirements for
the Degree of Doctor of Philosophy at the
University of Windsor

Windsor, Ontario, Canada
2010

Your file Votre référence
ISBN: 978-0-494-70569-8
Our file Notre référence
ISBN: 978-0-494-70569-8

Declaration of Co-Authorship/ previous publication

I. Co-Authorship Declaration

This thesis incorporates material that is the result of field work and lab analysis. Field work was carried out with the collaboration of Dr. M.A. Kavoosi, Dr. F. Ghazban and M. Seraj. Field work, laboratory analysis, data interpretation, key ideas and manuscript preparation were the responsibility of the first author. I certify that this thesis is the product of my own work but owe much to the scientific guidance, and precise editing of Dr. Ihsan Al-Aasm and Dr. Mario Coniglio, who are co-authors of the associated manuscripts. They provided me with valuable comments that led to the development of this thesis.

II. Declaration of previous publications

This thesis includes 3 original papers that have been published and/or submitted for publication in international peer- reviewed journals. The percentages given by the authors' names represent their relative scientific contribution.

Manuscript 1 (Chapter 2)

Hajikazemi, E., (70%), Al-Aasm, I.S., (15%), Coniglio, M.,(15%), 2010, Subaerial exposure and meteoric diagenesis of the Cenomanian-Turonian Upper Sarvak Formation, southwestern Iran , published in Special Publication 330 " Tectonic and Stratigraphic Evolution of Zagros and Makran during the Mesozoic-Cenozoic" by Geological Society of London, DOI: 10.1144/SP330.12. All co-authors provided insightful criticism on early versions of this manuscript. This project was possible through Natural Science and Engineering Research Council of Canada (NSERC) grants to I.S. Al-Aasm and M. Coniglio.

Manuscript 2 (Chapter 3)

Hajikazemi, E., (70%), Al-Aasm, I.S., (15%), Coniglio, M., (15%), 2010, Chemostratigraphy of Mid-Cretaceous carbonates in the Tethyan region: an example from the Sarvak Formation in southern Iran (submitted in October 2009 to the Journal of Petroleum Geology and accepted for publication in December 2009). Funding for this project was provided by NSERC grants to I.S. Al-Aasm and M. Coniglio. Additional funding was provided by StatoilHydro.

Manuscript 3 (Chapter 4)

Hajikazemi, E. (70%), Al-Aasm, I.S. (15%), Coniglio, M. (15%), 2010, The diagenetic history and reservoir potential of the Mid-Cretaceous Sarvak Formation in Southern Iran (submitted in March 2010 to the Journal of Petroleum Geology). All co-authors provided insightful criticism on early versions of this manuscript. This project was possible through a funding provided by contribution of StatoilHydro. Additional founding was provided by NSERC grants to I.S. Al-Aasm and M. Coniglio.

Abstract

This study presents integrated petrography, stable carbon and oxygen and also strontium isotopes and major and trace element data for the Cenomanian-Turonian carbonates of southern Iran. These data provide new insights into the diagenetic history and reservoir characteristics of the prolific Sarvak Formation and chemostratigraphy of Mid-Cretaceous strata in the Tethyan region.

The Cenomanian-Turonian Sarvak Formation forms one of the main hydrocarbon reservoirs in southern Iran and the Persian Gulf. The Sarvak carbonates are underlain by Kazhdumi Shales while a regional unconformity marks the top of the formation. These carbonates were deposited in a ramp setting. Detailed investigation using: well-logs, pertrography and geochemistry indicate that facies and diagenetic processes influenced reservoir quality.

Chemostratigraphy established from several sections confirms the presence of the regional Turonian and local Cenomanian-Turonian unconformities and reveals the presence of previously unrecognized subaerial exposure surfaces. The paleoexposure surfaces are recognized by their negative $\delta^{13}C$ and $\delta^{18}O$ values (as low as -6.4 and -9.4‰ VPDB, respectively) coupled with low Sr concentrations and higher $^{87}Sr/^{86}Sr$ ratios. These exposure surfaces have dual effects on reservoir quality: a constructive effect, which enhances the porosity through extensive dissolution of allochems and a destructive effect which includes occlusion of some of the porosity by meteoric cement precipitation.

Positive $\delta^{13}C$ values in the various carbonate phases reflect values of sea water coeval with Oceanic Anoxic Event (OAE) and Mid-Cenomanian Event (MCE). The $\delta^{13}C$ excursions identified in Sarvak carbonate have been correlated globally.

The interaction of the Sarvak carbonates with meteoric waters charged with atmospheric CO_2, caused dissolution, karstification and palaeosol and bauxite formation below the exposure surfaces in some localities. The latter is likely an indicator of a warm and humid climate during that time. Calcite cementation is the predominant contributor to the porosity loss.

The $\delta^{18}O$ and $\delta^{13}C$ values of various generations of calcite cements overlap to a large extent with calcite matrix and rudist shells, indicating their equilibration with fluids of similar isotopic composition (i.e. marine fluids). More negative $\delta^{18}O$ values suggest a significant meteoric component. The progressive decrease in $\delta^{18}O$ values of some of the calcite cements

(e.g. -12.3‰) and matrix-replacive dolomites could be related to precipitation at higher ambient temperatures. Their occurrence adjacent to stylolites suggests the formation during burial diagenesis. Partial dolomitization in some mud/wackestone intervals with shale interbeds is another factor in enhancement of the secondary porosity and reservoir development.

Acknowledgements

I would like to express my gratitude to my thesis advisors Dr. Ihsan Al-Aasm and Dr. Mario Coniglio for their funding and guidance through the course of this study. This project was funded through a contribution of individual NSERC grants to I.S. Al-Aasm and Mario Coniglio and partially by StatoilHydro. Field work in southwestern Iran was supported by the National Iranian South Oil Company, Tehran University and Geological Survey of Iran.

I am also appreciative of the assistance provided by Melisa Price and Martin Knyf with running stable isotope analyses, and to Dr. Brian Fryer for the use of his laboratory, Dr. ZhaopingYang and Mr. J.C. Barrette for their help during the ICP-MS analysis for elemental geochemistry. My special thanks to all the faculty and staff members in the Department of Earth and Environmental Sciences for their academic and administrative support during the last 4 years particularly Dr. I. Samson for offering excellent courses.

My acknowledgements would not be complete without expressing my gratitude to my family, especially my husband, who assisted me in field work. I would not have been able to finish this without his encouragement and cooperation. Last but not least I would like to thank my parents for all their love and support while I was busy with this work.

Table of Content

List of Tables

List of Figures

Chapter 1

1.1. Introduction

The Persian Gulf and southern Iran host a large number of proven hydrocarbon reserves. Hydrocarbon production is immence and exploration continues intensively at many localities. The petroliferous strata range in age from Silurian to Miocene and traps include both stratigraghic and structural types.

Globally, shallow-water Cretaceous carbonates form some of the thickest and most widespread platforms known (Beydoun et al., 1992). During the Mid-Cretaceous, extensive carbonate platforms covered the eastern part of the Arabian Plate, including the eastern Persian Gulf (Ziegler, 2001). A basin-wide, transgressive, shallow-water carbonate system was deposited from the late Albian to Turonian (Burchette, 1993; Van Buchem et al., 1996).

The Mid-Cretaceous carbonates in the Middle East are among the most productive oil-bearing stratigraphic intervals, containing numerous giant fields. The Sarvak Formation, which represents this succession in southern Iran and the Persian Gulf, is a prolific hydrocarbon reservoir and host to a number of giant oilfields in the region. Traps are mainly combination of stratigraphic and structural types, formed by reefs, near-reef and fore reef carbonates, but all are sealed by the regionally continuous basal marine shale of the overlying Laffan and in some of the oilfields by the Ilam or Gurpi formations (Ghazban, 2007).

Sarvak carbonates are typically associated with organic-rich source rocks and in some regions intruded by salt domes. There is high potential for unexplored areas within this petroleum system.

The Sarvak Formation is developed throughout southern Iran forming an extensive succession comprising a sequence, up to 1000 metres thick, including two important unconformities in late Cenomanian and Turonian. The sediments overlying the Sarvak Formation are represented by a regionally extensive flooding surface followed by deposition of Laffan Formation's shale or Gurpi Formation's marl (see Fig. 2.2 for stratigraphic column)

Several geologic and stratigraphic investigations have been carried on the Sarvak Formation. The work of James and Wynd (1964) marked the beginning of studies of the Sarvak Formation. Setudehnia (1978) reviewed the geology and facies determinations of the Sarvak

Formation in southwestern Iran and proposed depositional cycles. Boltz (1978) recognized intrashelf basins of the Sarvak carbonates and major hiatus and unconformity on top of the formation in several localities.

Hajikazemi et al. (2002) related the excellent reservoir quality of the Upper Sarvak to primary growth /framework porosity and secondary porosity which is mainly related to Turonian unconformity, subaerial exposure and associated karstification. They also concluded that diapirism affected the thickness of the reservoir rocks.

Sharp et al. (2003) divided the Upper Sarvak Formation into two progradational ramp sequences separated by a regionally extensive karst surface of Upper Cenomanian-Early Turonian age in the Lurestan area. Based on facies analysis and sequence stratigraphy, Taghavi et al. (2006) stated the complexity of Sarvak reservoir in Iran reflected its heterogeneity of depositional facies and diagenesis.

Previous studies (Videtich et al., 1988) indicated that major salt diapirs and basement structures formed different highs in Mid-Cretaceous, causing modification of facies distribution by localizing high energy grainstones and rudist reefs and generating local intraformational unconformities. The observations suggest that there is a significant tectonic influence on the general sedimentation pattern.

Based on the above review, it is clear that a major shortcoming in the studies related to the Sarvak Formation is the absence of geochemical investigations needed to unravel many existing problems including correlations and detailed diagenetic history. The few diagenetic investigations published refer to the role that diagenesis could have played without any particular documentation of the nature of the fluids involved or timing of events. Additionally, most previous work is focused on local sequence stratigraphy based on the well log information from selected oil fields with no regional perspective.

Geochemical analysis and trace element and isotope profiles for the Sarvak strata may identify the extent of the major Turonian hiatus and its correlation through the region. Thus, a good understanding of the sedimentology and diagenetic history of these strata forms the foundation of an effective exploration program. A chronostratigraphic framework is needed to better date and find the stratigraphic relationships of these tectonic influences in time.

1.2. General Geology and Sedimentology

The evolution of the Zagros depositional basin, developed on the northeastern margin of Arabian plate, was a long and complex process (Murris, 1980). From the Jurassic to the Mid-Cretaceous, the region was a tectonically passive, low- relief, carbonate shelf situated in an equatorial position (Zeigler, 2001).

Clastic and carbonate sediments were deposited in a variety of shallow-water settings in the basin. The repetitive interbedding of limestones with shales indicates a decreased input of terrigeneous clastics from the hinterland to the west. Such changes in lithology could also indicate the Oceanic Anoxic Event (OAE) which occurred throughout the world ocean at this time period. Generally, the succession developed into pure limestone toward the Late Cenomanian.

This time interval was also a period of major geologic events which had their influence on the development and subsequent submergence of the platform. These events included maximum sea level rise, salt diapirism, local subsidence, tilting and tectonic movements. Shallow water deposition was influenced by topographic features such as the Qatar-Fars Arch and salt-related structures (diapirs and salt walls) of smaller scale that were largely active during the Cretaceous (Farzadi, 2006).

Global sea level rose steadily to its highest level during the Cenomanian and Turonian coinciding with the global maximum flooding surface (Haq et al., 1988). Stable platform conditions persisted over the region until the Mid-Cretaceous, resulting in predominately carbonate deposition over a large area. The principal controls on sedimentation were sea level fluctuations and tectonic movements. Thick marine carbonates and marls predominated in the Md and Late Cretaceous sedimentary sequences over most of region (Sharland et al., 2001).

The interplay between sea level changes and syn-sedimentary salt diapirism influenced the stratigraphic evolution of the Sarvak succession (Sherkati and Letouzey, 2004; Sepehr and Cosgrove, 2004). Rising sea levels resulted in to onlap of new deposits on the topographic highs, where sedimentation occurred only during highstands (Sharland et al., 2001). Localized salt diapirism within the Sarvak Formation generated restricted topographic highs, with adjacent low areas subsiding further due to withdrawal of rock salt layers (Koop and Stoneley, 1982; Ghazban, 2007).

A major fall in sea level also occurred in the Turonian exposing carbonates of the Sarvak Formation. As a result, a considerable part of sedimentary succession was eroded away over the entire region (Harris and Frost, 1984). The widespread Turonian unconformity resulted from both a combination of localized uplift, following initiation of the ophiolite obduction on the northeast plate margin, and possibly a global eustatic fall in sea level (James and Wynd, 1965; Setudehnia, 1978; Farzadi and Hesthmer, 2007).

Major unconformities including the Turonian, which occurred in the sedimentary sequence in the region, are interpreted to have resulted from eustatic sea level fluctuations and/or regional tectonic events (Murris, 1980; Harris and Frost, 1984; Burchette and Briton, 1985). This major unconformity is recorded by karstic paleotopography and associated erosional surfaces. There have been some studies showing erosion and karstification of the Upper part of the Sarvak Formation in some of the oil fields.Several local and regional unconformities, in addition to thickness and facies variations have been related to reactivation of deep seated faults in the Zagros basement between Late Cretaceous and Early Miocene times (Koop and Stoneley, 1982). More recently, Farzadi (2007) using the geophysical data of the Sirri fields revealed that the Sarvak carbonates were subjected to periods of regionally extensive subaerial exposure.

Following subaerial exposure of the Sarvak Formation, a later relative sea level rise resulted in the flooding of the eroded surface and the transgressive deposition of shales. The unit on top of the Sarvak Formation is composed of fluvial deposits and the contact between the Sarvak limestone and overlying formation is locally characterized by the variegated red brown coloured clays.

1.3. Mid-Cretaceous Sea-level Change

Global sea level was at a highstand in late Cenomanian-early Turonian interval. The sedimentary succession in the Persian Gulf and southern Iran was greatly influenced by sea level fluctuations and also tectonic movements. Shallow marine carbonates accumulated due to flooding over the platform during the initial period of sea level rise. The Sarvak carbonates formed during the highstand where the sediments were deposited on a passive margin of the Neo-Tethys Ocean.

The lithofacies of the Sarvak Formation changed during the cycle of relative sea level. Thickness variations of the Sarvak Formation in the region are due to the effect of the Turonian

unconformity and basinal configuration and topography, as well as growing salt structures and diaprism.

Because of shoaling to the point of emergence, the Upper Sarvak was subjected to truncation resulting in a major unconformity. Simultaneous regional tilting towards north caused the Cretaceous succession to thicken in that direction with the depositional basin becoming deeper to the north accumulating deep water carbonates.

The platforms separated by various intrashelf basins are the sites of shallow-water carbonate deposition. The bioclastic grainstones are the 'rudist limestones' of James and Wynd (1965). In part, they are composed of rudistid banks (reefs) and aprons of large-scale, cross bedded bioclastic debris and brecciate limestones. Rudists are common components in the Cretaceous carbonates of the Persian Gulf basin.

A major sea-level fall at the Turonian boundary exposed carbonates and subarerial exposure and associated karsts carved into rudist-rich limestones in the Upper Sarvak Formation. By the end of the Turonian, regional uplift and associated unconformity resulted in erosion of the carbonates over the entire region. Conglomerate, breccia, ferruginous materials, and a weathered zone on top of the Sarvak Formation mark this event. Evidence of this pronounced unconformity is recognized almost everywhere in southern Iran and northern Persian Gulf. Thus, the Upper Sarvak succession terminates in an unconformity characterized by breccia-filled dolines, palaeosoles, and mature flint claystones (Pattinson and Takin, 1971; Burchette and Britton, 1985).

The Upper Sarvak possesses widespread good reservoir characteristics in different oil fields, particularly where it lies directly beneath the Turonian unconformity. The traditional concept of widespread uplift and erosion at the end of the Sarvak producing the major unconformity is confirmed in many areas including the Sirri fields in northern Persian Gulf (Hajikazemi et al., 2002). The reservoir quality is facies dependent to a large extent. It is particularly of a good quality where the carbonates were exposed to meteoric diagenesis and leaching due to subaerial exposure. As a result, the top of the Sarvak Formation is an exploration target for hydrocarbons (cf. Burchette and Britton, 1985).

Combination and interaction of several different factors have contributed to the formation of excellent quality reservoir facies in the Upper Sarvak. These include:

• Deposition of several lithofacies with different sedimentologic and petrophysical properties including porous reefal and forereef facies during deposition of the Upper Sarvak Formation.

• Occurrence of the major Turonian unconformity at the top of the Sarvak with the accompanying laterally extensive subaerial exposure, which has an important role in reservoir quality.

• Meteoric diagenesis of Sarvak carbonates and leaching of unstable carbonates during the Turonian with the formation of secondary porosity (i.e., moldic and vuggy) and fracturing, locally improving the permeability.

The combined effects of all these factors resulted in formation of superb quality reservoir facies in southern Iran and the Persian Gulf area.

1.4. Paleogeography and Paleoclimate

In a general paleogeographic sense, Murris (1980) and Koop and Stoneley (1982) believed that during the Early Cretaceous there was gradual establishment of ramp-type carbonate deposition related to a rise in sea-level, covering most of the Persian Gulf area. Although the area was predominantly a carbonate province during the Early Cretaceous, the presence of detrital clastics can not be ignored (Murris, 1980).

The Cretaceous period is referred to as one of several warm intervals of Earth's history (Huber et al. 2002). This period is generally divided into a relatively cool Early Cretaceous, a warm to very warm Mid-Cretaceous interval, and a relatively cool, Late Cretaceous. The movement of the Arabian plate to tropical or subtropical regions occurred at this time (Murris, 1980; Beydoun, 1991), while southern Iran and the Persian Gulf region was located just north of the Equator, with a semiarid or humid tropical climate (Parrish and Barron, 1986); no evaporites have been described from platform interiors.

1.5. Tectonics

During the Jurassic to Mid-Cretaceous times, sediments were deposited in a steadily subsiding Zagros Basin, in which subsidence was controlled by vertical movements and flexures along major basement faults (Berberian and King, 1981). Murris (1980) also pointed out that the basement faults influenced the Early Mesozoic sedimentation in the region. These structures

appear to have had periods of important activity alternating with intervals of relative quiescence. They were most active from the late Turonian to the early Campanian. These time periods correspond to major changes in basin configuration. They mark the early stages of regional compressive activity (Koop and Stoneley, 1982; Sherkati and Letouzey, 2004). Furthermore, isopach map patterns of facies distributions of Cretaceous sediments are more complex that for any the other period probably as a result of intense salt activity and reactivation of basement faults (e.g., Koop and Stoneley, 1982).

The early Cretaceous was a period of maximum rifting of the Neo-Tethys Ocean, while the major phase of tectonics occurred in late Cretaceous resulting in the closure of the Neo-Tethys Ocean accompanied by major continental collision. Thus, opening of Neo-Tethys probably ceased in mid-Cretaceous when the stable abrupt intensive reactivation of basement faults jostled the previously stable platform. This activity led to uplifting and subsequent erosion and triggering of structures in the Hormuz Salt.

Tectonic deformation of the northeastern edge of Arabian plate commenced with the obduction of the ophiolites during the early Coniacian- late Santonian (Falcon 1974). According to Berberian and King (1981), during the Turonian to Campanian, obduction of oceanic crust began along the modern eastern margin of the Arabian platform. Consequently, uplifting of the Arabian platform, associated with salt diapirism, resulted in a considerable period of non-deposition and erosion.Thus, the major phase of tectonic activity in the region appears to have occurred during the mid and late Cretaceous in response to the closure of Neo-Tethys and continental collision with the Arabian Plate (Zeigler, 2001).

Thick accumulations of Campanian-Maastrichtian sediments were deposited in front of the ophiolite nappes (Sherkati and Letouzey, 2004; Sepehr and Cosgrove, 2004). Thickness and facies of the Late Cretaceous and Paleogene sediments were considerably affected by progressive deformation following the ophiolite obduction (Koop and Stoneley, 1982; Sherkati and Letouzey, 2004).

Obduction of the Oman ophiolite in Late Cretaceous, together with complex facies changes within the Zagros Basin, heralded the onset of compressional tectonics and subduction of Neo-Tethys beneath Asia leading to eventual closure of Arabia and Iran (Haynes and McQuillan, 1974; Beydoun et al., 1992; Berberian and King, 1981).

1.6. Thesis Objectives

Despite over a century of intensive petroleum exploration, the sedimentology, diagenetic history and regional lithostratigraphic correlation of the Sarvak Formation are poorly known. Some information is available on the paleontology, sedimentology and petroleum geology, however, very little is known about the diagenetic history of this extensive carbonate succession. Previous studies of the Sarvak Formation have focused primarily on biostratigraphic correlations, as well as environmental interpretations. The main objectives of the present study are as follows:

1. To describe the sedimentary facies and to reconstruct the depositional environment of the Sarvak Formation.

2. To identify the nature of potential carbonate reservoir in the Sarvak Formation.

3. To identify the diagenetic features and to interpret the diagenetic environments in order to determine the diagenetic history of the Sarvak Formation. This includes the impact of the Turonian unconformity and other sedimentary break(s) on reservoir distribution and characteristics.

4. To establish a chemostratigraphic correlation of the Sarvak Formation in different parts of the basin. Since this formation is heterogenous in terms of facies, a thorough geochemical investigation will shed insight into regional correlation.

5. To determine palaeoclimatic conditions of the mid-Cretaceous based on study of the isotopic composition of the paleosol formed on the erosional surface. The mid-Cretaceous warm climate could have resulted in widespread weathering and dissolution of carbonates producing good reservoirs.

6. To conduct detailed geochemical work (stable isotope traverses) on rudists shells, which are considered here as an important tool to record the original isotopic signature of the ocean within the successions in order to define the temperature during the sedimentation.

This work incorporates observations from two outcrops and core samples from four productive wells in southern Iran and northeastern Persian Gulf (see Fig. 2.1 for location map of study area). A total of 360 petrographic sections were examined using standard petrographic techniques, cathodoluminescence, and scanning electron microscopy and the unaltered or the

least altered samples were processed and analyzed for stable carbon and oxygen isotopes, $^{87}Sr/^{86}Sr$ ratios and major, minor and trace element analysis.

1.7. Outline of the thesis structure

This thesis consists of 5 chapters. Chapter 1 is the introduction for the thesis and Chapter 5 presents a summary of this study. Chapters 2 to 4 are a collection of three manuscripts published or submitted to peer-reviewed scientific journals. A version of Chapter 2 was published as a research article in Memoir # 330 Geological Society of London: "Tectonic and Stratigraphic Evolution of Zagros and Makran during the Mesozoic-Cenozoic". This chapter investigates detailed field and geochemical evidence of meteoric diagenesis of the Upper Sarvak Formation and the effect of karstification on porosity evolution of the Sarvak reservoir. Through this chapter the Turonian unconformity and the resulting palaeo exposure surface is considered as the main factor in porosity enhancement of this formation.

A version of chapter 3 has been accepted for publication in Journal of Petroleum Geology. This chapter discusses the chemostratigraphy of the Sarvak Formation at the type section and correlation of the regional Turonian and local Cenomanian-Turonian unconformity in the study area utilizing stable isotope and elemental analysis. The global Oceanic Anoxic Event (OAE) and Mid Cenomanian Event (MCE) have been correlated through all surface and subsurface sections using high precision stable carbon isotope analysis. A version of chapter 4 has been submitted to Journal of Petroleum Geology. This chapter discusses the diagenesis and its role in reservoir quality of the Sarvak Formation in detail using the petrography, stable isotopes and elemental data of two dominant types of the calcite cement and dolomite and suggests three main diagenetic environments, including marine, meteoric and burial, for the Sarvak Formation.

1.8. References

Burchette, T.P., 1993. Mishrif Formation (Cenomanian-Turonian), southern Arabian Gulf: carbonate platform growth along a cratonic margin basin.In: Simo, J.A.T., Scott, R.W. and Masse, J.-P. (eds.): Cretaceous carbonates platforms. American Association of Petroleum Geologists, Mem. **56**, 185-199.

Burchette, T. P. and Britton, S. R. 1985. Carbonate facies analysis in the exploration for hydrocarbons: a case study from the Cretaceous of the Middle East. In: Brenchley, P. J.

R. and Williams, B. P. J. (editors) Sedimentology: Recent Developments and Applied Aspects. Geological Society, London, Special Publication **18**, 311-358.

Berbrian, M., and King, G. C. P., 1981. Towards a Paleogeography and Tectonic evolution of Iran. Canadian Journal of Earth Sciences 18, 210-265.

Beydoun, Z.R., 1991. Arabian plate hydrocarbon geology and potential- a plate tectonic approach: American Association of Petroleum Geologists Bulletin, Studies in Geology 33, 77p.

Beydoun, Z. R., Hughes Clarke, M. W., and Stoneley, R., 1992, Petroleum in the Zagros Basin: a late Tertiary foreland basin overprinted onto the outer edge of a vast hydrocarbon-rich Paleozoic–Mesozoic passive-margin shelf, in Macqueen, R. W., and Leckie, D. A. (editors), Foreland basins and fold belts: American Association of Petroleum Geologists Memoir 55, 309–339.

Boltz, H., 1978. The palaeogeographical evolution during the Cretaceous in the Operating Area with special emphasis on the Bangestan Group. Oil Service Company (OSCO) Internal Report 1274.

Falcon, N. L., 1974. An outline of the geology of the Iranian Makran. Geographical Journal, **140**, 284-291.

Farzadi, P., 2006. Seismic facies analysis based on 3d multi-attribute volume classification, Dariyan Formation, Persian Gulf. Journal of Petroleum Geology, **29**(2), 159-174.

Farzadi, P. and Hesthmer, J. 2007. Diagnosis of the Upper Cretaceous palaeokarst and turbidite systems from the Iranian Persian Gulf using volume-based multiple seismic attribute analysis and pattern recognition. Petroleum Geoscience, **13**, 227-240.

Ghazban, F., 2007. Petroleum geology of the Persian Gulf. Joint publication, Tehran University Press and National Iranian Oil Company. 706p.

Hajikazemi, E., Al-Aasm, S.I., and Coniglio, M, 2010. Subaerial Exposure and Meteoric Diagenesis of the Cenomanian-Turonian upper Sarvak Formation, southwestern Iran. In

"Tectonic and Stratigraphic Evolution of Zagros and Makran during the Mesozoic-Cenozoic" Geological Society of London. Special publication, 330, 253-272.

Hajikazemi, E., Ghazban, F. and Yousefpour M.R. 2002. Depositional and diagenetic history of the Middle Cretaceous sedimentary sequence in the Sirri Oil fields in the Persian Gulf, Iran. Middle East and North Africa Oil and Gas conference, Imperial College, London.

Haq, B. U., J. Hardenbol and P. R. Vail 1988. Mesozoic and Cenozoic chronostratigraphy and cycles of sea-level change. Society of Economic Paleontologists and Mineralogists, **42**, 71-108.

Harris, P. M. and Frost, S. H. 1984. Middle Cretaceous Carbonate Reservoirs Fahud Field and Northwestern Oman. American Association of Petroleum Geologists, Bulletin, **68**, 649-658.

Haynes, S.J. and McQuillan, H., 1974. Evaluation of the Zagros suture zone, Southern Iran. Geological Society of American Bulletin, **85**, 739-744.

Huber, B.T., Norris, R.D., and MacLeod, K.G., 2002: Deep-sea paleotemperature record of extreme warmth during the Cretaceous.Geology, **30**, 123–12.

James, G.A., and Wynd, J.G., 1965. Stratigraphical nomenclature of Iranian Oil Consortium Agreement Area. American Association of Petroleum Geologists Bulletin, **49**, 2182-2245.

Keyvani, F. and Heydari, E., 2002. Depositional environments and diagenesis of cretaceous (Albian to Maasterichtian) strata of the Abadan plain of the Persian platform in southwestern of Iran, Proceedings of The Geological Society of America Annual Meeting.

Koop, W. J., and Stoneley, R., 1982. Subsidence history of the Middle East Zagros basin, Permian to recent. In: Kent, P.E., Bott, M.P., McKenzie, D.P., and William,C.A.(Eds.), Philosophical Transactions Royal Society London, **305**, 149-168.

Murris, R.J., 1980. Middle East stratigraphic evolution and oil habitat: American Association of Petroleum Geologists Bulletin, **64**, 597-618.

Pattison, R., and Takin, M., 1971. Geological significance of the Dezful embayment boundaries. National Iranian Oil Company, Report 1166 (unpublished).

Sepehr, M., and Cosgrove., J. W. 2004. Structural framework of the Zagros Fold- Thrust Belt, Iran. Marine and Petroleum Geology. **21**, 829-843.

Setudehnia, A. 1978. The Mesozoic sequence in southwest Iran and adjacent area. Journal of Petroleum Geology, **1**(1), 3-42.

Sharland, P.R., Archer, R., Casey, D.M., Davies, R.B., Hall, S.H., Heward, A.P., Horbury, A.D., and Simmons, M.D., 2001. Arabian Plate sequence stratigraphy: GeoArabia Special Publication 2, Gulf Petrolink, Manama, Bahrain, 371 p.

Sharp, I, Bang, B., Morsalnezhad, D., Bargrizan, M., Taberner, C., Karpuz, R., Vergés, J., and Gillespie, P., 2003. Sedimentology And Sequence Stratigraphy Of The Bangestan Group, Lurestan Province, Zagros Mts, Iran, AAPG International conference, Barcelona Spain, September 21-24.

Sherkati, S., and Letouzey, J., 2004. Variation of structural style and basin evolution in the central Zagros (Izeh zone and Dezful Embayment), Iran: Marine and Petroleum Geology, **21**, 535-554.

Taghavi, A.A., Mork, A, and Emadi, M.A. 2006. Sequence stratigraphically controlled diagenesis governs reservoir quality in the carbonate Dehluran Field, southwest Iran, Petroleum Geoscience, **12**(2), 115-126.

Van Buchem, F.S.P., Razin, P., Homewood, P.W., Philip, J.M., Eberli, G.P., Platel, J.-P., Roger, J., Eschard, R., Desaubliaux, G.M.J., Boisseau, T., Leduc, J.-P., Labourdette, R., and Cantaloube, S. 1996. High resolution sequence Stratigraphy of the Natih Formation (Cenomanian/Turonian) in Northern Oman: Distribution of source rocks and reservoir facies: GeoArabia, **1**, 65–91.

Videtich, P.E., McLimans, R, K. Kim H., Watson, S., and Nag, R.M., 1988. Depositional, diagenetic, thermal, and maturation histories of Cretaceous Mishrif Formation, Fateh Field, Dubai. American Association of Petroleum Geologists Bulletin; **72**(10), 1143-1159

Ziegler, M. A., 2001. Late Permian to Holocene paleofacies evolution of the Arabian Plate and its hydrocarbon occurrence: GeoArabia, **6**, 445-504.

Chapter 2

Subaerial Exposure and Meteoric Diagenesis of the Cenomanian-Turonian Upper Sarvak Formation, Southwestern Iran

2.1. Introduction

The Mid-Cretaceous Sarvak Formation in southern Iran contains more than 20% oil-in-place of Iranian oil reservoirs forming the second most important reservoir rocks after the Asmari Formation of Oligo-Miocene. In addition to its petroleum significance, the Sarvak Formation forms productive ground water aquifers feeding karstic springs in the Zagros region (Raeisi and Karami, 1997; Ahmadipour, 2002).

Sarvak carbonates were deposited in a ramp environmental setting with extensive lateral and vertical facies variations (Setudehnia, 1978). These carbonates were affected by a major unconformity (Turonian) that caused extensive erosion and karstification. Therefore, the variability and extent of diagenesis and the distribution of diagenetic phases could be due to the presence of the unconformity and associated karstification. This unconformity has been reported in several localities in southern Iran as well as elsewhere in the Persian Gulf region (James and Wynd, 1965; Harris et al., 1984; Setudehnia, 1978).

Karstification of carbonate rocks by meteoric water during subaerial exposure is an important diagenetic process that contributes to the development of petroleum reservoirs by enhancing their porosity and permeability (e.g. Lousk, 1999; Wright, 1991; Wang and Al-Aasm, 2002; Fu et al., 2006). Karstified systems are commonly affected by later diagenesis including cementation.

Karstic features have great implications for sequence stratigraphy, palaeoenvironmental interpretation and more importantly the development of hydrocarbon reservoirs. However, identification of these features could be problematical in some instances in drilled cores. The high porosity and permeability of the karstified carbonates and the importance of palaeokarst processes in developing porosity have been widely documented in the literature (Mylroie and Carew, 1995; Lousk, 1999 among many others). Karstification could result in modification and redistribution of

porosity and permeability (Choquette and James, 1988; Hopkins, 1999), often significantly complicating exploration for oil and gas, as well as delineation of reservoir characteristics.

The aim of this investigation is to identify diagenetic processes in the Upper Sarvak Formation, including extensive karstification, that were mainly controlled by subaerial exposure. These processes also greatly influenced reservoir quality. To obtain a better understanding of the diagenetic processes, petrographic and stable carbon and oxygen isotope results of the Upper Sarvak carbonates from surface sections and subsurface cores from southwestern Iran have been integrated (see Fig. 2.1 for location of the study area). Data obtained from these investigations have been used to characterize the diagenetic fluid (s) involved. In addition these data have been utilized to substantiate the greenhouse condition, which is favoured for karst formation and the evolution of porosity in the Upper Sarvak Formation.

2.2. Previous Studies of the Sarvak Formation

The stratigraphy and sedimentology of the main lithostratigraphic units of the Zagros region in southwest Iran are now well established (Alavi, 2004). However; understanding the various petroleum systems in the region requires paleogeographic reconstructions of these units, focussing on their regional and local lithofacies variations.

The Mid-Cretaceous Sarvak Formation of the Bangestan Group (i.e., Albian-Santonian) in the Zagros Mountains was deposited in a ramp setting during Cenomanian to Early Turonian (Setudehnia, 1978; Taghavi et al., 2006). Stratigraphically, this formation is equivalent to Mauddud, Ahmadi and Mishrif formations in the Persian Gulf (Ghazban, 2007); Wara, Ahmadi and Mishrif formations in Iraq and Saudi Arabia (Fig. 2.2) and the Natih Formation in Oman (van Buchem et al., 2002).

James and Wynd (1965) conducted the first systematic stratigraphic investigation of the Zagros Mountains including the Cenomanian-Turonian Sarvak Formation. Their work was followed by Setudehnia (1978), who reviewed the geology of the formation and examined depositional facies and their cyclicity in southwestern Iran. Boltz (1978) recognized the deposition of the Sarvak carbonates within a restricted intrashelf basin in Dezful Embayment and suggested a significant tectonic influence on general sedimentation patterns.

Hajikazemi et al. (2002) demonstrated that much of the variability in diagenetic features and their spatial distribution in the Upper Sarvak Formation in the Sirri Oil fields in northeastern

Persian Gulf could be related to the presence of the major Turonian unconformity and associated karstification.

Taghavi et al. (2006) investigated the Upper Sarvak Formation in the Dehluran Field (~120 km northwest of Ahwaz) and identified three major transgressive-regressive sequences. According to these authors the diagenetic processes especially regressive parts of each major sequence, were controlled by sea-level fluctuations.

Beiranvand et al. (2007) recognized five facies association in the Sarvak Formation and identified different reservoir rock types with significant vertical and lateral heterogeneities in a giant oilfield near the northern head of the Persian Gulf while Farzadi and Hesthmer (2007) integrated the 3D geophysical and well-log data from the Sirri oilfields and introduced the volume-based interpretation technique as a proper method for detail stratigraphic interpretation of the Turonian palaeokarst in the Sarvak carbonates.

Based on these investigations it is apparent that lateral and vertical facies variations are important stratigraphic characteristics of the Upper Sarvak Formation. Furthermore, the major Turonian unconformity that has caused deep erosion and diagenesis greatly influenced the development of porosity and determined the reservoir characteristics in various areas. In spite of some important findings, the diagenetic processes and evolution of these heterogeneous carbonate reservoir rocks in southern Iran is not well understood and warrant more investigation.

2.3. Regional Geological Setting

The Permian-to-Cretaceous evolution of southern Iran and the Persian Gulf region ended with the establishment of an extensive carbonate shelf as the region became a passive margin of the Neo-Tethys Ocean (e.g. Murris, 1980; Harris et al., 1984; Van Buchem et al., 2002). The Early Cretaceous was a period of maximum rifting of the Neo-Tethys Ocean, while the major phase of tectonics occurred in Late Cretaceous resulting in the closure of the Neo-Tethys Ocean accompanied by major continental collision.

The Mid-Cretaceous sedimentary succession that includes the Sarvak Formation was dominated by widespread carbonate accumulation with an extensive development of carbonate platforms and rudist-foraminifera bioherms occurring widely throughout the Neo-Tethys Ocean (Burchette and Wright, 1992; Droste and Van Steenwinkel, 2004). In the early Cenomanian,

benthic foraminifera and rudists were widely distributed throughout the region and the latter formed rudist-debris rimmed shelves (Burchette and Britton, 1985).

During Cenomanian-Turonian, sedimentation rates varied considerably, from low-deposition (e.g., Northeast Persian Gulf), to accumulation of thick successions (e.g., Sarvak type section in the study area). This variability in sedimentation rate is evident when considering the total thickness of the formation and absence or very low thickness of some microfacies, especially the open marine microfacies of the lower Sarvak, in different areas in southern Iran and the Persian Gulf region. The variable thicknesses evident form the isopach map of the Mid-Cretaceous in different part of the sedimentary basin (Fig. 2.3). The thickness variation suggests a period of instability, characterized in some areas by active salt tectonism (Burchette and Britton, 1985). Thickness variations within the Sarvak Formation across some of the drilled wells in Persian Gulf area could also be due to erosion by the Turonian unconformity or variable subsidence rate in different parts of the basin (Ghazban, 2007).

The Mid to Late Cretaceous was also a period of major environmental changes with the global sea-levels steadily rising (Sharland et al., 2001). This is indicated by the early Turonian global maximum flooding surface (Haq et al., 1988). The Sarvak carbonates deposited when the global sea level was at a highstand. Following the deposition of the Upper Sarvak, a major sea level fall in mid Turonian exposed these carbonates and resulted in regional Turonian unconformity. This widespread unconformity is recorded by rubbly breccia, karstic topography and hematite nodules capping Cenomanian platform carbonates (Motiei, 1993) in southern Iran. It resulted from both a combination of localized uplift, following the initiation of ophiolite obduction and global eustatic sea level fall (James and Wynd, 1965; Setudehnia, 1978; Motiei, 1993; Ghazban, 2007). In addition there is evidence for the presence of a local erosional unconformity causing at the Cenomanian-Turonian boundary observed in drilled wells and examined outcrops of the Sarvak Formation in southwestern Iran (e.g., Beiranvand et al., 2007).

Sea level fluctuation left a recognizable imprint on sedimentation patterns; however local tectonic controls, notably salt tectonics and diapirism, were also of significant importance (Burchette, 1993).

2.4. Stratigraphy of the Sarvak Formation

The Sarvak Formation is named after Tang-e-Sarvak (Sarvak gorge) in the central part of the southern flank of Bangestan Mountain in southwestern Iran. At its type section, the Sarvak

Formation consists of three limestone units reaching a maximum thickness of 821 m (Motiei, 1993). The lower boundary of the Sarvak Formation conformably overlies the Kazhdumi Formation with a transitional contact, whereas the nature of the upper contact, which is the Turonian unconformity, is variable. For example in the type locality , marls of the Gurpi Formation (Maestrichtian) overlies the Sarvak Formation whereas in the Dezful embayment, the Sarvak carbonates and the overlying Ilam Formation (Santonian-Campanian) form an extensive continuous limestone unit, which appears to have been deposited in a shallow-marine environment.

The lower part of the Sarvak Formation (254 m thick) consists of argillaceous micritic limestones with lenticular bedding and thin-layered marl interbeds. The middle part of the succession (524 m thick) includes massive chalky limestones with iron-rich siliceous carbonate concretions and rudist fragments. Cross bedding is evident in a number of horizons. The top 42 m of the formation includes massive limestones with the topmost strata consisting of a weathered brecciated ferruginous limestone (Fig. 2.4).

The formation is interpreted to have been deposited in a shallow marine setting during the Cenomanian-Turonian. Three Third -order sequences have been distinguished within the Upper Sarvak Formation. VanBuchem et al. (2002) interpreted these sequences in Natih Formation (Upper Sarvak equivalent in Oman) as an alternation of two types of depositional systems, a mixed carbonate-clay ramp with benthic foraminifera as dominant fauna at the base and a carbonate-dominated ramp bordering an intrashelf basin with rudist in mid-ramp environment and organic-rich carbonates representing the basinal facies forming the top of each sequence. They invoked eustatic control as the main mechanism for the Third order sequences.

2.5. Material and Methods

This study is based on petrographic investigation of 360 repesentative samples derived from detailed field study of the Sarvak Formation type section, the Upper Sarvak Formation from another surface section at the Shahneshin Mountain 90 km northwest of Shiraz and samples from 2 cored wells in the Rag-e Sefid oilfield in southwestern Iran (see Fig.2.1 for study area). The type section and cores were logged and sampled based on facies and/or diagenetic variations.

Petrographic thin sections were stained with Alizarin red-S and potassium ferricyanide and carefully analyzed by standard optical transmitted light, fluorescence and cathodoluminescence microscopy, as well as by Scanning Electron Microscopy (SEM).

Cathodoluminescence (CL) microscopy of 98 representative carbonate samples was carried out using a Technosyn 8200 MKII model cold cathodoluminescence stage with a 12-15 kv beam and a current intensity of 420-430 μA on the unstained halves of the uncovered thin sections.

Carbonate rocks were classified according to Dunham's modified carbonates classification (Wright, 1992). In addition 48 core samples from mainly the most upper part of the formation were impregnated with an epoxy mixed with a blue dye for porosity identification.

Eighty samples of the least altered carbonate matrix (i.e., micrite), various generations of calcite cements and rudist shells were micro-sampled using a micoscope-mounted dental drill assembly. Extracted powders were reacted with 100% pure phosphoric acid at 25°C for 4 hours (Al-Aasm et al., 1990). The evolved CO_2 gas was analyzed for oxygen and carbon isotopic ratios using a Finnigan Mat Delta Plus mass spectrometer. All analyses for oxygen and carbon isotopes are reported in per mil (‰) notation relative to the Pee Dee Belemnite (VPDB) standard. Precision for both isotopes was better than 0.05‰.

2.6. Depositional Environment

Based on field and detailed petrographic investigations four main depositional environments identified in the ramp setting in the Upper Sarvak Formation using Burchette and Wright (1992) classification, comprising the inner- ramp, mid-ramp, outer-ramp and open marine or basinal environment. Each environment is characterized by several microfacies.

2.6.1. Inne- ramp

This environment can be subdivided into lagoonal and shoal/barrier environments in the lagoonal environment, benthic foraminiferal wackestone and packstones are the dominant microfacies. Miliolids, Textularia, *Praealveolina, Nezzazata* and *Orbitolina* are the main skeletal grains. Echinoiderms and gastropods are of lesser importance. Rudist biostroms are seen in surface sections can be identified as rudist floatstone or rudstone in core samples. Sedimentary features such as burrowing and geopetal fabric are abundant in this environment.

The Shoal/barrier environment is a high energy environment with the grainstones as the dominant microfacies. Benthic foraminifera grainstone, rudist –echinoderm grainstones, rudist rudstones and peloidal-bioclastic grainstones/packstones are the main microfacies representing this environment.

2.6.2. Mid-ramp

The mid-ramp environment is mainly represented by bioclastic wackestone to packstones. Bioclasts include benthic foraminifera (*Praealveolina, Dicyclina, Ovalveolina* and miliolids) and fragments of rudists and gastropods. Burrows, usually filled with calcite cement, are the most common sedimentary structure in this facies. At the Sarvak type locality this facies includes cross-bedding, which is a good indicator of a higher energy environment. This depositional environment appears to be restricted mainly to the Upper Sarvak Formation.

2.6.3. Outer-ramp

The outer-ramp environment is composed of meter-scale-bedded mudstone to wackestone with less variety of foraminifera (*praealveolina* and *Orbitolina*), some gastropod and echinoderm fragments, sponge spicules and rarely pelagic foraminefera. This environment is more dominant in the lower Sarvak Formation but occur in the lower part of the Upper Sarvak Formation as well.

1.6.4. Basinal Environment

The basinal environment is represented by organic-rich wackestones and packstones in the lowermost part of the Upper Sarvak Formation. *Hedbergella washitensis* and various Oligosteginids are the main skeletal grains in this microfacies indicating a low-energy open-marine depositional environment.

Based on wells and outcrops, intervals representing each sedimentary environment with their corresponding microfacies have variable thicknesses ranging from tens to hundreds of meters obtained from different wells and surface sections. Local thickness variations and presence or absence of each microfacies largely depend on topography and paleogeography of the basin at the time of deposition. Several factors including sea level change and salt movements (diapirism) affected basinal configurations and topography of the Cenomanian-Turonian basin in the area (Videtich et al., 1988).

2.7. Diagenesis

The Upper Sarvak Formation has been subjected to extensive and variable diagenetic modifications after its deposition in a shallow marine environment or during subaerial exposure (early diagenesis) and subsequent burial (late diagenesis). Major Diagenetic processes affecting

the Upper Sarvak carbonates include micritization, dissolution, karstification, compaction, dolomitization, calcite cementation, recrystallization, silicification and pyrite formation (Fig. 2.5).

2.7.1. Micritization

Micritization identified here is an early diagenetic process. Micritic envelopes surround some rudist and echinoderm fragments and wholesale micritization of some benthic foraminifera in bioclastic packstone microfacies makes the recognition of skeletal grains difficult in some intervals.

2.7.2. Dissolution

Dissolution and associated karstification was the most important diagenetic process to affect the porosity and permeability in the Upper Sarvak carbonates especially in grain-supported intervals. According to well data obtained from porosity logs and company reports, porosity in the Upper Sarvak Formation varies from 0.5 to more than 14%. However, the lower part of the Sarvak Formation has less than 1% porosity. Porosity is mainly secondary in nature and dominated by vuggy, mouldic, and intercrystalline types. Vugs are sub-spherical or irregular in shape and reach up to several millimetres in size in core samples and a few centimetres in surface sections. The vugs are partially or completely filled by ferroan calcite cement (Fig. 2.6A). Cavernous porosity is also observed in upper part of the Sarvak Formation underneath the unconformity surface (Fig. 2. 6B). Intercrystalline porosity occurs between calcite cement or dolomite crystals (Fig. 2.6C, D). Moulds of benthic foraminifera and gastropods are totally or partially filled with calcite cement whereas bitumen fills some of the vuggy and intercrystalline porosities (Fig. 2. 6E, F). Primary porosity is of lesser importance and mostly includes intraparticle porosity. The body cavity of the rudists forms the most important interaparticle porosity (Fig. 2.6G-H). The microfacies representing the shoal/ barrier deposits especially rudist grainstone/rudstone are the most porous intervals in the Upper Sarvak Formation, and they contain both primary and secondary porosity.

2.7.3. Karst Formation

Karstification can occur in different diagenetic realms, including meteoric (via dissolved CO_2 releasing carbonic acid), deep burial (thermal regime associated to deep CO_2 or H_2S production) and in mixing zones (mixing of fresh and seawater in coastal areas) (Ford 1988; Ford and Williams, 2007; Wright 1991). The effects discussed here are mainly related to meteoric dissolution. This is based on the presence of the prominent unconformity surfaces in the Upper

Sarvak Formation, resulted from regional exposure associated with the Turonian unconformity and local exposure of some areas at the Cenomanian-Turonian boundary. Karst development in the Upper Sarvak Formation occurred extensively on emergent portions of the ramp especially the inner ramp environment.

Subaerial exposure-related features in the Upper Sarvak Formation seen in Shahneshin Mountain surface section include:

(a) brecciation of carbonates,

(b) presence of cavernous porosity,

(c) boxwork texture showing extensive carbonate dissolution,

(d) erosional surfaces and incised channels filled with pisoids and clays,

(e) development of palaeosol and bauxite.

Breccia related to dissolution of carbonate rock is widespread in this area. Breccia fragments are angular to sub-angular varying in size from 2 mm to tens of centimetres. The breccia is either matrix-supported with calcite matrix being stained with iron oxides or grain-supported with bituminous calcite matrix (Fig. 2.7A, B). This breccia is interpreted to have resulted from dissolution widening associated with karstification and collapse of the overlying beds rather than being related to faults or major fractures. The brecciation observed in surface sections and core samples from Rag-e Sefid oil field is a strong support of our interpretation of subaerial exposure and karst development.

Boxwork texture (also known as honeycomb texture; Sweeting, 1973, p. 142) is a palaeokarst feature consisting of a network of thin blades of calcium carbonate projecting out from the rock surface. The blades enclose irregularly shaped and variably sized spaces and the overall appearance is that of sets of open, connected spaces (Fig. 2.7C). Boxwork texture forms in the meteoric diagenetic environments (Sweeting, 1973).

A scoured surface occurs on the top of the Sarvak Formation. On a two dimensional view the erosional feature appears as a flat-topped U-shaped depressions, typically 2-3 m wide and, with maximum depths ranging from 1-2 m (Fig. 2.7D). However, based on their lateral extension in 3D views, the scoured surfaces have channel morphologies extending at least for 30 m on the outcrop scale. The eroded surface appeared to be the highly karstified limestones, later covered

by fluvial deposits. Material filling the channels is composed mainly of black pisolites within a matrix composed of brown clay and silt-size calcitic sediments (Fig. 2.7E) and contained within the channel. Similar erosional surfaces have been reported within the Mid-Cretaceous Natih Formation of Oman by Van Buchem et al. (2002). Emersion features and erosional surfaces have been observed and interpreted to have developed during Turonian sea-level fall and filled during the subsequent transgression (Van Buchem et al. 1996; Van Buchem et al., 2002).

Palaeosols in the form of bauxite and laterite developed in the top 10-50 cm of the Sarvak Formation at Shahneshin Mountain (Fig. 2.7F). They overlie pisolites along the exposure surface. Although only one body of bauxite has been mined, many smaller masses, up to 3 m thick, are found in the region. The mined bauxite horizon, in the Firoozabad area near Shiraz is approximately 30 m thick covering an area of about 1 km^2 and is developed along the contact between Sarvak and Ilam formations (Liaghat et al., 2003). The relatively small thickness of most bauxite layers, which may indicate a short duration of exposure considering the humid climate at the time of their development.

Bauxite and laterite found in the study area could be classified as karst bauxite (Bardossy, 1982). They are perhaps the most persuasive and clear evidence of emergence, subaerial exposure and karstification of the Upper Sarvak Formation.

Clearly, the breccia, the occurrence of bauxite and laterites, palaeosol and extensive erosional truncation and karstification must have formed prior to the deposition of the overlying formation. The existence of warm and humid climatic conditions at this time would have intensified the hydrologic cycle.Under such conditions carbonate dissolution and karstification could be increased below the unconformity surface enhancing the overall porosity. This could be the main reason for porosity enhancement up to 15% in some intervals obtained from well data and surface section samples.

2.7.4. Compaction

Both mechanical and chemical compactions are observed in the Upper Sarvak Formation. Mechanical compaction resulted in porosity reduction by breakage the grains in packstones. Dissolution seams and stylolites are among the most common chemical compaction features in most of the rock units within the Sarvak succession.

2.7.5. Recystallization

Partial recrystallization of the matrix occurs in some intervals (i.e. below palaeoexposure surfaces and adjacent to some stylolites) causing the enlargement of the crystals of the micritic matrix (Fig. 2.8A). Recrystallization has also been locally important in modifying the internal structure in some of bioclasts such as benthic foraminifera.

2.7.6. Fracturing

Different sets of fractures with variable orientations occur in the Upper Sarvak Formation, but two sets of them are more common; vertical fractures and sub- horizontal fractures. Vertical fractures, which appear to have a wider opening (more than 2 mm in some cases) comparing to second set and are partially or completely sealed with calcite cement (Fig. 2.8B).The second set of fractures which is approximately horizontal, cross-cuts the earlier set and the calcite cement filling the ealier set and also stylolites and dissolution seams. Apertures do not exceed few micrometers and are devoid of cement.. The origin(s) of these small-scale fractures is not completely understood. They could be related to minor tectonic events (e.g. salt tectonic) in the area. There are large-scale fractures seen in the upper most part of the Sarvak Formation in surface sections which are in variable directions. They are devoid of cement and seem to be the product of the dissolution due the influence of meteoric water during the subaerial exposure.

2.7.7. Dolomitization

Three types of dolomite are recognized in the Upper Sarvak Formation; (a) fine crystalline(<20 μm) dolomite cement (dolomite I) filling the interparticle porosity in brecciated intervals underlying the unconformity; (b) subhedral-euhedral fine to medium-crystalline (40-60 μm) clear dolomite replacing calcite matrix in association of dissolution seams (dolomite II), and (C) euhedral medium-crystalline (>70 μm) cloudy center, clear rim dolomite (dolomite III), replacing the carbonate matrix and mainly associated with stylolites (Fig. 2.8C-E). Dolomite II and III are more common in mud-supported microfacies such as bioclastic wackestones.

2.7.8. Calcite Cementation

Calcite cementation is a dominant diagenetic feature in the Sarvak Formation specially in the upper part of the formation. Five main types of calcite cements are recognized in the Upper Sarvak Formation, from earliest to latest: (a) fine crystalline isopachous rim cement, (b) fine to medium equant calcite cement, (c) syntaxial overgrowth calcite, (d) drusy mosaic calcite, and (e) blocky sparry calcite.

The fine crystalline isopachous rim cement occurs around some of the skeletal grains growing into the primary intergranular pores in grainstones preventing the compaction of grains. It appears non-luminescent under CL. Equant calcite cements partially fill some of the rudist and foraminifera chambers and primary pores in packstones or grainstones reducing the porosity in some intervals. They consist of dark to non-luminescent crystals with thin bright luminescent rims surrounding them projecting toward the center of the pores. Syntaxial overgrowth calcite commonly surrounding echinoderm fragments in grainstone shoal deposits. Under CL, this type of cement appears to be non-luminescent. Drusy mosaic and blocky sparry calcite cement are the most abundant cements and fill the first generation of fractures, and partially or completely fill some moulds and primary pores in some of the rudists.

A consistent cathodoluminescence (CL) zonal succession is recognized in the fracture-filling drusy mosaic calcite cements. Based on CL microstratigraphy this cement is divided into three subzones which are referred from earliest to latest C1 to C3 (Fig. 2.8F). The earlier generation of fracture filling calcite cement (C1) is dull to non- luminescent with a small portion showing concentric zoning consisting of alternating bright, dull and non-luminescent bands.

The bright-rimmed-luminescent portion (C2) reflects a change in composition and chemistry of fluids involved in its precipitation. The following cement generations is zoned cement (C3) and shows dull-red to orange concentric luminescence zoning.

Coarse blocky sparry calcite cement is the latest cement (C4) and it partially fills remaining voids within the earlier sets of fractures and some rudist body cavities and partially or completely occludes some vugs, hence reducing the porosity and reservoir quality. This calcite cement is commonly ferroan and characterized by dull to non-luminescent crystals. Two phase fluid inclusions are visible in some of the larger crystals.

2.7.9. Discussion of Cement Stratigraphy

The non-luminescent characteristic of the isopachous rim cement, equant calcite cements and syntaxial cement indicates their precipitation under oxidizing conditions in either marine or meteoric vadose environments. The non-luminescent equant calcite crystals could be considered as both vadose meteoric or marine cement and the bright rims surrounding the crystals could indicate the influence of reducing conditions of phreatic meteoric environment (Moldovany and Lohmann, 1984).

Cathodoluminescence characteristics observed in drusy mosaic calcite cement (C1-C3), which fills fractures (I) throughout the Upper Sarvak Formation, also signifies meteoric water influence. The succession of non-luminescent to bright-yellow rimmed-luminescent cement (C1-C3) is interpreted as meteoric or shallow burial in origin (Meyers 1974; Moldovany and Lohmann 1984; Carpenter and Lohmann 1989). However the meteoric origin of these cements further supported by stable carbon and oxygen isotope results obtained from them (see below). Therefore, the cement succession is interpreted to reflect the effect of meteoric water on the entire Upper Sarvak formation during the subaerial exposure. The repeating of dark and bright banding of this cement might be due to sea-level fluctuation and periodic emplacement of the Upper Sarvak Formation in phreatic and vadose meteoric environments and changes in the available oxygen level. The dull-luminescent blocky spar (C4) could be interpreted as burial cement. The two-phase fluid inclusions observed in this type of cement confirm its formation in an environment with ambient temperature greater than 50°C.

2.7.10. Pyrite Formation

Two types of pyrite occur in the Upper Sarvak Formation: (a) fine-crystalline framboidal pyrite (pyrite I) and (b) Coarse-crystalline authigenic pyrite (pyrite II), which replaces either matrix or calcite cement in some intervals.

Framboidal morphology displays a spheroidal cluster consisting of smaller, discrete, equant individual crystals of microcrysts. Framboidal pyrites are interpreted to have formed during the early stages of diagenesis and under reducing conditions (Butler and Rickard, 2000a). It is important to note that some of Fe-staining of the carbonates in the upper most part of the Sarvak Formation might be the product of alteration of these pyrites. Authigenic pyrite (i.e. pyrite II) occurs as octahedral crystals, as well as cubic grains. Partial replacement of fracture–filling calcite cement with pyrite (II) in some intervals could indicate its occurrence during the last stages of diagenesis.

2.7.11. Silicification

Minor silica precipitation partially replaces some of the calcitic rudist shells and the latest fracture-filling blocky calcite cements, in the latter case retaining the shape of the original calcite crystals. The silica was probably provided by the dissolution of the sponge spicules, common in the intervals representing the outer ramp environment of the Upper Sarvak Formation.

2.8. Stable Isotope Geochemistry

On the basis of petrography, individual generations of cement, matrix and rudist shells were micro-sampled for their carbon and oxygen isotopic composition in order to further determine the diagenetic environments and their significance (Table 1 and Fig. 2.9).

2.8.1. Calcite Matrix

The $\delta^{13}C$ and $\delta^{18}O$ values of the carbonate matrix range from -0.3‰ to 2.9‰ VPDB and -6.3 to -0.9‰ VPDB, respectively. Compared to the postulated $\delta^{13}C$ and $\delta^{18}O$ values of Mid-Cretaceous marine carbonates (Veizer et al., 1999, see Fig. 2.5 for values), the $\delta^{13}C$ values of the Upper Sarvak Formation carbonates reported here fall well within the range of marine carbonates, whereas the $\delta^{18}O$ values reflect a 1‰ to 2‰ depletion.

2.8.2. Calcite cements

Drusy mosaic calcite cements in the fractures (referred as early cement in Table 2.1 and Fig. 2.9), display $\delta^{13}C$ and $\delta^{18}O$ values ranging from 0.00 ‰ to 3.5‰ VPDB and -6.6‰ to -1.8‰ VPDB, respectively. The blocky calcite cement (referred as late cement in Table 2.1 and Fig. 2.9) also display extreme depletion in $\delta^{18}O$ compared to matrix and early cements and $\delta^{13}C$ values show a significant overlap. The $\delta^{13}C$ and $\delta^{18}O$ values for the blocky calcite cement range from +0.5‰ to +2.5‰ VPDB and from -12.3‰ to -4.5‰ VPDB, respectively. Compared to the matrix the $\delta^{13}C$ and $\delta^{18}O$ values obtained from calcite cements show a wider range.

2.8.3. Rudist shells

The $\delta^{13}C$ and $\delta^{18}O$ values of the rudist shells range from 0.1‰ to 2.1‰ and -5.3‰ to -3.0‰ VPDB, respectively. The range of isotopic compositions of the rudist shells is similar to the range of carbonate matrix.

2.8.4. Palaeosol

Four samples of palaeosol were analyzed and yielded $\delta^{13}C$ and $\delta^{18}O$ values of -5.8 to -3.0 ‰ and -6.2 to -4.2‰ VPDB, respectively.

2.9. Discussion of Stable Isotope Geochemistry

2.9.1. Oxygen Isotopes

The $\delta^{18}O$ of diagenetic carbonate phases are mainly controlled by fluid composition, temperature and water/rock ratios (Brand and Veizer, 1981) and consequently the $\delta^{18}O$ values are expected to be reset by diagenetic alteration. Similarity of stable isotopic compositions of the drusy mosaic calcite cements (early cement), carbonate matrix and rudist shells reflects their equilibration with pore fluids of similar isotopic composition. By contrast, the blocky calcite cements (late cement) have $\delta^{18}O$ values that are relatively depleted.

In most Cretaceous carbonates studied by Scholle and Arthur (1980), the $\delta^{18}O$ data show significant depletion in $\delta^{18}O$ values at or near the Cenomanian-Turonian boundary. Such depletion corresponds closely to the major $\delta^{13}C$ maxima (see Fig. 2.3 in Scholle and Arthur, 1980). The majority of the early cements and matrix analyzed here displayed similar depletion in $\delta^{18}O$ values. Such depleted $\delta^{18}O$ values in conjunction with CL and petrographic observations in association with extensive karstification suggest an important meteoric water influence.

Meteoric diagenesis of marine carbonates typically results in a shift toward more negative values of both $\delta^{13}C$ and $\delta^{18}O$ (e.g., Al-Aasm and Veizer, 1986b). The $\delta^{18}O$ values for some of the Sarvak matrix and cements are more negative than Mid-Cretaceous marine values (Fig. 2.9), suggesting their modification due to either meteoric water influence with variable composition or precipitation from warm fluids, or combination of both (see Given and Lohmann 1985; Carpenter et al., 1991). The interaction with isotopically light waters would have depleted ^{18}O signature of the carbonates. This could have occurred while meteoric water percolated through the Sarvak carbonates during the exposure of the Sarvak carbonates, a hypothesis that is supported by our field and petrographic observation.

The $\delta^{18}O$ values of the blocky calcite cement (late cement) are lower than the $\delta^{18}O$ values of the matrix or early cement suggesting their precipitation from meteoric water or under higher ambient temperatures due to increase of burial depth or combination of both.

2.9.2. Carbon Isotopes

The magnitude of $\delta^{13}C$ exchange between carbonates and meteoric water is controlled by the duration of meteoric diagenesis and extent of the water-rock interaction (James and Choquette, 1990), where the $\delta^{13}C$ of diagenetic phases are mainly buffered by isotopic

composition of the precursor rock (Brand and Veizer, 1981). Stable-isotope patterns in peritidal carbonates also suggest that micrites can retain the original $\delta^{13}C$ if the duration of subaerial exposure is brief (Joachimski, 1994).

The analyzed Upper Sarvak carbonates at the type section, lack the negative $\delta^{13}C$ commonly seen in meteoric diagenetic environments below subaerial exposure surfaces and unconformities (see Allan and Matthews, 1982). One of the most important processes that could account for absence of negative $\delta^{13}C$ excursions on top of the Sarvak Formation is missing sedimentary section or removal of the rocks (see Allan and Matthews, 1982) due to extensive erosion of the uppermost layer during the palaeoexposure. However, depleted $\delta^{13}C$ (i.e.,-1.6 to -5.8‰ VPDB) has been observed in palaeosols and recrystallized matrix sampled at the unconformity surfaces at the top of the Sarvak Formation in Shahneshin area or core samples from wells.

The Cenomanian-Turonian transition is marked by a major positive $\delta^{13}C$ excursion (i.e., 3 to 5‰, Arthur et al., 1988; Voigt, 2000). The widespread accumulation of organic carbon-rich sediment accompanied by a positive $\delta^{13}C$ excursion in marine carbonates across the Cenomanian-Turonian boundary is one of the most prominent episodes of the Mesozoic, described as the Oceanic Anoxic Event (OAE) (Jenkyns, 1980; Arthur et al., 1988). In addition, carbonates immediately above and below the Cenomanian-Turonian boundary level have exhibited $\delta^{13}C$ values of +2.0 to +3.0 ‰ (Schlanger et al., 1983).

Some of the depleted $\delta^{13}C$ values measured for Sarvak carbonate matrix (< +1.0‰) underlie the Cenomanian-Turonian boundary and display a departure from $\delta^{13}C$ positive excursion. Such depleted $\delta^{13}C$ values are due to subaerial exposure and influence of the unconformity surface.

The highly enriched $\delta^{13}C$ values characteristic of the Cenomanian-Turonian boundary is missing in the Sarvak carbonates due to fall in sea level and non-deposition.

2.10. Palaeotemperature and Climatic Considerations

The Mid-Cretaceous was a time of unusually warm climate and is one of the best examples of "greenhouse" conditions in the geologic record (Barron, 1983; Bice and Norris, 2002). Diverse sets of biotic and marine geological data provide convincing evidence that Mid-Cretaceous oceans were extremely warm by today's standards. Global average surface

temperatures were more than 10°C higher than today (Bice and Norris, 2002). The cause of the warm temperatures is unclear but it has been widely attributed to high levels of atmospheric greenhouse gases (Barron, 1987). Atmospheric CO_2 concentrations up to four times present day concentrations increased averaged precipitation rates by 25% (Barron, 1987). Global climate changes at the Cenomanian-Turonian boundary have been linked to changes of oceanic water temperature (Arthur et al., 1988) and to changes in atmospheric CO_2 (Bice and Norris, 2002).

Existing marine records based on $\delta^{18}O$ thermometry suggest that mean sea surface temperatures (SSTs) were highest during the Cretaceous thermal maximum, mostly in Turonian time (Huber et al., 2002; Wilson et al., 2002). To be more specific the SSTs exceeding 34°C are evident from the late Cenomanian to late Turonian (Forster et al., 2007). During the greenhouse period, meteoric water, with increased P_{CO2} would be more aggressive (James and Choquette, 1990). In such warm climates the supply of meteoric water was important in determining the rate, intensity and direction of diagenetic alteration. Thus, the Cenomanian-Turonian interval constitutes an ideal candidate for investigations of the changing climatic conditions. The dominance of warm climate and high amounts of rainfall during exposure of the Sarvak carbonates are important factors in determining the ultimate effect of subaerial exposure

Since the $\delta^{18}O$ of calcite is dependent on the temperature of the water from which it is precipitated, in this study we have used the technique as a thermometer for the Mid-Cretaceous Sea by analyzing the shells of rudists collected from the Upper Sarvak Formation. Calcite palaeotemperatures have been calculated using the equation modified by Anderson and Arthur (1983) that is specifically based on bivalve calcite. This expresses the $\delta^{18}O$ of the water ($\delta^{18}O_{water}$), directly relative to the SMOW standard:

$$T\ (°C) = 16.0 - 4.14\ (\delta^{18}O_{Calcite} - \delta^{18}O_{water}) + 0.13\ (\delta^{18}O_{calcite} - \delta^{18}O_{water})^{2}$$

To obtain the best palaeotemperature results, we analyzed the $\delta^{18}O$ of the rudist shells for their potential in preserving the original stable isotope signatures due to their outer shell layer mineralogy which originally consisted of low-Mg calcite (Al-Aasm and Veizer, 1986b). To produce quantitative temperature estimates it was essential that the original shell $\delta^{18}O$ did not change over time. The $\delta^{18}O$ values obtained from the rudist shells (-3.0 to -5.3‰) are similar to those from the well preserved rudist shells derived from Campanian Carbonates obtained by Immenhauser et al. (2005).

The $\delta^{18}O$ values obtained from the Sarvak rudist shells, would provide a temperature minimum of 25°C (using $\delta^{18}O_{Rudist\ shell}$= -3.0‰VPDB) and a maximum of 36°C (with $\delta^{18}O_{Rudist\ shell}$= -5.0‰VPDB), assuming seawater compositions for the Mid- Cretaceous (no ice build-up) of -1.2 ‰ PDB (White et al., 2001). Such calculated temperatures are in accordance with the proposed Mid-Cretaceous SST values ranging between 28 and 36°C for tropical open marine settings (Steuber, 1996; Huber et al., 2002; Wilson and Norris, 2002; Immenhauser et al., 2005 and Forster et al., 2007). Therefore, warm oceanic temperatures that characterize the Mid-Cretaceous greenhouse conditions appear to have been preserved in the rudist shells found in Upper Sarvak Formation.

A possible objection using $\delta^{18}O$ values here is that they may have been affected by meteoric water, biasing the $\delta^{18}O$ values towards more negative values and therefore higher palaeotemperatures. We do not consider this to be a significant problem for the samples analyzed here because under careful examination using CL and SEM microscopy, we have found no evidence of recrystallization within the rudist shells and the obtained $\delta^{18}O$ and $\delta^{13}C$ results fall well within the range of Mid-Cretaceouse marine carbonates. The calculated temperatures also match the proposed temperatures by other workers (see above).

Temperature of cement precipitation can be also estimated by assuming a value for the isotopic composition of local meteoric water and then calculating a temperature range over which the calcite cements precipitated in equilibrium with this water. Estimation of the ancient meteoric water composition depends on palaeolatitude and palaeotopography at the time of recharge, as well as the degree of water rock interaction in the infiltration zone. During the Mid-Cretaceous, the study area was at an equatorial position, with a humid tropical climate. Thus, the $\delta^{18}O$ of meteoric water could not have been less than -6‰ (White et al., 2001). Precipitation of early cements with $\delta^{18}O$ of -4.1 ± 1.5‰ and formation of palaeosol with $\delta^{18}O$ = -4.2‰ VPDB with such meteoric water gives palaeotemperature estimates of about 25°C. Such calculated warm palaeotemperatures are consistent with warm climate in the Mid-Cretaceous.

That Mid-Cretaceous precipitation rates were likely elevated relative to modern values is supported by the globally widespread distribution of coeval laterites (Sigleo and Reinhardt, 1988). Bauxites development was also widespread during the Mid- Cretaceous, a consequence of the periodic emergence of the carbonate shelves (Mameli et al., 2007). Starting in the Mid-Cretaceous a large scale expansion of lateritic bauxite formation took place on surfaces of several

continents. Bauxites occurred with periodic emergences of the carbonate shelf, under favourable climatic conditions (e.g., warm and humid) that allowed lateritic weathering.

The Upper Sarvak lateritic horizons are sound geologic evidence and in good accordance with the global warming and increased precipitation of Mid-Cretaceous period. Limonitic and reddish soil covers on the exposure surface and bauxite deposits are an indication of humid climate at the time of their development (Wopfner and Schwarzbach, 1976). The palaeosols observed in the study area could be the result of the cumulative weathering effects of long-term exposure largely associated with sea level lowstands.

2.11. Conclusions

By combining detailed field and core examination with petrographic and geochemical analyses, several conclusions can be made regarding the diagenesis and evolution of reservoir porosity of the Sarvak Formation, as follows:

1. Emergence of the Sarvak carbonate ramp due to relative sea- level fall, local salt tectonics and uplift caused large areas of the carbonate succession to be subaerially exposed and subjected to warm and humid conditions. This resulted in profound changes such as the development of vuggy and cavernous porosity within the system, which contributed to elevated rates of additional karst formation.

2. Petrographic, sedimentologic and stable isotope evidence indicate that the subaerial exposure and meteoric diagenesis were the most important diagenetic process affecting the Upper Sarvak Formation.

3. Meteoric dissolution resulted in enhancement of the porosity and permeability especially in rudist –bearing grain/rudstone intervals of the Upper Sarvak Formation.

4. The positive $\delta^{13}C$ of the matrix carbonates, rudist shells and calcite cements are within the range of marine Cretaceous carbonates while the $\delta^{18}O$ values show depletions due to precipitation/equilibration with meteoric water. The $\delta^{18}O$ values of the late cement are distinctly lighter than early cement indicating some exchange reaction or contribution from an isotopically light waters or precipitation in burial environment under higher ambient temperatures.

5. Recognition of the Cenomanian-Turonian and Turonian unconformities is a key factor in locating high porosity and permeability zones in the succession and is based on the presence of (a) sediment filling scoured surface; (b) preserved palaeosols and bauxite rich horizons; (c) iron oxide staining of underlying horizons; and (d) solution-collapse breccia. These are compatible with warm tropical and greenhouse conditions dominating the region during Cenomanian-Turonian.

6. Depleted $\delta^{13}C$ values measured within the Sarvak succession is an indicative of subaerial exposure associated with porosity enhancement.

7. The $\delta^{18}O$ values obtained from the Sarvak rudist shells provide a sea surface temperature (SST) minimum of 25°C and a maximum of 36°C.

2.12. Acknowledgments

The senior author wishes to thank National Iranian South Oil Company for access to samples and making the field work possible. Reviewers are thanked for critically reading an earlier version of this manuscript and their constructive comments. The cooperation of Mr. A.M. Zadeh Mohammadi and Mr. M. A. Kavoosi and Miss F. Pakar is greatly appreciated. Dr. F. Ghazban and Mrs. F. Keyvani were instrumental not only for leading us to excellent outcrop locations but also for their valuable comments and discussions. Funding for this project was provided by Natural Science and Engineering Research Council of Canada (NSERC) to I. Al-Aasm and M. Coniglio. Additional funding was provided by StatoilHydro.

2.13. References

Ahmadipour, M. R., 2002. The role of Sarvak Formation in supplying pol-e- dokhtar town (Iran) with drinking water. Acta Carsologica, **31**(2/4), 93-103.

Al-Aasm, I.S. and Veizer, J., 1986b. Diagenetic stabilization of aragonite and low-Mg calcite, II. Stable isotopes in rudists. Journal of Sedimentary Petrology, **56**, 763-770.

Al-Aasm, I.S., Taylor, B.E. and South, B., 1990. Stable isotope analysis of multiple carbonate samples using selective acid extraction. Chemical Geology, **80**, 119-125.

Alavi, M., 2004. Regional stratigraphy of the Zagros fold-trust belt of Iran and its proforeland evolution. American Journal of Science, **304**, 1–20.

Allan, J. R. and Matthews, R. K., 1982. Isotope signature associated with early meteoric diagenesis. Sedimentology, **29**, 797-897.

Anderson, T.F. and Arthur, M. A., 1983. Stable isotopes of oxygen and carbon and their application to sedimentologic and palaeoenvironmental problems. In: Arthur, M.A., Anderson, T.F., Kaplan, I.R., Veizer, J. and Land, L.S. (editors.): Stable isotopes in sedimentary geology. Society of Economic Palaeontologist and Mineralogist Short Course, **10**, 1-15.

Arthur, M.A., Dean, W.E. and Pratt, L.M., 1988. Geochemical and climatic effects of increased marine organic carbon burial at the Cenomanian-Turonian boundary. Nature, **335**, 714–717.

Barron, E. J. 1983. A warm, equable Cretaceous: the nature of the problem. Earth Science Review, **19**, 305–338.

Barron, E.J., 1987. Cretaceous plate tectonic reconstructions. Palaeogeography, Palaeoclimatology, Palaeoecology, **59**, 3–29.

Bardossy G. 1982. Karst bauxites, bauxite deposits on carbonate rocks, Elsevier Scientific, Amsterdam, 441p.

Beiranvand, B. Ahmadi, A. and Sharafodin, M. 2007. Mapping and classifying flow units in the upper part of the Mid-Cretaceous Sarvak Formation (western Dezful embayment, SW Iran) based on a determination of the reservoir types. Journal of Petroleum Geology. **30** (4), 357-373.

Bice, K.L. and Norris, R.D. 2002. Possible atmospheric CO_2 extremes of the Middle Cretaceous (late Albian-Turonian). Palaeoceanography, **17**(4), 1070.

Boltz, H., 1978. The palaeogeographical evolution during the Cretaceous in the Operating Area with special emphasis on the Bangestan Group. Oil Service Company (OSCO) Internal Report 1274.

Bordenave, M.L.2002. The Middle Cretaceous to Early Miocene Petroleum System in the Zagros Domain of Iran and its Prospect Evaluation. AAPG Annual Meeting, March 10-13, 2002, Houston, Texas.

Brand, U. and Veizer, J., 1981. Chemical diagenesis of a multicomponent carbonate system-2. Stable isotopes. Journal of Sedimentary Petrology, **51**, 987–997.

Burchette, T.P., 1993. Mishrif Formation (Cenomanian-Turonian), southern Arabian Gulf: carbonate platform growth along a cratonic margin basin. In: Simo, J.A.T., Scott, R.W. and Masse, J.-P. (Editors): Cretaceous carbonates platforms. American Association of Petroleum Geologists, Memoir **56**, 185-199.

Burchette, T.P. and Wright, V.P., 1992. Carbonate ramp depositional systems. Journal of Sedimentary Geology, **79**, 3 -57.

Burchette, T.P.and Britton, S.R. 1985. Carbonate facies analysis in the exploration for hydrocarbons: a case study from the Cretaceous of the Middle East. In: Brenchley, P.J. and Williams, B.P.J. (editors): Sedimentology. Recent developments and applied aspects, Black well, Oxford, 311-338.

Butler, I.B. and Rickard, D. 2000a. Framboidal pyrite formation via the oxidation of iron (II) monosulfide by hydrogen sulphide. Geochimica et Cosmochimica Acta, **64**, 2665–2672.

Carpenter, S.J. and Lohmann, K.C., 1989: $\delta^{18}O$ and $\delta^{13}C$ variations in late Devonian marine cements from the Golden Spike and Nevis reefs, Alberta, Canada. , Journal of Sedimentary Petrology, **59**(5), 792-814.

Carpenter, S.J., Lohmann, K.C., Holden, P., Walter, L.M., Huston, T.J. and Halliday, A.N., 1991. $\delta^{18}O$ values, $^{87}Sr/^{86}Sr$ and Sr/Mg ratios of Late Devonian abiotic marine calcite: implications for the composition of ancient seawater. Geochimica et Cosmochimica Acta, **55**, 1991-2010.

Choquette, P.W. and James, N.P., 1988. Palaeokarst. Springer-Verlag, New York, 416p.

Droste, H. and Van Steenwinkel, M., 2004. Stratal geometries and patterns of platform carbonates: The Cretaceous of Oman, in Eberli, G., Masaferro, J.L., and Sarg, J.F.R.,

eds., Seismic Imaging of Carbonate Reservoirs and Systems: American Association of Petroleum Geologists, Memoir **81**, 185–206.

Farzadi, P. and Hesthmer, J., 2007. Diagnosis of the Upper Cretaceous palaeokarst and turbidite systems from the Iranian Persian Gulf using volume-based multiple seismic attribute analysis and pattern recognition. Petroleum Geoscience, **13**, 227-240.

Ford, D., 1988. Characteristics of dissolutional cave systems in carbonate rocks. In Paleokarst, edited by James, N.P. and Choquette, P.W. Springer-Verlag, 25-57.

Ford, D.C. and Williams, P., 2007. Karst Hydrogeology and Geomorphology. John Wiley and Sons, 562 p.

Forster, A., Schouten, S., Bass, M. and J. Sinninghe Damste, 2007. Middle Cretaceous (Albian–Santonian) sea surface temperature record of the tropical Atlantic Ocean, Geology, **35**(10), 919-922

Fu, Q., Qing, H. and Bergman, C. M., 2006. Paleokarst in Middle Devonian Winnipegosis mud mounds, subsurface of south-central Saskatchewan, Canada. Bulletin of Canadian Petroleum Geology; **54**(1) 22-36.

Ghazban, F. 2007. Petroleum geology of the Persian Gulf. Joint publication, Tehran University Press and National Iranian Oil Company. 706p.

Given, R.K. and Lohmann, K.C. 1985. Derivation of the original isotopic composition of Permian Marine cements. Journal of Sedimentary Petrology, **55**, 430-439.

Hajikazemi, E., Ghazban, F. and Yousefpour, M.R., 2002. Depositional and diagenetic history of the Middle Cretaceous sedimentary sequence in the Sirri Oil fields in the Persian Gulf, Iran. Middle East and North Africa Oil and Gas conference, Imperial College, London.

Haq, B. U., J. Hardenbol and P. R. Vail, 1988. Mesozoic and Cenozoic chronostratigraphy and cycles of sea-level change. Society of Economic Paleontologists and Mineralogists, **42**, 71-108.

Harris, P.M., Frost, S.H., Seiglie, G.A. and Schneidermann, N., 1984: Regional unconformities and depositional cycles, Cretaceous of the Arabian peninsula, in J.S. Schlee, ed,

Interregional uncoformities and hydrocarbon accumulations. American Association of Petroleum Geologists, Mem. **36**, 67-80.

Hopkins, J.C., 1999. Characterization of reservoir lithologies within subunconformity pools: Pekisko Formation, Medicine River Field, Alberta, Canada. American Association of Petroleum Geologists, **83**, 1855-1870.

Huber, B.T., Norris, R.D., and MacLeod, K.G., 2002: Deep-sea paleotemperature record of extreme warmth during the Cretaceous.Geology, **30**, 123–126.

Immenhauser, A., Nagler, T.F., Steuber, T.and Hippler, D., 2005. A critical assessment of mollusk $^{18}O/^{16}O$, Mg/Ca, and $^{44}Ca/^{40}Ca$ ratios as proxies for Cretaceous seawater temperature seasonality. Palaeogeography, Palaeoclimatology, Palaeoecology, **215**, 221–237.

James, N.P., and Choquette, P.W., 1990. Limestone diagenesis, the meteoric environment. In Sediment diagenesis. Edited by I. McIlreath and D. Morrow. Geological Association Canada, Reprint Series 4, 36–74.

James, G.A. and Wynd, J.G., 1965. Stratigraphic nomenclature of Iranian oil consortium, Agreement area, American Association of Petroleum Geologists Bulletin, **49** (12), 2182-2245.

Jenkyns, H.C, 1980. Cretaceous anoxic events: from continent to ocean, Journal of Geological Society, London, **137**, 171-188.

Joachimski, M., 1994. Subaerial exposure and deposition of shallowing upward sequences: evidence from stable isotopes of Purbeckian peritidal carbonates (basal Cretaceous), Swiss and French Jura Mountains. Sedimentology, **41**, 805–824.

Liaghat, S. and Hosseini Zarasvandi, A., 2003. Determination of the origin and mass change geochemistry during bauxitization process at the Hangam deposit, SW Iran. Geochemical Journal, **37**, 627 - 637.

Lousk, R., 1999. Paleocave carbonate reservoirs; origins, burial-depth modifications, spatial complexity and reservoir implications. American Association of Petroleum Geologists Bulletin , **83**(11), 1795-1834.

Mameli, P., Mongelli G., Oggiano, G and Dinelli, E, 2007. Geological, geochemical and mineralogical features of some bauxite deposits from Nurra (Western Sardinia, Italy): insights on conditions of formation and parental affinity. International Journal of Earth Science, **96**, 887–902.

Meyers, W.J., 1974. Carbonate cement stratigraphy of the Lake Valley (Mississippian) Sacramento Mountains, New Mexico. Journal of Sedimentary Petrology, **44**, 837-861.

Moldovany, E.P. and Lohmann, K.C., 1984.Isotopic and Petrographic Record of Phreatic Diagenesis: Lower Cretaceous Sligo and Cupido Formations. Journal of Sedimentary Petrology, **54**(30), 927-958.

Motiei, H., 1993. Geology of Iran. The stratigraphy of Zagros. Geological survey of Iran (in Farsi).

Murris, R.J., 1980. Middle East: Stratigraphic evolution and Oil habitat. American Association of Petroleum Geologists Bulletin, **64**, 597–618.

Mylroie, J.E. and Carew, J.L., 1995. Karst Development on Carbonate Islands. In: Budd, D.A., Saller, A.H., Harris, P.M. (editors), Unconformities and Porosity in Carbonate Strata. American Association of Petroleum Geolgists Mem. **63**, 55–76

Raeisi, E. and Karami, G., 1997. Hydrochemographs of Berghan karst spring as indicators of aquifer characteristics. Journal of Cave and Karst Studies, **59**(3), 112-118.

Schlanger, S. O., Arthur, M. A., Jenkyns, H. C. and Scholle, P. A., 1983. Stratigraphic and paleoceanographic setting of organic carbon-rich strata deposited during the Cenomanian-Turonian "Oceanic Anoxic Event". Association of Petroleum Geologists Bulletin, **67**, 545.

Scholle, P. A. and Arthur, M. A., 1980: Carbon isotope fluctuations in cretaceous pelagic limestones: potential stratigraphic and petroleum exploration tool. American Association of Petroleum Geologists Bulletin, **64**, 67-87.

Setudehnia, A., 1978. The Mesozoic succession in S.W. Iran and adjacent areas. Journal of Petroleum Geology, **1**, 3-42.

Sharland, P.R., Archer, R., Casey, D.M., Casey, R.B., Hall, S.H., Heward, A.P., Horbury, A.D. and Simmons, M.D., 2001. Arabian Plate Sequence Stratigraphy. GeoArabia Special Publication, **2**, 371p.

Sigleo, W. and Reinhardt, J., 1988. Palaeosols from some Cretaceous environments in the southeastern United States In: Reinhardt, J. and Sigleo, W.R. (editors): Palaeosols and weathering through geologic time.

Steuber, T., 1996. Stable isotope sclerochronology of rudist bivalves: Growth rates and Late Cretaceous seasonality, Geology; **24**(4), 315–318.

Sweeting, M. M., 1973. Karst landforms, London, MacMillan publishing Company, 362 p.

Taghavi, A.A., Mork, A, and Emadi, M.A., 2006. Sequence stratigraphically controlled diagenesis governs reservoir quality in the carbonate Dehluran Field, southwest Iran, Petroleum Geoscience, **12**(2), 115-126.

Van Buchem, F.S.P., Razin, P., Homewood, P.W., Philip, J.M., Eberli, G.P., Platel, J. P., Roger, J., Eschard, R., Desaubliaux, G.M.J., Boisseau, T., Leduc, J.-P., Labourdette, R., and Cantaloube, S., 1996. High resolution sequence Stratigraphy of the Natih Formation (Cenomanian/Turonian) in Northern Oman: Distribution of source rocks and reservoir facies: GeoArabia, **1**, 65–91.

Van Buchem, F.S.P., Razin, P., Homewood, P.W., Oterdoom, H. and Philip, J., 2002, Stratigraphic organization of carbonate ramps and organic-rich intrashelf basins: Natih Formation (middle Cretaceous) of northern Oman: American Association of Petroleum Geologists, Bulletin, **86**, 21–54.

Veizer, J., Ala, D., Azmy, K, Bruckschen, P., Buhl, D., Bruhn, F., Carden, G.A.F., Diener, A., Ebneth, S., Godderis, Y., Jasper, T., Korte, C., Pawellek, F., Podlaha, O.G. and Strauss, H., 1999. $^{87}Sr/^{86}Sr$, $\delta^{13}C$ and $\delta^{18}O$ evolution of Phanerozoic seawater. Chemical Geology, **161**, 59–88.

Videtich, P.E., McLimans, R.K., Watson, H.K. and Nagy, R.M. 1988. Depositional, diagenetic , thermal and maturation histories of Cretaceous Mishrif Formation, Fateh Field, Dubai. American Association of Petroleum Geologists Bulletin, **72**, 1143-1159.

Voigt, S., 2000. Cenomanian–Turonian composite $\delta^{13}C$ curve for Western and Central Europe: the role of organic and inorganic carbon fluxes. Palaeogeography, Palaeoclimatology, Palaeoecology. **160**, 91–104.

Wang, B. and Al-Aasm, I. S., 2002. Karst-controlled diagenesis and reservoir development: Example from the Ordovician main reservoir carbonate rocks on the eastern margin of the Ordos basin, China. American Association of Petroleum Geologists Bulletin, **86**(9), 1639-1658

White, T., Gonzales, L., Ludvigson, G. and Poulson, C., 2001. Middle Cretaceous greenhouse hydrologic cycle of North America. Journal of Geology, **29**, 363-366.

Wilson, P.A., Norris, R.D. and Cooper, M. J., 2002. Testing the Cretaceous greenhouse hypothesis using glassy foraminiferal calcite from the core of the Turonian tropics on the Demerara Rise. Geology, **30**, 607–610.

Wopfner, H. and Schwarzbach, M., 1976. Ore deposits in the light of paleoclimatology. In: Wolf, K. H. (editor): Handbook of Strata-bound and Stratiform Ore Deposits, **3**, 43–92.

Wright, V.P., 1991. Palaeokarst: types, recognition, controls and associations. In: Paleokarsts and paleokarstic reservoirs, (editors) Wright, V.P., Esteban, M. and Smart, P.L., Postgraduate Research Institute for Sedimentology, University of Reading Contribution, **152**, 56-88.

Wright, V.P., 1992. A revised classification of limestones. Journal of Sedimentary Geology, **76**(4), 177-185.

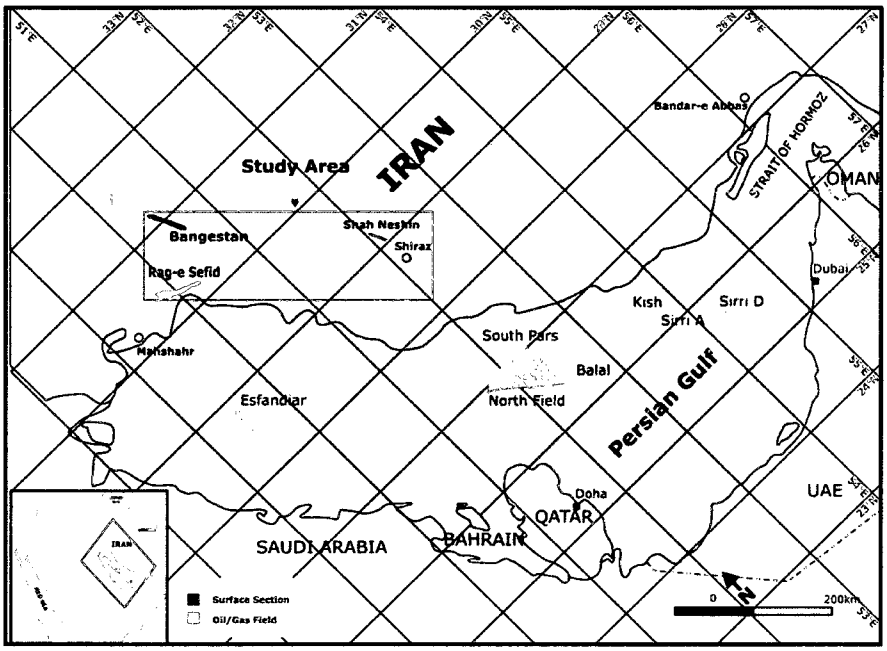

Figure 2.1 Map of southwest Iran and Persian Gulf showing the location of the study area. Inset map at bottom left.

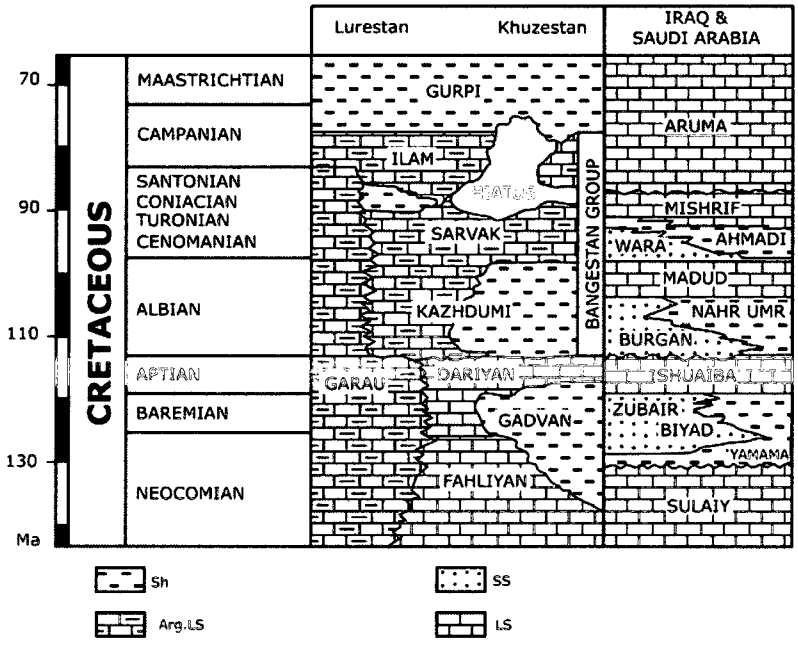

Figure 2.2 Simplified table of Cretaceous rock units from southwestern Iran (after Bordenave 2002).

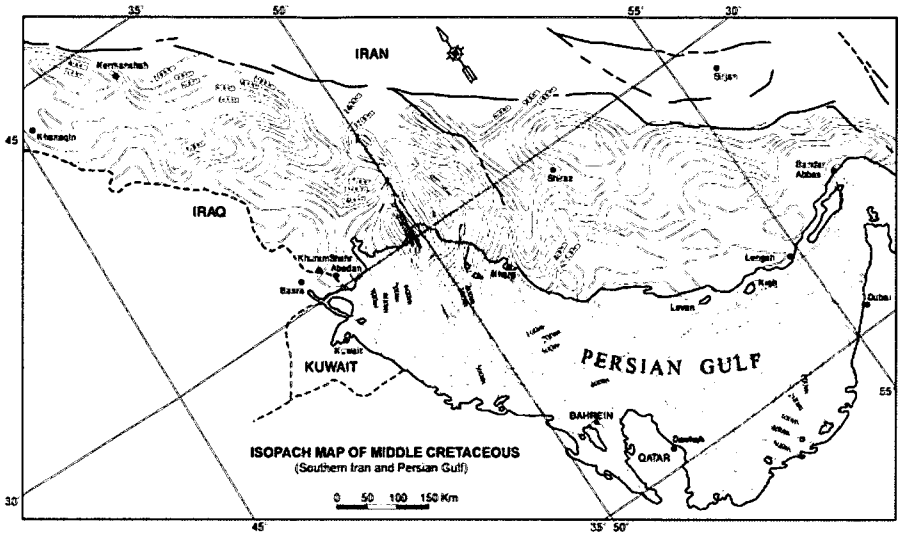

Figure 2.3 Isopach map of Mid-Cretaceous sedimentary rocks in southern Iran and Persian Gulf region (modified from Motiei 1993).

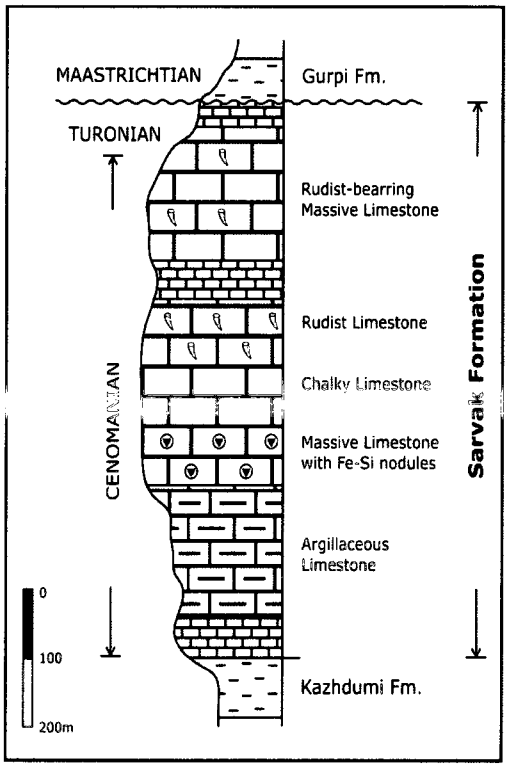

Figure 2.4 General stratigraphic column of the Sarvak Formation at its type section in the Bangestan Mountain in southwestern Iran (Modified from Motiei 1993).

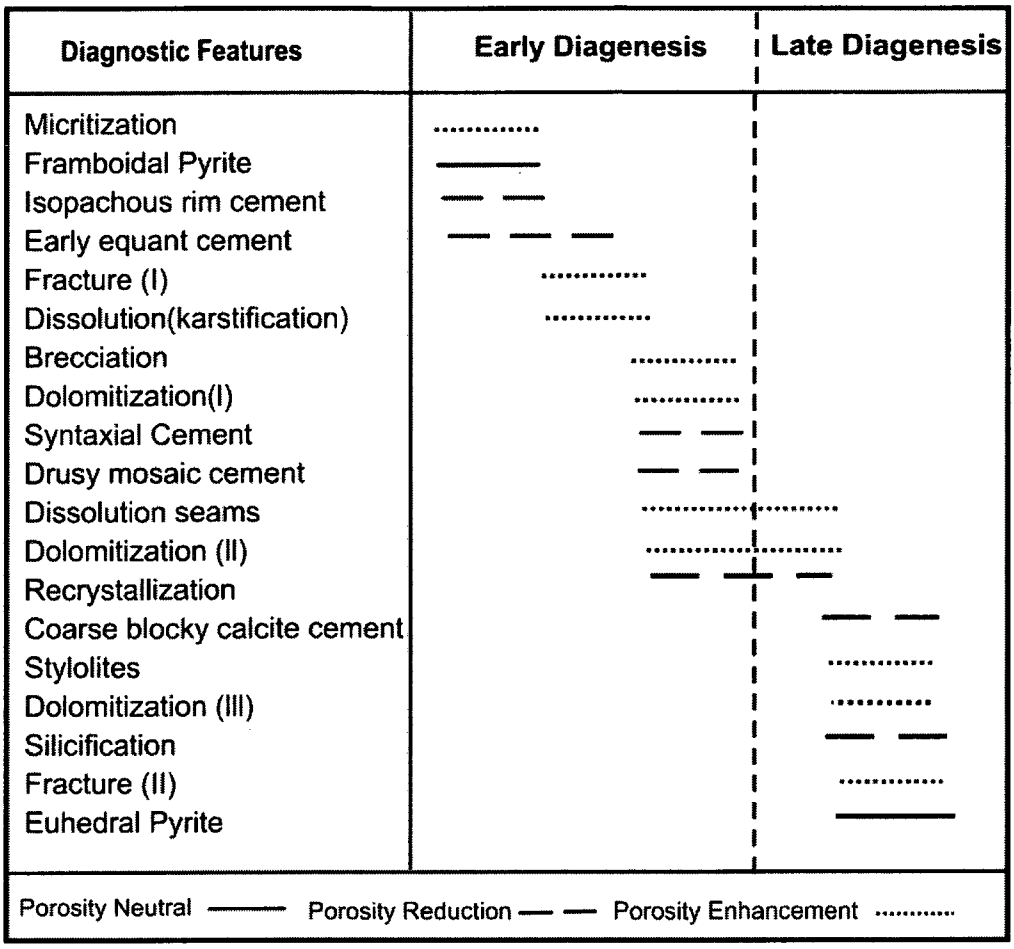

Figure 2.5. Paragenetic sequence of the diagenetic processes affecting the Upper Sarvak Formation.

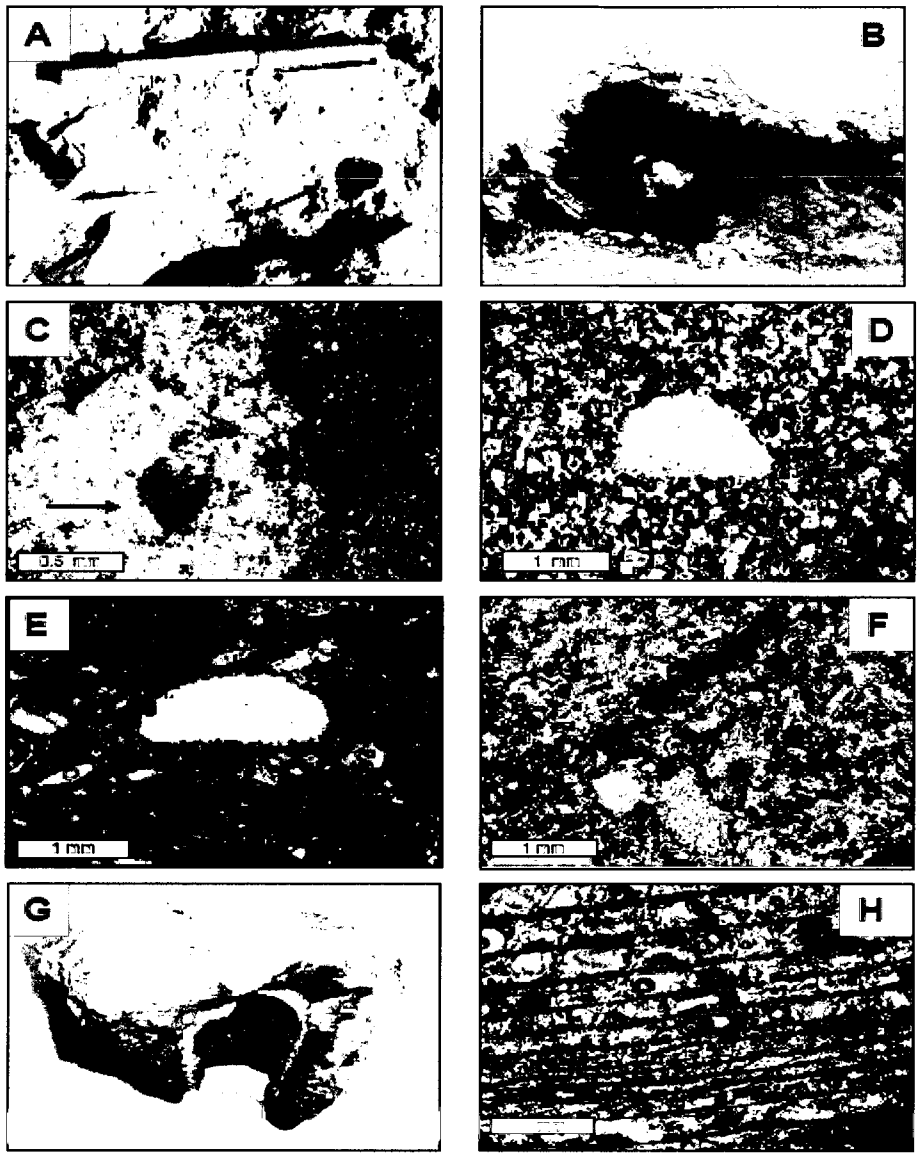

Figure 2.6 Field photograph and photomicrograph of different type of porosity in the Upper Sarvak Formation. A: Vuggy porosity partially filled with rusty-weathering, ferroan calcite cement. B: Cavernous porosity in the Upper Sarvak Formation, Shahneshin Mountain. C: Intercrystalline porosity in calcite cement. D: Intercrystalline porosity in a matrix selective dolomite in rbitolina wackestone or pack stone filled with organic matter. E: Mouldic porosity in bioclastic wackestone filled with blue dye. F: Interparticle porosity filled with blue dye. G, H: Preserved primary porosity in rudist.

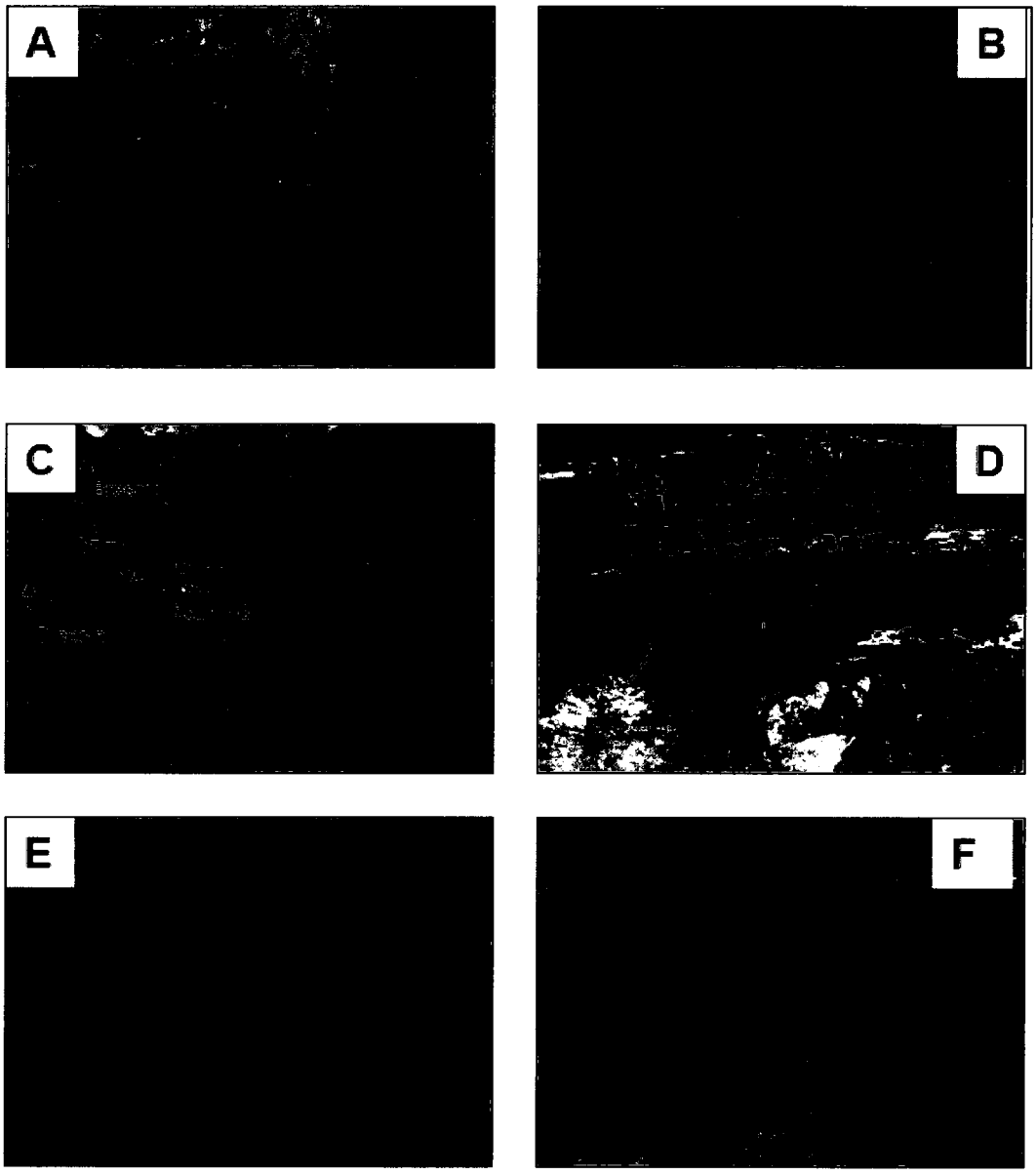

Figure 2.7. Field photographs of karst-controlled diagenetic features in the Upper Sarvak Formation (Shahneshin Mountain). A: Chaotic, solution-collapse breccia within the Sarvak Formation cemented by Fe-stained carbonate matrix. B: Solution-collapse breccia with bituminous carbonate cement on top of the Sarvak Formation C: Boxwork texture with fragments of the Sarvak Formation cemented by fringing calcites, Calcite blades form a honeycomb or network of open space. D: Subaerial exposure surface (arrows) and channel erosion of the Upper Sarvak Formation. E: The ferroan pisolites filling the channel shown in Figure 2.7D. F: Limonitic and reddish soil crust overlying pisolites along the exposure surface.

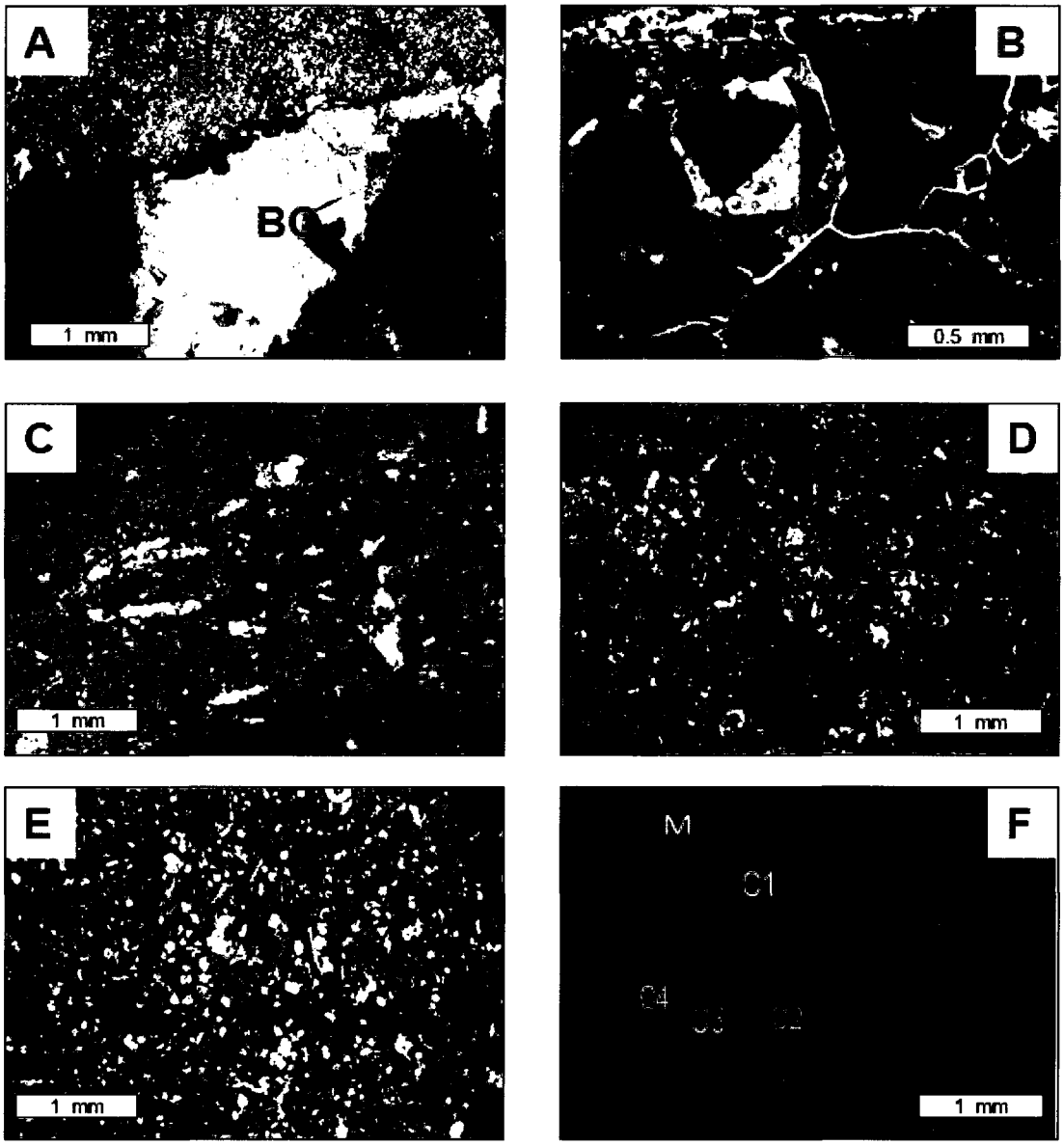

Figure 2.8. Photomicrographs of diagenetic features in the Upper Sarvak Formation. A: Partial recrystallization (R) of matrix and blocky calcite cement (BC) in bioclastic wackestone. B: Fluorescence photomicrograph of equant calcite cement filling vertical fractures retaining the hairline fractures. C: Dolomitic cement in dissolution breccia D: Cloudy center clear rim dolomite (III) partially replacing matrix. E: Clear dolomite partially replacing the calcitic matrix (II). F: Cathodoluminescence view of calcite cement microstratigraphy in a fracture, M: carbonate matrix with limited pore space filled with luminescent orange calcite, C1, C2, C3 (drusy mosaic calcite cement) and C4 (coarse blocky calcite cement).

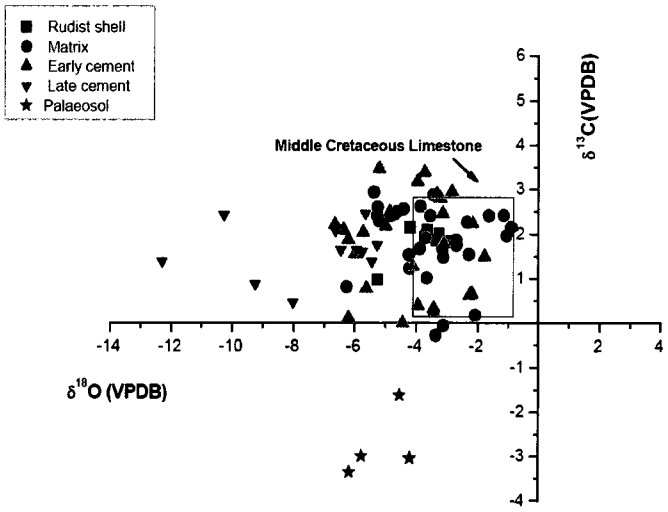

Figure 2.9 Carbon and oxygen isotopic composition of carbonate components of the Upper Sarvak Formation in the study area.

Table-2.1 Carbon and oxygen isotopic composition of the calcitic components of the Upper Sarvak Formation.

Sample No.	Mineralogy	$\delta^{13}C_{VPDB}$ (‰)	$\delta^{18}O_{VPDB}$ (‰)	Component Type
8952- SHELL	Calcite	**2.1**	**-3.6**	Rudist Shell
91-SHELL	Calcite	**2.0**	**-3.7**	Rudist Shell
92-SHELL	Calcite	**1.9**	**-3.3**	Rudist Shell
98-SHELL	Calcite	**1.8**	**-3.0**	Rudist Shell
BH-101	Calcite	**1.0**	**-5.3**	Rudist Shell
BH104-3-M	Calcite	**1.9**	**-3.7**	Rudist Shell
BH104-4-M	Calcite	**2.0**	**-3.3**	Rudist Shell
BH-4	Calcite	**2.1**	**-4.2**	Rudist Shell
SE-21	Calcite	**-3.0**	**-4.2**	Palaeosol
SE-22	Calcite	**-1.6**	**-4.5**	Palaeosol
SK-1	Calcite	**-3.5**	**-6.2**	Palaeosol
SK-2	Calcite	**-3.0**	**-5.8**	Palaeosol
2525-M	Calcite	**2.9**	**-3.4**	Matrix
2517-M	Calcite	**2.4**	**-5.3**	Matrix
BH-6-M	Calcite	**1.5**	**-4.2**	Matrix
BH-3-M	Calcite	**2.6**	**-5.3**	Matrix
BH-2-M	Calcite	**2.4**	**-4.8**	Matrix
BH-12-M	Calcite	**2.5**	**-4.6**	Matrix
BH107-M	Calcite	**0.8**	**-6.3**	Matrix
BH106-M	Calcite	**2.9**	**-5.4**	Matrix
BH104-M	Calcite	**2.3**	**-5.2**	Matrix
BH-0-M	Calcite	**2.6**	**-4.4**	Matrix
9211.5-M	Calcite	**1.2**	**-4.2**	Matrix
8961-M	Calcite	**1.9**	**-3.7**	Matrix
8943-M	Calcite	**1.5**	**-3.1**	Matrix
8700-M	Calcite	**1.0**	**-3.7**	Matrix
8688-M	Calcite	**1.7**	**-3.1**	Matrix
8686-M	Calcite	**1.9**	**-2.7**	Matrix
166-M	Calcite	**-0.3**	**-3.4**	Matrix
165M	Calcite	**0.2**	**-2.1**	Matrix
164-M	Calcite	**1.5**	**-2.3**	Matrix
162-M	Calcite	**1.7**	**-3.9**	Matrix
161-M	Calcite	**2.0**	**-2.4**	Matrix
159-M	Calcite	**1.7**	**-2.7**	Matrix
151-M	Calcite	**-0.1**	**-3.1**	Matrix
150-M	Calcite	**2.0**	**-1.0**	Matrix
143-M	Calcite	**2.1**	**-0.9**	Matrix
139-M	Calcite	**2.4**	**-1.6**	Matrix
129-M	Calcite	**2.4**	**-3.5**	Matrix

Table 2.1 (Continued)

128-M	Calcite	**2.6**	**-3.9**	Matrix
120-M	Calcite	**2.4**	**-1.1**	Matrix
2517-C	Calcite	**2.4**	**-4.8**	Early Cement
BH-4-C1	Calcite	**1.9**	**-6.2**	Early Cement
BH104-5	Calcite	**2.0**	**-5.7**	Early Cement
BH101-1	Calcite	**1.3**	**-4.1**	Early Cement
BH-0-1	Calcite	**2.2**	**-6.6**	Early Cement
9211.5-C	Calcite	**2.2**	**-2.2**	Early Cement
8961-C	Calcite	**2.2**	**-4.0**	Early Cement
8943.8-C1	Calcite	**0.4**	**-3.9**	Early Cement
8943-C1	Calcite	**0.2**	**-3.4**	Early Cement
8688-C	Calcite	**0.3**	**-3.4**	Early Cement
166-C	Calcite	**0.1**	**-6.2**	Early Cement
165-C	Calcite	**0.0**	**-4.4**	Early Cement
160-C	Calcite	**1.5**	**-1.8**	Early Cement
159-C	Calcite	**3.2**	**-3.9**	Early Cement
158-C	Calcite	**3.4**	**-3.7**	Early Cement
155-C	Calcite	**0.6**	**-2.2**	Early Cement
153-C	Calcite	**0.7**	**-2.2**	Early Cement
147-C	Calcite	**1.8**	**-3.1**	Early Cement
143-C	Calcite	**2.8**	**-3.2**	Early Cement
140-C	Calcite	**2.9**	**-2.8**	Early Cement
129-C	Calcite	**2.9**	**-3.3**	Early Cement
128-C	Calcite	**3.5**	**-5.2**	Early Cement
120-C	Calcite	**2.5**	**-3.1**	Early Cement
8688-C3	Calcite	**1.6**	**-4.5**	Late Cement
8951-C2	Calcite	**1.6**	**-5.8**	Late Cement
8952-C2	Calcite	**1.4**	**-5.4**	Late Cement
BH104-C3	Calcite	**1.6**	**-5.9**	Late Cement
BH2-C2	Calcite	**2.5**	**-5.6**	Late Cement
BH4-C2 R	Calcite	**2.1**	**-6.6**	Late Cement
165-C2	Calcite	**0.5**	**-8.0**	Late Cement
BH106-C2	Calcite	**2.4**	**-10.3**	Late Cement
BH106-CR	Calcite	**0.8**	**-9.3**	Late Cement
BH106-C	Calcite	**1.4**	**-12.3**	Late Cement
BH104-C2	Calcite	**1.5**	**-5.3**	Late Cement

Chapter 3

Chemostratigraphy of Mid-Cretaceous Carbonates in the Tethyan Region: an Example from the Sarvak Formation in Southern Iran

3.1. Introduction

Regional unconformities are commonly used to separate stratigraphic units (Sloss 1963, 1988). The recognition of unconformities and subaerial exposure surfaces in carbonate platforms can help to refine the diagenetic framework (e.g. Saller et al., 1994; Flugel, 2004). However, the identification of palaeoexposure surfaces is not always straightforward.

The Cenomanian-Turonian Sarvak Formation in southern Iran is poorly documented. Based on field investigations and well log data, previous researchers considered the Sarvak carbonates to form a continuous succession with only one major break occurring at the top of the formation (e.g. Pattison and Takin, 1971; Setudehnia, 1978). However recent investigations have indicated the occurrence of two unconformities (Beiranvand et al., 2007; Taghavi et al., 2006; Hajikazemi et al., 2010). Furthermore, base on palaeontological data (Ghabeishavi et al., 2010) the apparent depositional continuity of the succession has been questioned, suggesting the presence of a "gap" prior mid-Cenomanian time. Using paleontological evidence, at the type section locality, the formation has been divided into early-mid and late Cenomanin (Ghabeishavi, 2009).

The Cenomanian-Turonian time interval in southern Iran is poorly understood. In some areas such as Lurestan, Cenomanian-Turonian sediments are pelagic. Shallow-marine carbonates dominate other areas, including the study locations.

Substantial erosion of the Sarvak carbonates took place after regional exposure during the Turonian (Moteie, 1993; Ghazban, 2007). This resulted in the removal of the upper part of the formation in many areas. Locally, older unconformity surface within the formation were also removed (Motiei, 1993).

The regional Turonian unconformity and the consequence palaeoexposure surface at the top of the Sarvak Formation which is recognized by brecciation, karstification and lateritization

appear to be responsible for the creation and enhancement of favourable reservoir characteristics. The Upper Sarvak Formation was affected by a major unconformity reported in several localities in southern Iran and elsewhere in the region (James and Wynd, 1965; Harris et al., 1984; Setudehnia, 1978; Beiranvand et al., 2007; Taghavi et al., 2006; Hajikazemi et al., 2010). Other sedimentary gaps or breaks may similarly have affected the carbonates elsewhere in the formation. Therefore, it is important to investigate the possible occurrence of breaks within the succession, as well as the presence and regional distribution of the upper Cenomanian (post-Cenomanian) unconformity.

Stable carbon isotopes and $^{87}Sr/^{86}Sr$ stratigraphy have been used for high-resolution global correlation in carbonate sequences (e.g. McArthur et al., 2001; Tsikos et al., 2004). These methods are valuable for shallow-water carbonate sequences where there is often inadequate palaeontological information for dating and correlation. These methods are effective particularly when secular variations of isotope data occur. This is demonstrated when $^{87}Sr/^{86}Sr$ ratios are integrated with $\delta^{18}O$, $\delta^{13}C$ and Sr concentration data and petrographic observations.

The Diagenetic effects of the palaeoexposure surfaces are restricted mainly to the Upper Sarvak Formation. Hence the present work focuses on the upper part of the Sarvak Formation in SW Iran (see Fig. 3.1 for locations).This interval records the diagenetic effects associated with Cenomanian-Turonian exposure and also the global isotopic events associated with Cenomanian-Turonian time interval.

Biostratigraphic resolution in Cenomanian-Turonian interval is extremely coarse in the region. In addition, in shallow-water carbonates such as the Upper Sarvak, the record of sea-level changes is often severely limited by the low-stratigraphic resolution attained by the classical methods of biostratigraphy (Jenkins et al., 1994). However, this stratigraphic interval is particularly favorable for chemostratigraphy technique which is applied here. The objectives of this paper are (1) to investigate temporal and spatial variations and changes in geochemical characteristics within the succession, including stable carbon and oxygen isotopes, and Mn and Sr concentrations in conjunction with strontium isotope ($^{87}Sr/^{86}Sr$) data; and (2) to identify palaeoexposure surfaces and to evaluate the application of geochemical signatures as stratigraphic markers for local, regional and global correlation.

3.2. Regional Geological Setting

The Cenomanian-Turonian sedimentary succession that includes the Sarvak Formation was dominated by widespread carbonate accumulation with an extensive development of carbonate platforms with rudist-foraminifera reef rimmed shelves (Motiei, 1993; Hajikazemi et al., 2010). Many of the major hydrocarbon accumulations are found in the Mid-Cretaceous reservoir rocks, which developed as the carbonate platforms evolved.

Emergence of the Sarvak carbonates due to relative sea-level drop, local salt tectonics and uplift caused large areas of the carbonate succession to be subaerially exposed, resulting in profound changes such as the development of vuggy and cavernous porosity within the system, which contributed to elevated rates of additional karst formation (Hajikazemi et al., 2010).

Sedimentation rates varied considerably. The rate was low in the NE of the Persian Gulf, but rapid accumulation of a thick succession occurred in some places like the type section of the Sarvak Formation at the Bangestan Mountains (Hajikazemi et al., 2010). Salt diapirs and basement structures formed palaeo-highs during the Mid-Cretaceous. This influenced patterns of deposition by localizing high-energy grainstones and rudist reefs, and also resulted in the generation of local intraformational unconformities (Burchette and Britton, 1985; Videtich et al., 1988; Hajikazemi et al., 2010).The Sarvak Formation (Cenomanian-Turonian) has a thickness of about 800 m at the type locality in Bangestan Mountain. It conformably overlies the shales of the Kazhdumi Formation with a transitional contact while the upper contact, consists of marls of the Gurpi Formation of Maestrichtian age (Motiei, 1993).

The lower part of the Formation, with a thickness of about 255 m, consists of argillaceous limestones with lenticular bedding and thin-layered marl interbeds. The middle part is about 525 m in thickness, consists of massive chalky limestones with iron-rich siliceous nodules and rudist fragments. The top 42 m of the Formation consists of massive limestone with the topmost strata consisting of a weathered brecciated ferruginous limestone. In some areas (i.e. Persian Gulf) this formation includes Ahmadi member which is composed of shale/marl. An unconformity occurs at the top of the Formation marks the boundary between the Sarvak and the overlying strata.

The late Cenomanian was marked by the initiation of tectonic activity and major continental collision in the region, leading to the closure of the Neo-Tethys Ocean. As a result, the carbonate platform began to undergo tectonic movements by the late Turonian (88 Ma) and

regional uplift caused truncation of the upper part of the Turonian carbonates and locally over the complete Turonian succession (Berberian and King, 1980).

3.3. Regional and Local Unconformities

Regional uplift and sea-level fall in Turonian caused a major unconformity marked by conglomerates, breccias, karstification and haematite nodules (Setudehnia, 1978; Ghazban, 2007; Hajikazemi et al., 2010).The Upper Sarvak was eroded during the Turonian and the channel-like features developed on top of the Sarvak Formation have been attributed to the Turonian unconformity observed close to Bangestan Mountain (Farzadi and Alaei, 2006). This unconformity has also been reported elsewhere in the Persian Gulf region (Harris et al., 1984; Van Buchem et al., 2002)

In southern Iran, erosional surfaces in Mid-Cretaceous rocks have been recognized and mapped over long distances. Based on oil company reports and previous publications (e.g. Beiranvand et al., 2007) two principal unconformities have been identified: (i) the Turonian unconformity which occurs throughout the southern Iran and Persian Gulf; and (ii) a more local Cenomanian-Turonian boundary break in the area which is reported in some local studies of wells or surface sections but has not been mapped in the area in the previous works.

The Turonian unconformity occurs at the top of the Sarvak Formation and equivalent units (Aqrawi et al., 1998; van Buchem et al., 2002.) (Fig.3.2a). Hajikazemi et al. (2002, 2010) demonstrated that diagenetic features (i.e. dissolution, cementation, etc.) and their spatial distribution in the Upper Sarvak Formation are related to the presence of the Turonian unconformity and associated karstification. This unconformity influenced the development of porosity in the Upper Sarvak Formation in the region. Farzadi and Hesthmer (2007), using seismic reflection data, provided a regional framework for the Turonian unconformity by integrating 3D geophysical and well-log data from the Sirri oilfields.

Alsouki et al. (2008) showed that the Turonian unconformity on seismic profiles is overlain by shales of the Laffan Formation, and is subcropped by the Sarvak Formation limestones near the Strait of Hormoz. Although the unconformity is a strong seismic reflector, the presence of multiples makes its interpretation difficult, especially below structural highs.

The presence of an underlying (Cenomanian-Turonian) unconformity of more local extent has not previously been well documented; although Keyvani and Heydari (2002) attributed

diagenetic alterations to Cenomanian-Turonian unconformity and Beiranvand et al. (2007) classified flow units in the Upper Sarvak Formation with reference to an unconformity of this age. Therefore, an unconformity forms a boundary between Upper Cenomanian–Turonian succession and the overlying deep-marine Coniacian Laffan shales or Coniacian-Santonian Gurpi Marls.Due to the magnitude of the Turonian unconformity, the underlying Cenomanian-Turonian unconformity may locally have been removed, and as a result, the two unconformities can be difficult to distinguish. In some locations, such as Shahneshin Mountain however, both unconformity surfaces are present and show cross-cutting relationships with evidence of deep erosion and significant truncation (Fig. 3.2b)

Evidence of two unconformities was recorded on top of the Sarvak Formation in a road cutting across the Navdan anticline in Shahneshin Mountain (north of the city of Shiraz: Fig. 1). Erosional surfaces in the Shanheshin Mountain were examined during the course of this investigation. At this locality, a conformable fluvial bed with an average thickness of about 20 cm and a palaeosol horizon devoid of organics overlies Upper Sarvak carbonates (Fig.3.2c). The surfaces show pedogenic features such as Fe-Mn nodules which occur below the discontinuity surface and rest on a karstified horizon (Fig. 3. 2d). Fe-staining of underlying strata due to pedogenesis also occurs.

3.4. Material and Methods

Surface and subsurface sections of the Sarvak Formation were examined in south and SW Iran and samples were collected systematically along continuous profiles. A total of 360 samples were collected from the formation at its type section locality in the Bangestan Mountains, from well-exposed outcrops in the Shahneshin Mountains and from four wells in the Rag-e Sefid, Bibi Hakimeh and Sirri oilfields where there was good collection of cores of the Upper Sarvak available (see Fig.1 for locations). Hand specimens from type section (Bangestan Mountain) were collected approximately every 1-2 m through the uppermost part of the Sarvak Formation and every 3-5 m elsewhere.

The Shahneshin Mountain was chosen for extensive sampling due to field evidences such as recognizable and well exposed paleoexposure surfaces, bauxite horizon, presence of fluvial channel, and paleosol. The outcrop samples were taken every 1 m from the Upper Sarvak at Shahneshin Mountain with respect to the well exposed subaerial exposure surface. Samples taken from the Bangestan type section profile were analyzed for stable isotopes and treated as a reference section.

Core samples were restricted to the upper part of the formation, which contains the main reservoir units. Slabs were taken from split core samples in 0.5 m intervals where available. However, core recovery was below 20% in some intervals.

Thin sections were stained with Alizarin Red-S and potassium ferricyanide and analyzed under transmitted light. Cathodoluminescence microscopy of 138 representative carbonate samples was carried out using a Technosyn 8200 MKII model cold cathodoluminescence stage with a 12-15 kv beam and a current intensity of 420-430μA on the unstained halves of the uncovered thin sections.

Elemental data were obtained using an ICP-MS apparatus at the University of Windsor. A total of 58 samples of calcite matrix and rudist shells were analyzed for their Sr and Mn concentrations. Each sample was weighed, reacted with 1% HNO3 acid, and then diluted with about 50 grams of laboratory internal standard with a dilution factor about 50. Calibration of the ICP-MS was achieved using reference materials and a procedural blank, selected to cover the range of elemental concentrations expected in the samples. Precision (described by relative standard deviation: RSD) was 5%, and accuracy (described by relative difference to the USGS standard) was 0.25%.Surface and subsurface sections were examined and samples were collected systematically along continuous profiles in south and southwestern Iran. A total of 360 samples were collected from the Sarvak Formation at its type section locality in the Bangestan Mountain, well-exposed outcrops of the Upper Sarvak Formation in the Shahneshin and from four wells drilled through the Sarvak Formation in the Rag-e Sefid, Bibi Hakimeh and Sirri-D oilfields (see Fig. 3.1 for locations). Hand-specimens were collected approximately every 1-2 m through the uppermost part of the Sarvak Formation and 3-5 m through the rest of the section.

Limited subsurface core samples were available, which prevented systematic and extensive sampling from some wells. Core samples were restricted to the upper part of the formation, which contains the main reservoirs. However, in some intervals the core recovery was below 20%. Due to the lack of production from the lower part of the formation this part was not cored. Core samples were taken every 0.5 m where ever they were available.

Petrographic thin sections were stained with Alizarin red-S and potassium ferricyanide and carefully analyzed by standard optical transmitted light. Cathodoluminescence (CL) microscopy of 138 representative carbonate samples was carried out using a Technosyn 8200

MKII model cold cathodoluminescence stage with a 12-15 kv beam and a current intensity of 420-430 μA on the unstained halves of the uncovered thin sections.

Elemental data were obtained using an ICP-MS at Great Lake Environmental Institute for Environmental Research at the University of Windsor. A total of fifty eight samples of calcite matrix and rudist shells were analyzed for their Sr and Mn concentrations. Each sample was weighed, reacted with 1% HNO_3 acid, and then diluted with about 50 grams of laboratory internal standard with a dilution factor about 50. Calibration of the ICP-MS was achieved using well characterized rock reference materials and a procedural blank, selected to cover the range of elemental concentrations expected in the samples. Precision (described by relative standard deviation RSD) is at the range of 5%, and accuracy (described by relative difference to the recommended value, U.S.G.S recommended, 1998) is at the range of 0.25%.

Some 161 samples of the least altered carbonate matrix (i.e. micrite) and rudist shells were micro-sampled using a microscope-mounted dental drill assembly. Extracted powders were reacted with 100% phosphoric acid at 25°C for 4 hours (Al-Aasm et al., 1990). The evolved CO_2 gas was analyzed for oxygen and carbon isotopic ratios using a Finnigan Mat Delta Plus mass spectrometer at the University of Windsor. All analyses for oxygen and carbon isotopes are reported in per mil (‰) notation relative to the Vienna Pee Dee Belemnite (VPDB) international standard. Precision for both isotope delta values was better than 0.05‰.

In addition, 54 samples of carbonate matrix and rudist shells were analyzed for strontium isotopes on a Finnigan MAT 262 with five fixed collectors. NBS-87 and ocean water were used as standard references, and $^{87}Sr/^{86}Sr$ ratios were normalized to $^{88}Sr/^{86}Sr = 8.375209$. Precision for $^{87}Sr/^{86}Sr$ ratios was better than 0.000010.

3.5. Textural and Chemical Preservation of the Sarvak Carbonates

In chemostratigraphic studies, the degree of chemical and textural preservation of the samples analyzed is critical. Thus, an important step was to carefully select samples whose textures and original chemical compositions were most likely preserved. Previous researchers (e.g. Veizer, 1983) have applied co-variation trends in elemental and stable isotope systematics in conjunction with petrographic methods (e.g. cathodoluminescence and SEM) to identify the least-altered carbonates. These approaches were followed to investigate the preservation and alteration of the samples, the goal being to use the preserved carbonate chemistry for correlation and chemostratigraphy.

Previous investigations (e.g. Al-Aasm and Veizer, 1986a and b; Steuber, 1996, 2001, 2003; Immenhauser et al., 2005; Frijia and Parente, 2008), have shown low-Mg calcite shell layers in rudists to have a high potential to preserve their original chemical compositions. Petrographic examinations suggest that the rudist shells in the studied samples are relatively well preserved and show no evidence of diagenetic alteration (Fig. 3.3).Further evidence of good preservation is that most of the rudist shell samples analyzed had $\delta^{18}O$ values similar to those expected from precipitation in equilibrium with Mid-Cretaceous seawater (see Table 3.2 and Fig. 3.6 for values). Rudists collected from the surface sections were compared geochemically with those sampled from cores at depths ranging from 2 to 3.5 km. The rudists had similar petrographic and geochemical signatures and were therefore used as an internal reference for the original marine geochemical signature.

The degree of alteration of calcite matrix was also examined using optical and CL petrography and SEM observations in conjunction with trace element and stable isotope analyses. Most samples of calcite matrix showed no sign of diagenetic alteration. In addition, they displayed constant geochemical values.

According to previous investigations (e.g., Al-Aasm and Veizer, 1986a and b; Steuber, 1996, 2001, 2003; Immenhauser et al., 2005; Frijia and Parente, 2008), low-Mg calcite shell layers in rudists have great potential to preserve their original chemical compositions. Petrographic examinations suggest that most of the rudist shell layers in the studied samples are relatively preserved and show no evidence of diagenetic alteration in the portions which have been sampled (Fig. 3.3).

Evidence of good preservation is that most of the rudist shell samples analyzed in this investigation have $\delta^{18}O$ values similar to those expected from precipitation in equilibrium with Mid-Cretaceous seawater (see Table 3.2 and Fig. 3.6). In addition, rudists collected from the surface sections and those sampled from cores at different depths ranging from 2 to 3.5 km in subsurface sections were compared geochemically in order to determine their preservation or alteration. Most of the rudist display similar petrographic and geochemical signatures and therefore can be used as an internal reference for original marine geochemical signature.

We also examined the degree of the alteration of calcitic matrix, using optical and CL petrography and SEM observations in conjunction with trace element and stable isotope analysis.

Most of the measured samples from calcitic matrix show no appreciable sign of diagenetic alteration. In addition they display constant geochemical values.

3.6. Results

The concentrations of Sr and Mn, and carbon, oxygen and strontium stable isotope ratios were determined for samples of carbonate matrix (micrite), rudist shells and carbonate fraction of the palaeosols from the Sarvak Formation. The results are presented in Tables 3.1 and 3.2.

3.6.1. Manganese and Strontium

Mn concentrations in most of the Sarvak carbonates (matrix and rudist shells) range from 2 to 38 ppm. These values fall within the range of calcite precipitated at equilibrium with sea water, and also of modern marine carbonates (i.e. <50 ppm as reported by Veizer, 1983a). Two samples collected from below the Turonian unconformity surface at the Shahneshin Mountain locality, where Fe-Mn nodules are present, show Mn concentration of about 170 ppm (Table 3.1).

Figure 3.4 shows the Mn concentration in a profile of the Sarvak Formation at the type section in the Bangestan Mountains. Al-Aasm and Veizer (1982) used trace element compositions to identify well-preserved brachiopod material, and considered that samples with Mn contents higher than 70 ppm were altered. Using their criteria, the Mn values obtained from matrix and rudist shells indicate that the Sarvak Formation at this location appears not to be altered (Tables 3.1 and 3.2). The peaks and troughs could signify the minor changes in the environmental conditions affecting the input of Mn into the carbonates. Strontium concentrations range from 15 to 1336 ppm, with a mean of 353 ppm. Most Sr values fall within the range of Sr concentration driven from unaltered Cretaceous marine calcite which has an average value of 320 ppm (Veizer, 1977).

Sr concentrations are fairly uniform in matrix samples along a vertical profile from the Upper Sarvak Formation, although values are higher in argillaceous limestones of the Lower Sarvak Formation. Samples from the unconformity surface and other sedimentary breaks or palaeoexposure surfaces in the Upper Sarvak Formation of the Bangestan section have the lowest concentrations compared to the rest of the section (Fig. 3.5). Similar low values were measured in samples from the uppermost part of the Sarvak Formation at Shahneshin and Rag-e Sefid-A, which are approximately 200 km apart.

3.6.2. Stable Carbon and Oxygen Isotopes

The $\delta^{13}C$ values of the carbonate matrix from surface sections and core samples of the Sarvak Formation range from -6.4 ‰ to +4.1‰ (VPDB) and $\delta^{18}O$ values range from -9.4‰ to -0.9‰ (VPDB). The $\delta^{13}C$ and $\delta^{18}O$ values of palaeosol samples collected from the uppermost part of the formation at Shahneshin Mountain range from -9.0 to -3.0‰ and from -6.2 to - 4.0 ‰, respectively (Tables 3.1, 3.2). Figure 3.6 shows the majority of the $\delta^{13}C$ and $\delta^{18}O$ values of carbonate matrix analyzed fall within the range of Mid-Cretaceous marine carbonates plotted by Veizer et al. (1999) and the data from rudist shells of the Tethyan region from Immenhauser et al. (2005). The only exceptions are the samples taken immediately at or below the unconformity surfaces which show depleted carbon and oxygen isotope values.

$\delta^{13}C$ and $\delta^{18}O$ profiles were constructed for the entire Sarvak Formation along a stratigraphic column at the relatively complete type section in Bangestan Mountain (Fig. 3.7a), and at the Rag-e Sefid A and Bibi Hakimeh subsurface sections. The successions in the subsurface sections were identified as Upper Sarvak based on oil company paleontological reports. The Upper Sarvak Formation was sampled from outcrops in Shahneshin Mountain where the sampling was performed with respect to the subaerial exposure surface. In all profiles, there is a positive shift in $\delta^{13}C$ values within the strata with values of between +3.3 and +4.1 ‰ (Fig. 3.7b).

Depth profiles of $\delta^{13}C$ and $\delta^{18}O$ values show distinct peaks with some minor variations. In addition to the negative $\delta^{13}C$ and $\delta^{18}O$ values measured at the unconformity surface(s) in the uppermost part of the section, other negative excursions show simultaneous decreasing values of $\delta^{13}C$ and $\delta^{18}O$ corresponding to palaeoexposure surfaces or might reflect the sequence boundaries (SB), which are referred to previously in oil company reports and by Ghabeishvi (2010) and the rest might be the sequence boundaries of parasequences (Fig. 3.7a). Distinct negative peaks identified along the Bangestan section occur at 220 m, 456 m, 545 m and 745 m. Positive values occur at 450 m ($\delta^{13}C$ = 3.3 ‰; $\delta^{18}O$ = -5.2‰).

3.6.3. Strontium Isotope Analysis

Strontium isotope ratios ($^{87}Sr/^{86}Sr$) were obtained for 54 samples taken from the Sarvak Formation at the type section and from the studied wells. $^{87}Sr/^{86}Sr$ ratios range from 0.70728 to 0.70878 for matrix and 0.70736 - 0.70749 for rudist shells (Tables 3.1 and 3.2).

A plot of Sr ratio versus oxygen isotope composition (Fig. 3.8a) showed no particular trends or variations in the Sarvak carbonates over the stratigraphic interval studied, indicating that the samples have not been significantly affected by meteoric diagenetic alteration (c.f. Derry et al., 1994) because in the case of meteoric diagenesis alteration the samples with the most negative $\delta^{18}O$ values should show the highest $^{87}Sr/^{86}Sr$ ratios.

$^{87}Sr/^{86}Sr$ ratios of micrite samples from the Bangestan section are plotted versus stratigraphic height in Fig. 8a. $^{87}Sr/^{86}Sr$ values from Bangestan Mountain samples can be divided into three groups. The $^{87}Sr/^{86}Sr$ ratios for argillaceous pelagic limestones in the lower 300 m of the Bangestan section, which correspond to the Lower Sarvak Formation, have values of 0.70740 - 0.70745. At about 362 m, there is a sharp increase in the $^{87}Sr/^{86}Sr$ ratio (i.e. 0.70784). Above this point, $^{87}Sr/^{86}Sr$ ratios remain within the range of the Mid-Cretaceous values. A profile of $^{87}Sr/^{86}Sr$ in the Mid-Cretaceous strata could help in identification of this major gaps and hiatus in the succession. An anomalously high $^{87}Sr/^{86}Sr$ value was measured (0.70878) at the top of the formation at Bangestan (Fig. 3.8b). Similar high values were also obtained from carbonate matrix below the Turonian unconformity surface at Rag-e-Sefid-A ($^{87}Sr/^{86}Sr$ = 0.70832), Bibi Hakimeh ($^{87}Sr/^{86}Sr$ = 0.70786) and Sirri-D ($^{87}Sr/^{86}Sr$ = 0.70776) (Fig. 3.8c). These higher isotopic values are good indications of diagenetic alteration at the unconformity surface. By contrast, the majority of the measured $^{87}Sr/^{86}Sr$ ratios show little variation over most of the sections and fall within the values that characterize Cenomanian-Turonian marine carbonates (0.70720 to 0.70750: Burke et al., 1982; McArthur et al., 2001).

The values from surface and subsurface samples plotted on the Cenomanian-Turonian portion of the secular seawater curve of Burke et al. (1982) (Fig. 3.8d). This plot shows the majority of the obtained values fallow the Cenomanian portion of the curve.

3.7. Discussion

Stable carbon isotopes and $^{87}Sr/^{86}Sr$ stratigraphy have been used as powerful chronostratigraphic tools for high-resolution global correlation in carbonate sequences by many researchers and oil companies (e.g. McArthur et al., 2001; Tsikos et al., 2004). These geochemical methods are very valuable especially for shallow-water carbonate sequences where there is normally inadequate palaeontological information for dating and correlation. Such methods are effective particularly when secular variations of isotope data occur and retention of these data is confirmed. This is demonstrated when $^{87}Sr/^{86}Sr$ data are integrated with $\delta^{18}O$, $\delta^{13}C$,

Sr concentration data and petrographic observations. In general, diagenetically altered intervals have higher $^{87}Sr/^{86}Sr$ values, low $\delta^{13}C$ and $\delta^{18}O$ values relative to adjacent intervals, a combination that is consistent with open-system meteoric diagenesis (Banner, 2004).

3.7.1. Strontium Concentrations

Meteoric waters generally have low Sr concentrations, and carbonates in equilibrium with these waters will have low Sr contents (Morse and Mackenzie, 1990). Moreover, there is often a negative covariance between Mn and Sr in carbonates exposed to meteoric diagenesis (Veizer, 1983). Flushing of the carbonate sediments by meteoric waters may lead to significant loss of Sr (Land and Epstein, 1970). Mn may be incorporated during diagenetic alteration and modification by meteoric waters, whereas Sr may be expelled from the carbonates (Brand and Veizer, 1980; Veizer, 1983). Therefore, the influence of meteoric water on low-Mg calcite may decrease the Sr content and increase the Mn content. Considering the lower Sr concentrations in samples from the uppermost part of the sections and close proximity to the exposure surface, it appears that the uppermost part of the formation has been subjected to surface diagenetic alteration. The depletion in Sr concentrations observed here correlates well with the depletion in $\delta^{13}C$ and $\delta^{18}O$ values (see below) and slight increase in Mn concentrations. The depletion of Sr concentrations in other parts of the stratigraphic column (i.e. 480 m in Fig. 3.5) could also indicate the influence of meteoric water due to presence of a palaeo-exposure.

3.7.2. Mn stratigraphy

Mn is a redox-sensitive element which can be solubilized under reducing conditions while forming insoluble oxides in contact with oxygenated sediments (Calvert and Pedersen, 1993). Mn is generally present in low concentrations in marine carbonates (Arthur et al., 1988). Thus, if carbonate precipitation and/or recrystallization occur in anoxic conditions, then high values of Mn may occur in carbonates. In the case of Sarvak limestones, the relatively low values of Mn could be due to a lack of Mn in the depositional environment.

During early Cenomanian, Mn could have been incorporated into the shales of the Ahmadi member or other shale intervals in the Sarvak Formation, resulting in depletion of Mn in mid Cenomanian-Turonian carbonates. Because Mn precipitates in oxic conditions, low concentrations of Mn in water reflect removal of dissolved Mn onto particle surfaces (Frakes and Bolton, 1984; Dickens and Owen, 1993). These processes could have been responsible for the depletion of the sea water with respect to Mn. The low Mn values (< 10 ppm) recorded in matrix

and rudist shells of the Upper Sarvak carbonates are consistent with carbonate precipitation from Mn-depleted sea water. The Mn concentrations are similar to values given by Immenhauser et al. (2005) and Firijia and Parente (2008) for marine carbonates of similar age.

Diagenetic alteration can cause an increase in Mn concentrations in low-Mg calcite (Marshall, 1992). Mn concentrations increase with intensity of diagenesis and in proximity to an unconformity surface. At the Bangestan section, there is a slight increase in Mn content towards the unconformity surface (s). This is evident from the high concentrations of Mn in the samples taken from unconformity surface (i.e. 170 ppm) and the Fe-Mn nodules and concretions in the uppermost part of the Sarvak Formation.

3.7.3. Carbon and Oxygen Stratigraphy

A well-known feature of the carbon-isotope curve is the positive $\delta^{13}C$ excursion and the Cenomanian–Turonian Boundary Event (CTBE; see Jarvis et al., 2006 for a review), which is inferred to represent a geochemical expression of Oceanic Anoxic Event 2 (OAE2). OAE 2 and the associated carbon isotope excursion have been described from numerous sections and cores (e.g. Arthur et al., 1988; Tsikos et al., 2004; Erbacher et al., 2005).

The $\delta^{13}C$ profiles in this study display significant Cenomanian-Turonian events, which can be correlated throughout the study area. The data presented here can be partially correlated with the global Cenomanian-Turonian $\delta^{13}C$ curve (Jenkyns et al., 1994). The reference curves of $\delta^{13}C$ show several well-defined events that have been already successfully used for global correlations (Jenkyns, 1985).

Superimposing our data on the Cenomanian-Turonian $\delta^{13}C$ seawater curve of Voigt et al. (2000) shows that there is very good correlation with the Cenomanian portion of the curve up to the Cenomanian/Turonian boundary event spike (Fig. 3.9). However, the well-documented Cenomanian-Turonian boundary event, which corresponds to OAE2 or the Bonarelli Event of Schlanger et al. (1987) and Arthur et al. (1988), is missing from the Bangestan data. The absence of the positive $\delta^{13}C$ excursion (CTBE) in the Upper Sarvak Formation indicates that this part of the succession has been erosively removed or that there was a hiatus in sedimentation.

The depleted $\delta^{13}C$ values obtained from the topmost Cenomanian strata in the Bangestan section confirm subaerial exposure and consequent erosion or a gap in sedimentation.

Detailed field and geochemical investigation at Shahneshin Mountain show the presence of the Cenomanian-Turonian Boundary (CTB) unconformity and /or sedimentary break (Hajikazemi et al., 2010). The lower subaerial exposure surface presented in this section may represent the Cenomanian-Turonian unconformity.

Prior to OAE2 in the mid Cenomanian a short-term anoxic event (Mid Cenomanian Event) occurred and is characterized by a positive excursion in the $\delta^{13}C$ profile although $\delta^{13}C$ values are smaller in magnitude than those expected from the Cenomanian-Turonian Boundary unconformity (see Ernst et al., 1983; Paul et al., 1994; Voigt, 2000; Jarvis et al., 2006). This event is associated with a pair of closely-spaced, positive $\delta^{13}C$ excursions at the base of the mid Cenomanian (Jenkyns et al., 1994). There is no widespread deposition of organic-rich sediments linked with the positive excursions of $\delta^{13}C$ during the Mid Cenomanian Event and in addition the records of $\delta^{13}C$ excursions from oceanic settings are rare (Jenkyns et al., 1994; Huber et al., 2002).

The isotope profiles of the Sarvak Formation sections (Fig. 3.7b) show the same positive $\delta^{13}C$ excursions with values between +3.3 and +4.1‰ in three different sections. These isotope peaks that show the most positive $\delta^{13}C$ values coincide closely with the positive $\delta^{13}C$ excursion of the Mid Cenomanian Event. This is evidence of the occurrence of the Mid Cenomanian Event in the study region, as observed elsewhere (e.g., Cenomanian chalks in England: Jarvis, 2006).

The widespread occurrence of the Mid Cenomanian Event (MCE) in the western Tethyan realm and elsewhere implies a geographically extensive event (Friedrich et al., 2009). Our investigations indicate further extension of this event and occurrence of the MCE in southern Iran.

The MCE excursion in $\delta^{13}C$ can be correlated in the Sarvak type section locality at Bangestan Mountain and two other subsurface sections from wells (see Fig. 3.7). Therefore, the co-occurrence and co-variation of $\delta^{13}C$ in different sections suggests that our $\delta^{13}C$ values could reflect the ancient sea water signals.

It is important to note that in the Tethyan region the sedimentary environments before the MCE were relatively highly oxygenated while above that oxygen-depletion occured (Friedrich et al., 2009). This is also indicated by relatively higher concentration of Mn in the intervals below the MCE (below 460 m) in our records from the Lower Cenomanian (Fig. 3.4). This general trend

toward lower oxygenation of bottom waters above the MCE was accompanied by climate warming in combination with rising sea-level and the development of vast shallow epicontinental seas during the Mid to late Cenomanian (Friedrich et al., 2009).

The $\delta^{18}O$ values of the micritic matrix analyzed show a significant range from -0.89 to -9.4‰ VPDB. Considering the stratigraphic column in the region which includes about 3 km of sediments above the Sarvak Formation, this formation has been buried to a minimum depth of about 3 km. As a result, some of the $\delta^{18}O$-depleted matrix could be attributed to diagenetic modification. In contrast to $\delta^{18}O$, $\delta^{13}C$ values are less affected by diagenetic processes because pore waters have low concentration of carbon (Brand and Veizer, 1980). Thus, $\delta^{13}C$ values should not be significantly modified by diagenetic alteration. The only exceptions are samples taken from palaeoexposure surfaces and few metres below them which are highly influenced by atmospheric CO_2 and pedogenic depleted $\delta^{13}C$.

The most depleted $\delta^{18}O$ values coincide with the most depleted carbon values at or below palaeoexposure surfaces where the water–rock interaction was maximized. Thus, we would expect to see the $\delta^{18}O$ values to be heavier above the palaeoexposure surfaces than underneath it.

A mechanism that could cause ^{13}C depletion of platform-top carbonates is meteoric diagenesis associated with high-frequency, low-amplitude oscillations in sea level that episodically exposed the shallow-platform. Isotopically light meteoric water and light soil zone CO_2 commonly cause a marked depletion in ^{13}C and ^{18}O in carbonates beneath exposure horizons (Allan and Matthews, 1982).

3.7.4. Strontium Isotopes

The Cenomanian-Turonian part of the $^{87}Sr/^{86}Sr$ seawater curve consists of high slope segments (McArthur et al., 2001). Many of the values obtained from surface sections fit well with the portion of $^{87}Sr/^{86}Sr$ curve corresponding to Cenomanian-Turonian age interval.

Generally, diagenetic processes tend to increase the $^{87}Sr/^{86}Sr$ ratios in carbonate sediments relative to pristine (coeval seawater) values. Thus, it is generally appropriate to draw a best-estimate curve along the lower limits defined by the data (Burke et al., 1982).

A major drop in sea level, which occurred in Turonian exposed the older sediments and subjected them to chemically aggressive meteoric fluids. Thus, during the sea level fall the

palaeoexposure surface and adjacent shallow basin could have been subjected to fluids characterized by higher $^{87}Sr/^{86}Sr$ values (reflecting Sr from riverine sources) affecting the values of the precipitated carbonates at that time. Samples collected immediately below the unconformity surface show radiogenically enriched $^{87}Sr/^{86}Sr$ ratios while further below this horizon the underlying strata display values similar to the Turonian values. Therefore the major features and absolute values of $^{87}Sr/^{86}Sr$ compare well with reference curves while the departures from this are recognized by values that plot away from a consistent trend. The $^{87}Sr/^{86}Sr$ ratios are by far more radiogenic than any other values within the curve.

The extremely sharp increase in $^{87}Sr/^{86}Sr$ ratio (i.e., 0.70878) of carbonate matrix measured at the topmost part of the studied surface sections and wells show a departure from the normal sea water curve implying alteration due to their exposure to fluids other than normal sea water.

Considering the complexity of recognition the unconformity surfaces in core and cutting samples of the wells by petrographic methods, utilizing the$^{87}Sr/^{86}Sr$ ratios could well represent the major unconformity in the region which appears to be well developed spatially. Short duration palaeoexposure surfaces or sedimentary breaks (e.g. Cenomanian-Turonian unconformity) with little diagenetic modification seem to be incapable of modifying $^{87}Sr/^{86}Sr$ ratios and leaving no traceable changes.Therefore, using carbon and oxygen isotopes, which are more susceptible to meteoric diagenesis, seems the most reliable method to recognize palaeoexposures of short duration.

There is no discernible trend in a plot of 1/Sr versus $^{87}Sr/^{86}Sr$ (Fig. 3.10a), implying that the strontium was supplied from a uniform source namely the contemporaneous sea water and no external Sr was added to the precipitating carbonates. This is the reason that $^{87}Sr/^{86}Sr$ ratios of the matrix limestone generally remained relatively constant (between 0.70728 and 0.70758). Therefore, strontium isotope stratigraphy of the type section generally follows similar trends expected from the seawater Sr isotope curve. The only exceptions are the values obtained from the samples at or below the unconformity surface at the top of the Sarvak Formation, which shows extremely high $^{87}Sr/^{86}Sr$ ratio (0.70878) and the other one in Lower Sarvak Formation, which may correspond to early Cenomanian sedimentary break that has been recognized as paleontological gap by other workers. (see Fig. 6 in Ghabeishavi et al., 2010).

3.8. Sea-level Change

Shifts in the stable isotope composition of marine carbonates in response to sea-level changes are well known from the geologic record (e.g. Jenkyns, 1980; Kuypers et al., 1999). The relationship between $\delta^{13}C$ excursions and sea level has been debated (e.g. Jarvis et al., 2001, 2006). For example, Mabrouk et al. (2007) noted a long-term decline in $\delta^{13}C$ values associated with falling sea-levels, and that when the eustatic sea level fluctuated, the $\delta^{13}C$ follows in the same manner. During transgressions, large amounts of organic matter can be stored in marginal areas resulting in an enrichment of ^{13}C; whereas during regressive phases, the stored organic matter is eroded and oxidized, resulting in ^{12}C enrichment in deep basins (Broecker, 1982). Thus, $\delta^{13}C$ values and associated changes can indicate eustatic sea-level changes.

The $\delta^{13}C$ profile obtained from the surface and subsurface sections show negative and positive peaks (Figs. 3.7a, b). Major shifts toward negative $\delta^{13}C$ values observed in isotope profiles are interpreted to be a result of sea level fall and meteoric water influence with subaerial exposure of the carbonates. At this time the carbonates were subjected to meteoric diagenesis under the influence of ^{13}C-depleted atmospheric CO_2. Pedogenic calcites in the Shahneshin area have a range of $\delta^{13}C$ values between -9.1 and -1.6 ‰ (see Table 3.1 for values). Consequently, the $\delta^{13}C$ and $\delta^{18}O$ patterns are a good indicator for sea level changes if associated with subaerial exposures. Based on the presence of horizons with different negative $\delta^{13}C$ and $\delta^{18}O$ values, a number of subaerial exposure surfaces may be present. This is consistent with the presence of erosional surfaces, bauxite formation and pedogenic features in surface sections (Hajikazemi et al., 2010). Dissolution processes during exposure as well as erosion and reworking of the soil and the presence of Fe-Mn nodules and pisoids during subsequent marine flooding are all indicative of exposure surfaces (Fig. 3.11).

The negative $\delta^{13}C$ values displayed in the isotope profiles are interpreted as being due to sea- level fall and incorporation of pedogenic carbonates. Hence, the presence of negative $\delta^{13}C$ excursions in bulk-rock profiles is a reliable way of detecting these surfaces in the Sarvak carbonates. Thus, the shift toward negative $\delta^{13}C$ values of similar form may be related to the presence of subaerial exposure particularly in subsurface sections with no other evidence of the palaeoexposure surface.

The short-lived exposure period could result in the absence of pedogenesis or vertical zonation of pedogenic fabrics at the erosional surface (see Flugel, 2004, p. 206), which makes

identification of the palaeoexposures of shorter durations difficult. In addition, the petrographically altered horizons may be very thin and difficult to recognize, or they may have been removed during transgression, whereas the geochemical signal of exposure was preserved in the underlying rocks.

3.9. Conclusions

The Upper Sarvak carbonates contains many potential hydrocarbon reservoirs highly effected by meteoric diagenetic during the periods of subarerial exposures.

The present work utilized applied chemostratigraphy to constrain the age of the most significant unconformity event and correlate them. The results of this study also added new data to the isotopic composition records of the Mid-Cretaceous seawater, filling the Cenomanian-Turonian gap of documentation.

Two pronounced unconformities have been identified in the Sarvak carbonate succession; 1) during the period of sea-level fall at the Cenomanian-Turonian Boundary leading to subaerial exposure of the shallow-water platform, and 2) the Turonian transgression and subsequent subaerial exposure coinciding with a mid Turonian sea-level fall.

The Cenomanian-Turonian unconformity was recognized by the geochemical signals including depleted $\delta^{13}C$ values coupled with depleted Sr concentrations. Based on the $^{87}Sr/^{86}Sr$ ratios, the Cenomanian-Turonian exposure was of shorter duration than the Turonian unconformity, characterized by the lack of a pronounced peak in the $^{87}Sr/^{86}Sr$ ratio.

Negative $\delta^{13}C$ and $\delta^{18}O$ values observed in the stratigraphic profiles indicate that other palaeoexposure surfaces exist within the Sarvak Formation, attributed to sea-level changes.

Co-variations and close agreement is observed in $\delta^{13}C$, Sr and Mn concentration profiles showing their temporal and spatial extent in the region during the Sarvak depositional period. Most of the geochemical records obtained in this study are in agreement with changes in the geochemical records through the Cenomanian-Turonian. The results also demonstrate the potential of the combined $\delta^{13}C$ and $^{87}Sr/^{86}Sr$ reference curve as a prime criterion for surface and subsurface correlation.

The positive $\delta^{13}C$ excursions obtained represent the primary signatures. The most positive values determined along the stable isotope profiles represent MCE (Mid Cenomanian Event), which has been identified and correlated both on the surface and subsurface sections and could be correlated with such event globally.

3.10. Acknowledgments

This manuscript has been greatly improved from indepth review by Dr. Thomas Steuber. Our special thanks to him for his useful suggestions. Funding for this project was provided by Natural Science and Engineering Research Council of Canada (NSERC) to I.S. Al-Aasm and M. Coniglio. Additional funding was provided by StatoilHydro.

3.11. References

Al-Aasm, I.S. and Veizer, J., 1982. Chemical stabilization of aragonite and low-Mg calcite: An example of brachiopods. Journal of Sedimentary Petrology, 52, 1101-1109.

Al-Aasm, I.S. and Veizer, J.,1986a. Diagenetic stabilization of aragonite and low-Mg calcite, I. Trace Elements in rudists. Journal of Sedimentary Petrology, **56**, 138-152.

Al-Aasm, I.S. and Veizer, J., 1986b. Diagenetic stabilization of aragonite and low-Mg calcite, II. Stable isotopes in rudists. Journal of Sedimentary Petrology, **56**, 763-770.

Al-Aasm, I. S.; Tylor, B. E. and South, B., 1990. Stable isotope analysis of multiple carbonate samples using selective acid extraction. Chemical Geology, **80**, 119-125.

Alsouki, M., Hassani, H, Irannejad, M., and Riahi, M. 2008. The structural imaging in offshore area of Strait of Hormoz based on 3-D seiemic data. Journal of Applied Sciences. **15**, 2726-2731.

Aqrawi, A.A.M., Thehni, G.A., Sherwani, G. H. and Kareem, B.M.A., 1998. Mid-Cretaceous rudist-bearing carbonates of the Mishrif Formation: An important reservoir sequence in the Mesopotamian Basin, Iraq. Journal of Petroleum Geology. **21**(1), 57-82

Arthur, M.A., Dean, W.E. and Pratt, L.M., 1988. Geochemical and climatic effects of increased marine organic carbon burial at the Cenomanian/Turonian boundary. Nature. **335**, 714–717.

Arthur, M. A., Jenkyns, H. C., Brumsack, H. J. and Schlanger, S. O. 1990. Stratigraphy, geochemistry and paleooceanography of organic carbon-rich Cretaceous sequences. In Cretaceous Resources Events and Rhythms: Background and Plans for Research (editors R. N. Ginsburg and B. Beaudoin), 75–119. NATO Science Series C: Mathematical and Physical Sciences no. 304. Dordrecht, The Netherlands: Kluwer Academic Publishers.

Banner, J.L., 2004. Radiogenic isotopes: systematics and applications to earth surface processes and chemical stratigraphy Earth Science Reviews. **65**, 141–194.

Beiranvand, B. Ahmadi, A. and Sharafodin, M. 2007. Mapping and classifying flow units in the upper part of the Middle Cretaceous Sarvak formation (western Dezful embayment, SW Iran) based on a determination of the reservoir types. Journal of Petroleum Geology, **30**(4), 357-373.

Brand, U. and Veizer, J. 1980. Chemical diagenesis of a multicomponent carbonate system-1: Trace elements, Journal of Sedimentary Petrology. **50**, 1219–1236.

Boltz, H., 1978. The palaeogeographical evolution during the Cretaceous in the Operating Area with special emphasis on the Bangestan Group. Oil Service Company (OSCO) Internal Report 1274.

Broecker, W.S., 1982, Glacial to interglacial changes in ocean chemistry: Progress in Oceanography, **11**(2), 151-197.

Burchette, T.P., 1993. Mishrif Formation (Cenomanian-Turonian), southern Arabian Gulf: carbonate platform growth along a cratonic margin basin. In: Simo, J.A.T., Scott, R.W. and Masse, J. P. (editors): Cretaceous carbonates platforms. American Association of Petroleum Geologists, Memoir. **56**, 185-199.

Burchette, T.P. and Britton, S.R., 1985. Carbonate facies analysis in the exploration for hydrocarbons: a case study from the Cretaceous of the Middle East. In: Brenchley, P.J. and Williams, B.P.J. (editors): Sedimentology. Recent Developments and Applied Aspects, 311-338.

Calvert, S.E. and Pedersen, T.F., 1993. Geochemistry of recent oxic and anoxic marine sediment: implications for the geological record. Marine Geology. **113**, 67–88.

Derry, L.A., Brasier, M.D., Corfield, R.M., Rozanov, A. Yu. and Zhuravlev, A. U., 1994. Sr and C isotopes in Lower Cambrian carbonates from the Siberian craton: A paleoenvironmental record during the 'Cambrian explosion' Earth and Planetary Science Letters, **128,** 671-681

Dickens, G.R. and Owen, R.M., 1993. Global change and manganese deposition at the Cenomanian–Turonian boundary. Marine Georesources and Geotechnology, **11**, 27–43.

Dickens, G. R.and Owen, R. M., 1995. Rare earth element deposition in pelagic sediment at the Cenomanian–Turonian boundary, Exmouth Plateau. Geophysical Research Letters, **22**, 203–206.

Dunnington, H.V., 2005. Generation, Migration, accumulation and dissipation of oil in northern Iraq. GeoArabia, **6**(2), 39-84.

Erbacher, J., Friedrich, O., Wilson, P.A., Birch, H.and Mutterlose, J., 2005. Stable organic carbon isotope stratigraphy across Oceanic Anoxic Event 2 of Demerara Rise, western tropical Atlantic. Geochemistry, Geophysics, Geosystems, **6** (Q06010).

Ernst, G., Schmid, F.and Seibertz, E., 1983. Event-Stratigraphie im Cenomanian und Turonian von NW-Deutschland. Zitteliana , **10**, 531–554.

Farzadi, P. and Alaei, B., Submitted. Stratigraphic architecture of the Zagros Basin: towards an objective comparison of the Fold-Thrust Belt and Foreland provinces.

Farzadi, P. and Hesthmer, J., 2007. Diagnosis of the Upper Cretaceous palaeokarst and turbidite systems from the Iranian Persian Gulf using volume-based multiple seismic attribute analysis and pattern recognition. Petroleum Geoscience, **13**, 227-240

Firijia, G. and Parente, M. 2008. Strontium isotope stratigraphy in the upper Cenomanian shallow-water carbonates of the southern Apenninen: Short- term perturbations of marine $^{87}Sr/^{86}Sr$ during the Oceanic Anoxic Event 2. Palaeogeography, Palaeoclimatology, Palaeoecology, **261**, 15–29.

Flugel, E., 2004. Microfacies of carbonatre rocks. Analysis, Interpretation and Application, Springer, 976p.

Frakes, L.A. and Bolton, B.R., 1984. Origin of manganese giants: Sea level change and anoxic-oxic history. Geology, **12**, 83– 86.

Friedrich, O, Erbacher, J, Paul A. Wilson, P.A., Moriya , K., and Mutterlose, J. 2009. Paleoenvironmental changes across the Mid Cenomanian Event in the tropical Atlantic Ocean (Demerara Rise, ODP Leg 207) inferred from benthic foraminiferal assemblages. Micropaleontology, **71**, 28–40

Gale A. S., Jenkyns, H. C., Kennedy, W. J. and Corfield, R. M., 1993. Chemostratigraphy versus biostratigraphy: data from around the Cenomanian–Turonian boundary.Journal of the Geological Society, London **150**, 29–32.

Gale, A. S., Kennedy, W. J., Voigt, S. and Walaszczyk, I., 2005. Stratigraphy of the Upper Cenomanian–Lower Turonian Chalk succession at Eastbourne, Sussex, UK: ammonites, inoceramid bivalves and stable carbon isotopes. Cretaceous Research, 26, 460–87.

Ghabeishavi, A., 2009. Stratigraphy of the Ilam and Sarvak formations in Bangestan anticline and Parsi oilfield. University of Esfahan. 200p.

Ghabeishavi, A., Vaziri-Moghaddam, H., Taheri, A. and Taati, A., 2010. Microfacies and depositional environment of the Cenomanian of the Bangestan anticline, SW Iran. Journal of Asian Earth Sciences, **37**, 275-285.

Ghazban, F., 2007. Petroleum geology of the Persian Gulf. Joint publication, Tehran University Press and National Iranian Oil Company. 706p.

Hajikazemi, E., Al-Aasm, S. I. and Coniglio, M., 2010. Subaerial exposure and meteoric diagenesis of the Cenomanian-Turonian Upper Sarvak Formation, southwestern Iran. Geological Society of Londoan. Special publications, **330**, 253-272.

Hajikazemi, E., Ghazban, F. and Yousefpour M.R., 2002. Depositional and diagenetic history of the Middle Cretaceous sedimentary sequence in the Sirri Oil fields in the Persian Gulf, Iran. Middle East and North Africa Oil and Gas conference, Imperial College, London.

Haq, B.U., Hardenbol, J.and VAIL, P.R., 1987. Chronology of fluctuating sea levels since the Triassic (250 million years ago to present). Science, **235**, 1156– 1167.

Haq, B. U., Hardenbol, J. and Vail, P., 1988. Mesozoic and Cenozoic chronostratigraphy and cycles of sea level change. In Sea-Level Changes – An Integrated Approach (eds. C. K. Wilgus, B. S. Hastings, C. A. Ross, H. Posamentier, J. Van Wagoner and C.G. S.C. Kendall), 71–108. SEPM Special Publication no. 42. Tulsa: The Society of Economic Paleontologists and Mineralogists.

Harris, P.M., Frost, S.H., Seiglie, G.A. and Schneidermann, N., 1984. Regional unconformities and depositional cycles, Cretaceous of the Arabian peninsula, in J.S. Schlee, ed, Interregional uncoformities and hydrocarbon accumulations. American Association of Petroleum Geologists, Memoir. **36**, 67-80.

Huber, B.T., Norris, R.D.and Macleod, K.G., 2002. Deep-sea paleotemperature record of extreme warmth during the Cretaceous. Geology, **30**, 123–126.

Immenhauser, A., Nagler, T.F., Steuber, T. and Hippler, D., 2005. A critical assessment of mollusk $^{18}O/^{16}O$, Mg/Ca, and $^{44}Ca/^{40}Ca$ ratios as proxies for Cretaceous seawater temperature seasonality. Palaeogeography, Palaeoclimatology, Palaeoecology, **215**, 221–237.

Jarvis, I., Murphy, A.M. and Gale, A.S., 2001. Geochemistry of pelagic and hemipelagic carbonates: criteria for identifying systems tracts and sea-level change. Journal of the Geological Society, London, **158**, 685-695

Jarvis, I., Gale, A.S., Jenkyns, H.C.and Pearce, M.A., 2006. Secular variation in Late Cretaceous carbon isotopes: a new $\sigma^{13}C$ carbonate reference curve for the Cenomanian–Campanian (99.6–70.6 Ma). Geological Magazine, **143**, 561–608.

Jenkyns, H.C., Gale, A.S. and Corfield, R.M., 1994. Carbon and oxygen isotope stratigraphy of the English Chalk and Italian Scaglia and its palaeoclimatic significance. Geological Magazine, **131**, 1–34.

Jenkyns, H. C., 1980. Cretaceous anoxic events: from continents to oceans. Journal of the Geological Society London, **137**, 171–88.

Keyvani, F. and Heydari, E., 2002. Depositional environments and diagenesis of cretaceous (Albian to Maasterichtian) strata of the Abadan plain of the Persian platform in southwestern of Iran, Proceedings of the Geological Society of America Annual Meeting.

Koop, W. and Stoneley, R., 1982. Subsidence history of the Middle East Zagros Basin, Permian to Recent. Phil. Trans. Roy. Soc. Lond., **305**, 149–168.

Kuypers, M.M.M., Pancost, R.D. and Sinninghe Damste, J.S., 1999. A large and abrupt fall in atmospheric CO2 concentration during Cretaceous times: Nature, **399**, 342–245.

Land, L, S. And Epstein, S., 1970. Late Pleistocene diagenesis and dolomitization, North Jamaica Sedimentology, **14**, 187-200.

Lawrence, A. and Hardie, L.A., 1996. Secular variation in seawater chemistry: An explanation for the coupled secular variation in the mineralogies of marine limestones and potash evaporites over the past 600 m.y. Geology, **24**(3), 279–283.

Mabrouk, A., Jarvis, I., Belayouni, H., Murphy, A. and R. T.J. Moody, 2007. Sequence Stratigraphy, Sea Level Change and Palaeoenvironments via Chemostratigraphy: Regional to Global Correlations. Extended abstract prepared for oral presentation at AAPG Annual convention, Long Beach, California.

Marshall, J. D., 1992, Climatic and oceanographic signals from the carbonate rock record and their preservation: Geological Magazine, **129**, 143–160.

McArthur, J.M., Howarth, R.J. and Bailey, T.R., 2001. Strontium isotope stratigraphy: LOWESS Version 3. Best-fit to the marine Sr-isotope curve for 0 to 509 Ma and accompanying look-up table for deriving numerical age. Geology, **109**, 155–170.

Motiei, H. 1993. Geology of Iran. The stratigraphy of Zagros. Geological survey of Iran.

Pattison, R. and Takin, M., 1971. Geological significance of the Dezful embayment boundaries. National Iranian Oil Company, Report 1166 (unpublished).

Paul, C.R.C., Mitchell, S.F., Marshall, J.D., Leary, P.N., Gale, A.S., Duane, A.M. and Ditchfield, P.W., 1994. Palaeoceanographic events in the Middle Cenomanian of Northwest Europe.Cretaceous Research, **15**, 707–738.

Pratt, L. M., Arthur, M. A., Dean, W. E. and Scholle, P. A., 1993. Paleoceanographic cycles and events during the Late Cretaceous in the Western Interior Seaway of North America. In Cretaceous Evolution of the Western Interior Basin of North America (editors W. G. E.Caldwell and E. G. Kauffman), 333–353. Geological Association of Canada, Special Paper no. 39.

Saller, A.H., Budd, D.A., and Harris, P.M., 1994. Unconformities and porosity development in carbonate strata: Ideas from a Hedberg Conference: American Association of Petroleum Geologists, Bulletin, **78**, 857–872.

Schlanger, S.O., and Jenkyns, H.C., 1976. Cretaceous oceanic anoxic events: causes and consequences. Geologie en Mijnbouw, 55, 179–184.

Schlanger, S. O., Arthur, M. A., Jenkyns, H. C., and Scholle, P. A., 1987, The Cenomanian-Turonian Oceanic Anoxic Event, I. Stratigraphy and distribution of organic carbon-rich beds and the marine $\delta^{13}C$ excursion, J., and Fleet, A. J., editors, Marine Petroleum source Rocks: Geological Society of London Special Publication. **26**, 371–399.

Scholle, P.A. and Arthur, M.A., 1980. Carbon isotope fluctuations in Cretaceous pelagic limestones: potential stratigraphic and petroleum exploration tool. American Association of Petroleum Geologists, Bull. **64**, 67–87.

Setudehnia, A., 1978. The Mesozoic succession in S.W. Iran and adjacent areas. Journal of Petroleum Geology, **1**, 3-42.

Sharland, P.R., Archer, R., Casey, D.M., Casey, R.B., Hall, S.H., Heward, A.P., Horbury, A.D. and Simmons, M.D., 2001. Arabian Plate Sequence Stratigraphy. GeoArabia Special Publication, **2**, 371p.

Sloss, L.L., 1988. Tectonic evolution of the craton in Phanerozoic time. In: Sedimentary Cover-North American Craton, The Geology of North America, D-2, 25–51. Geological Society of America, Boulder Company.

Steuber, T., 1996. Stable isotope sclerochronology of rudist bivalves: growth rates and Late Cretaceous seasonality. Geology, **24**, 315–318.

Steuber, T., 2001, Strontium isotope stratigraphy of Turonian-Campanian Gosau-type rudist formations in the Northern Calcareous and Central Alps (Austria and Germany). Cretaceous Research, **22**, 429-441.

Steuber, T., 2003. Strontium isotope stratigraphy of Cretaceous hippuritid rudist bivalves: rates of morphological change and heterochronic evolution. Palaeogeography, Palaeoclimatology, Palaeoecology, **200**, 221–243.

Taghavi, A.A., Mork, A, and Emadi, M.A., 2006. Sequence stratigraphically controlled diagenesis governs reservoir quality in the carbonate Dehluran Field, southwest Iran, Petroleum Geoscience, **12**(2), 115-126.

Tsikos, H., Jenkyns, H.C., Walsworth-Bell, B., Petrizzo, M.R., Forster, A., Kolonic, S., Erba, E., Premoli Silva, I., Baas, M., Wagner, T. and Sinninghe Damste, J.S., 2004. Carbon-isotope stratigraphy recorded by the Cenomanian–Turonian Oceanic Anoxic Event; correlation and implications based on three key localities. Journal of Geological Society of London, **161**, 711-719.

Tucker, M. E. and V. P. Wright, 1990. Carbonate Sedimentology: Oxford: Blackwell Scientific Publications, 482 p.

Van Buchem, F. S. P., Razin, P., Homewood, P.W., Oterdoom, H. and Philip, J., 2002. Stratigraphic organization of carbonate ramps and organic-rich intrashelf basins: Natih Formation (middle Cretaceous) of northern Oman: American Association of Petroleum Geologists, Bulletin, **86**, 21–54.

Veizer, J., Ala, D., Azmy, K, Bruckschen, P., Buhl, D., Bruhn, F., Carden, G.A.F., Diener, A., Ebneth, S., Godderis, Y., Jasper, T., Korte, C., Pawellek, F., Podlaha, O.G. and Strauss, H., 1999. $^{87}Sr/^{86}$ Sr, $\delta^{13}C$ and $\delta^{18}O$ evolution of Phanerozoic sea water. Chemical Geology, **161**, 59–88.

Veizer, J., 1977. Diagenesis of Pre-Quaternary carbonates as indicated by tracer studies. Journal of Sedimentary Petrology, **47**(2), 565–81.

Veizer, J., 1983. Chemical diagenesis of carbonates: Theory and trace element technique. in Arthur, M.A., Anderson, T.F., Kaplan, I.R., Veizer, J., and Land, L.S. (editors), Stable

Isotopes in Sedimentary Geology: Society of Economic Paleontologists and Mineralogists Short Course no. 10, Dallas, p. 3.1–3.100.

Videtich, P.E., Mclimans, R.K., Watson, H.K. and Nagy, R.M., 1988. Depositional, diagenetic, thermal and maturation histories of Cretaceous Mishrif Formation, Fateh Field, Dubai. American Association of Petroleum Geologists Bulletin, **72**, 1143-1159.

Voigt, S., 2000. Cenomanian–Turonian composite $\delta^{13}C$ curve for Western and Central Europe: the role of organic and inorganic carbon fluxes. Palaeogeography, Palaeoclimatology, Palaeoecology, **160**, 91–104.

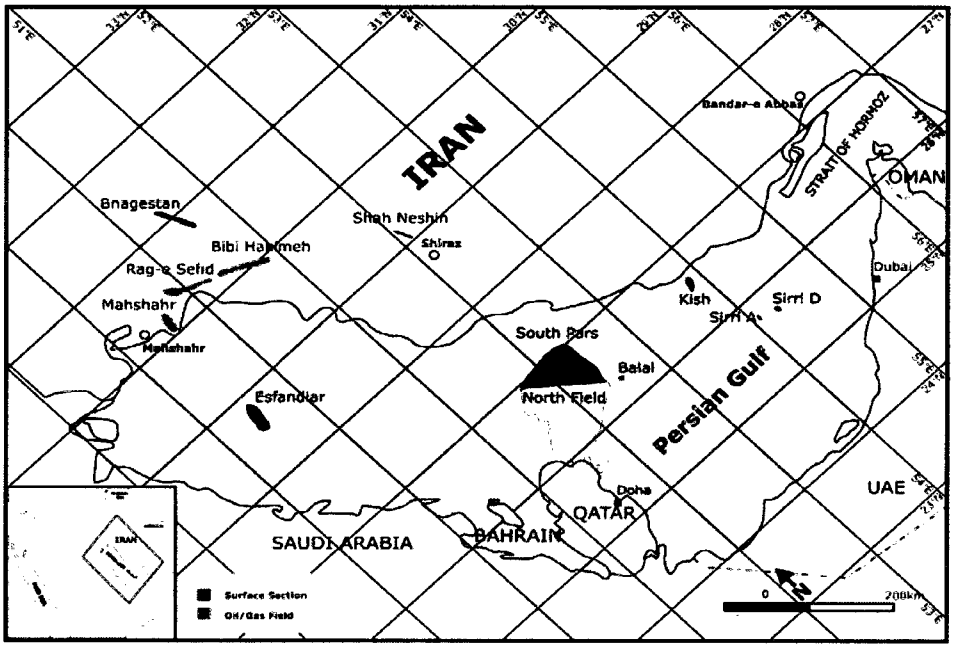

Figure 3.1 Map of SW Iran and Persian Gulf showing the location of the study area.

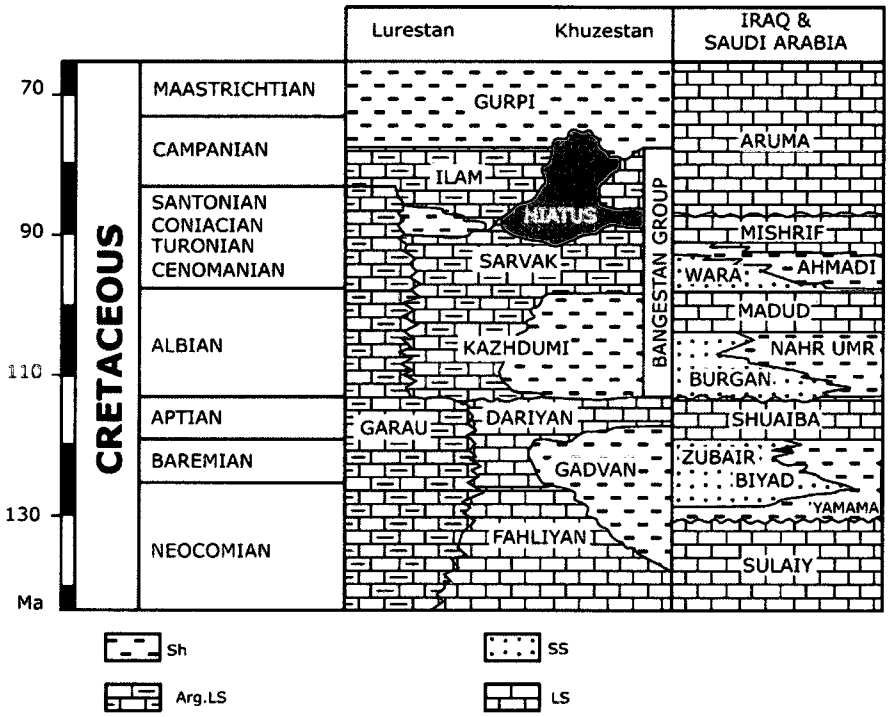

Figure 3.2 a) Stratigraphic correlation chart showing the regional Turonian unconformity on top of the Sarvak Formation (after Bordenave 2002).

Figure 3.2b) Palaeosol formed below the unconformity surface on Upper Sarvak Formation in Shahneshinn section.

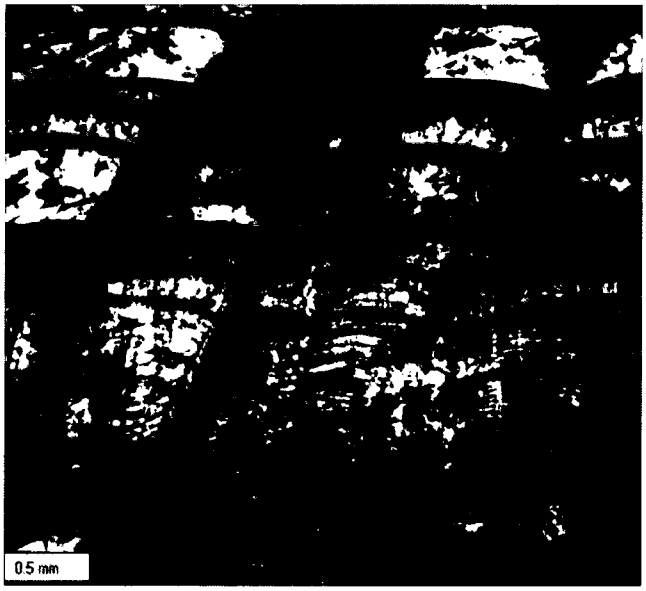

Figure 3.3 Photomicrograph of a rudist shell showing the preservation of internal microstructures of the shell.

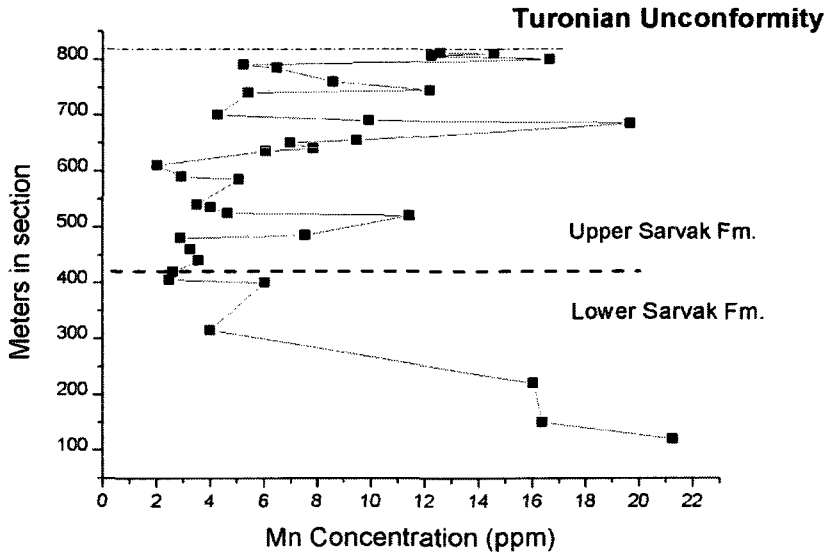

Figure 3.4 Variation of Mn concentrations along the Sarvak Fm. at the type section locality in Bangestan Mountain.

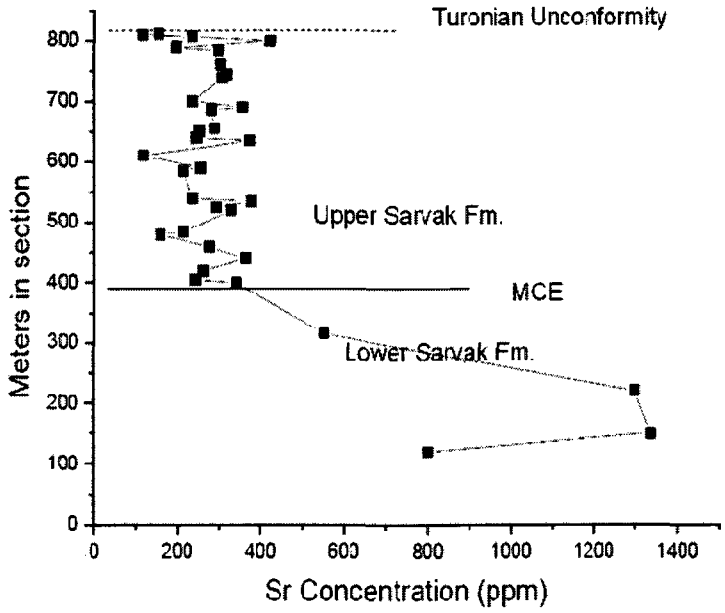

Figure 3.5 Sr concentration profile of the Sarvak Formation along the type section locality in Bangestan Mountain.

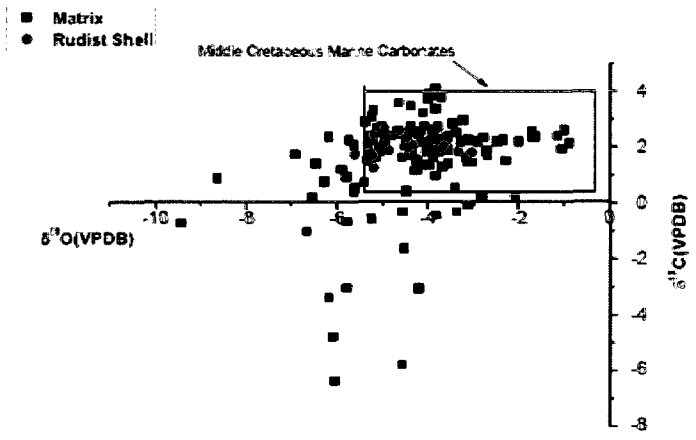

Figure 3.6 Carbon and oxygen isotopic composition of micrite and rudist shells of the Sarvak Formation in the study area.The marine carbonate box is based on global carbon and oxygen curve by Veizer et al. (1999) and carbon and oxygen data of Tethyan region (Immenhauser et al., 2005).

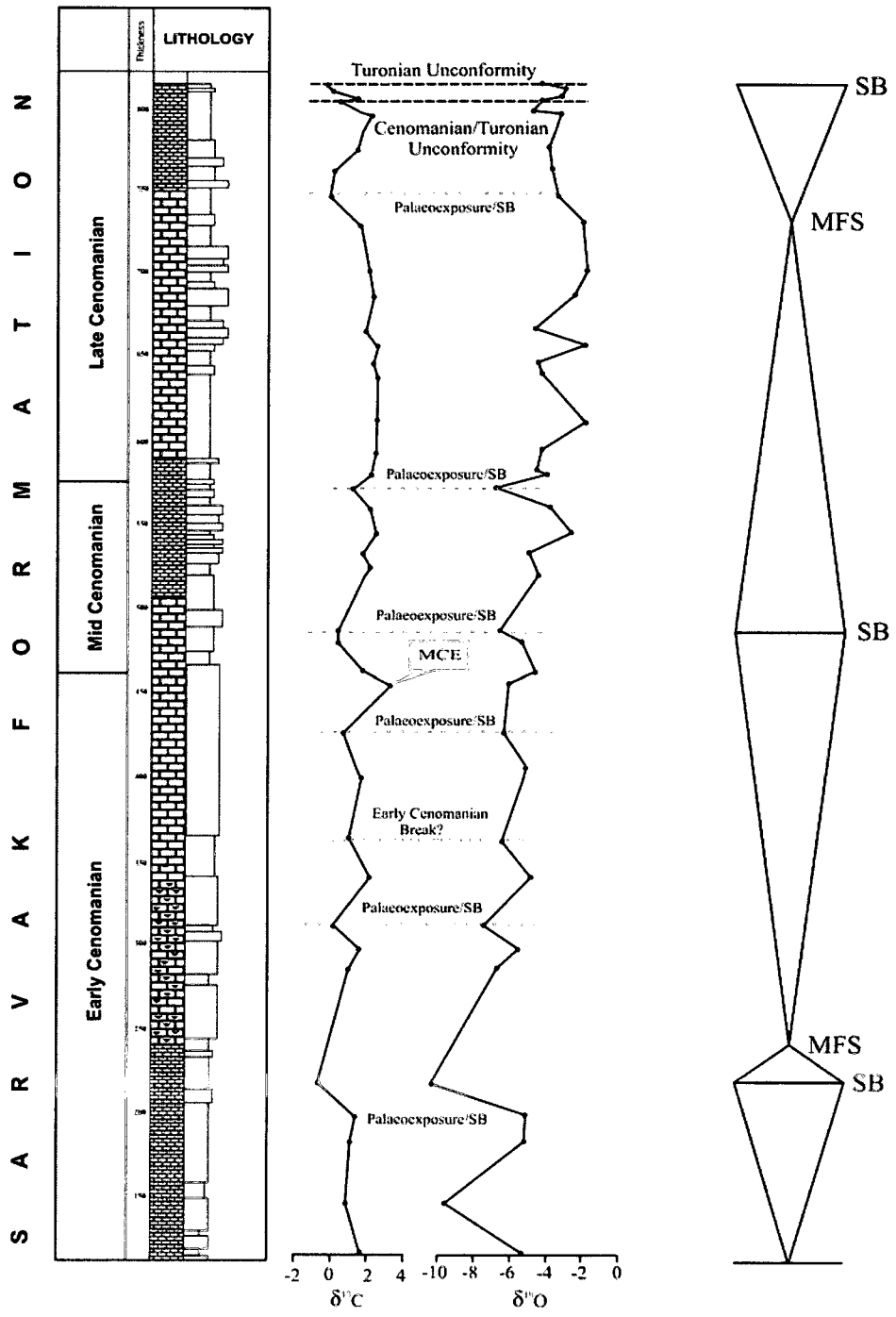

Figure 3.7a $\delta^{13}C$ and $\delta^{18}O$ variation along the Sarvak Formation at the type section locality, Bangestan Mountain.Some of sequence boundaries (right side of plot) are comparable with sequence stratigraphic column of Ghabeishavi et al. (2009).

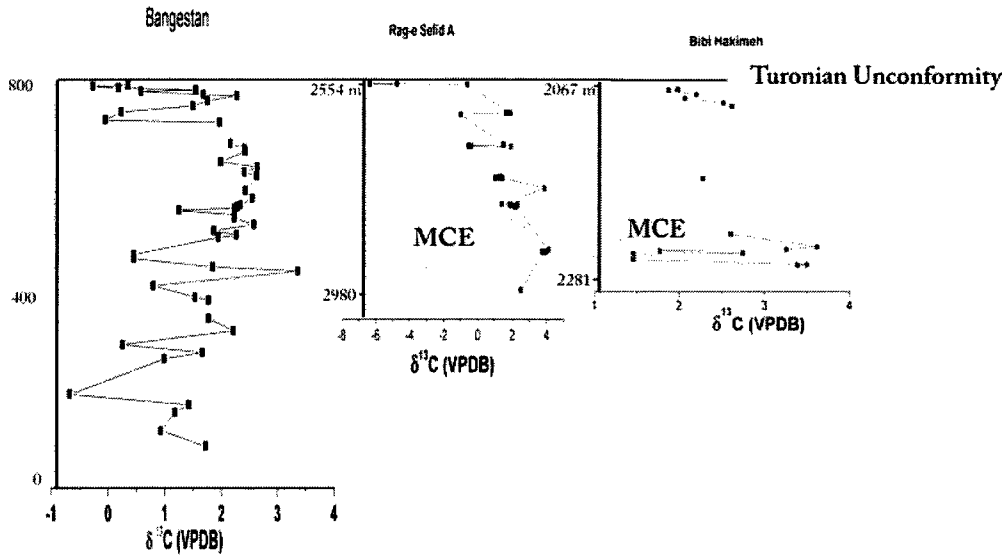

Figure 3.7b $\delta^{13}C$ profile of Bangestan section, Rag-e sefid A and Bibi Hakimeh wells shows the correlation of Mid Cenomanian Event (MCE).

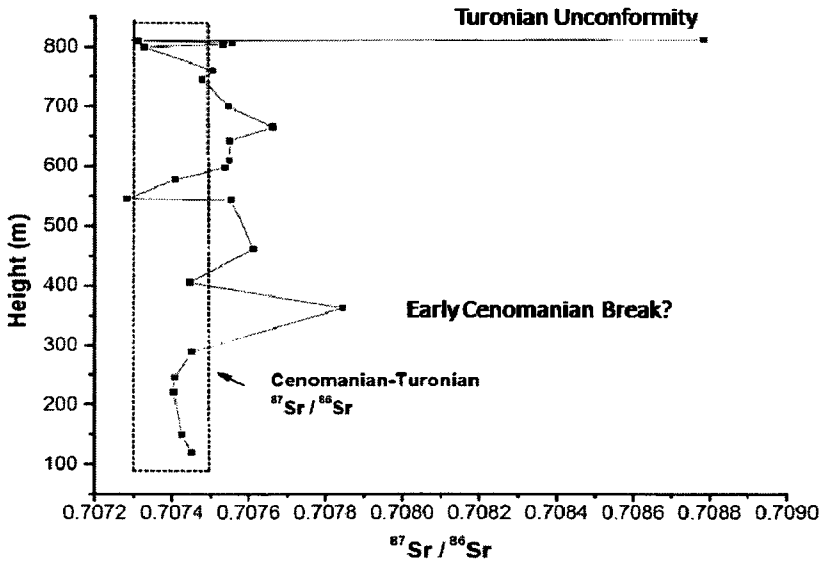

Figure 3.8a Strontium isotope stratigraphy of the Sarvak Formation at the type section locality, Bangestan Mountain.

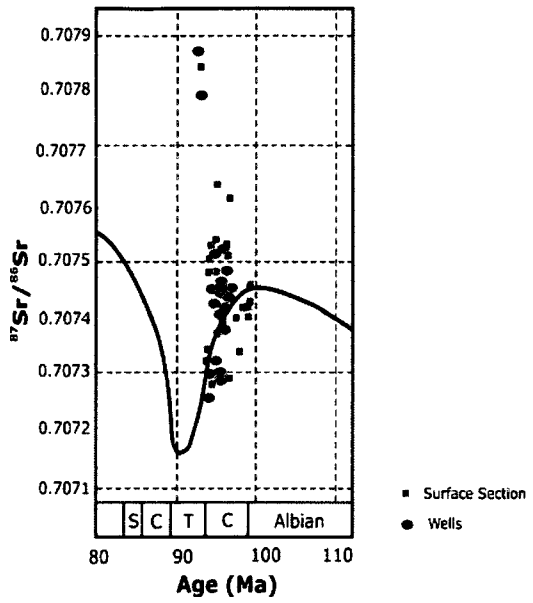

Figure 3.8b $^{87}Sr/^{86}Sr$ values of the Sarvak Formation plotted on Cenomanian-Turonian portion of global $^{87}Sr/^{86}Sr$ curve of Burke et al. (1982).

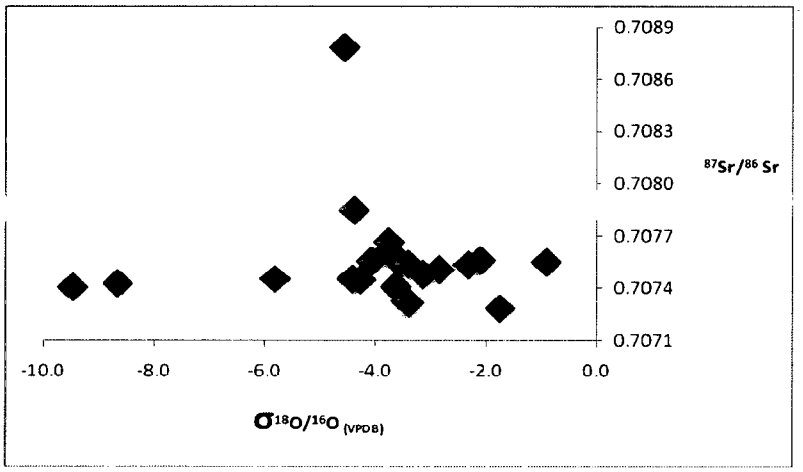

Figure 3.8c $^{87}Sr/^{86}Sr$ ratios of the samples taken from Bangestan section, plotted versus $\delta^{18}O$ shows no relationship indicating the chemical preservation of the micrite matrix.

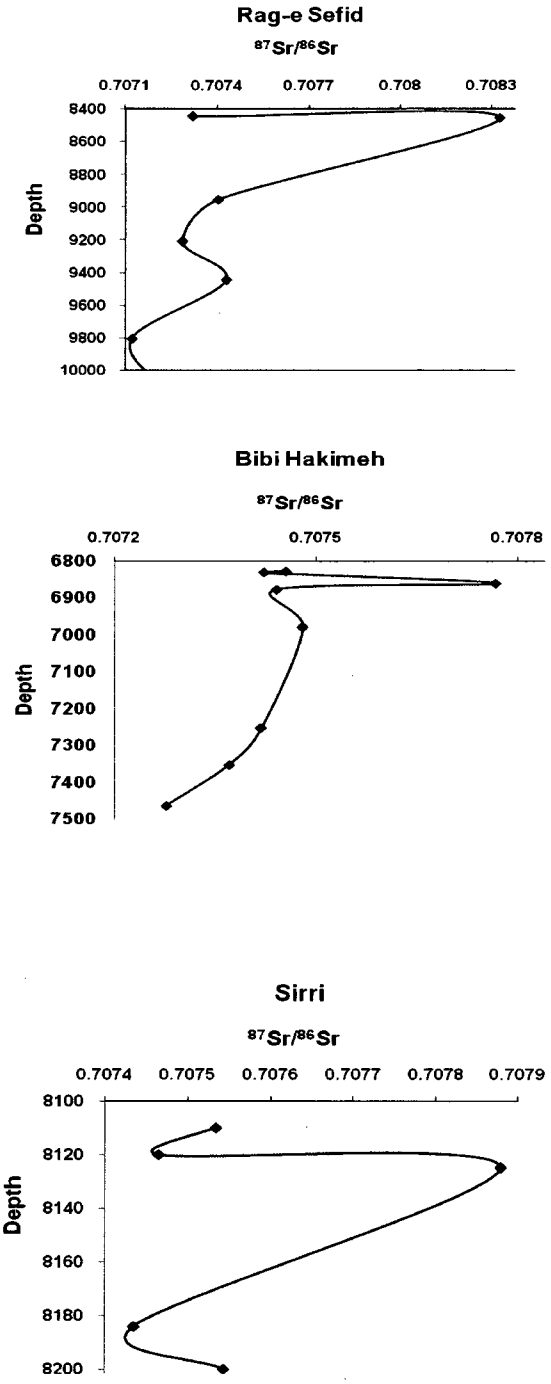

Figure 3.8d $^{87}Sr/^{86}Sr$ profile along the Sarvak Formation in subsurface sections showing the high $^{87}Sr/^{86}Sr$ ratio below the Turonian unconformity surface.

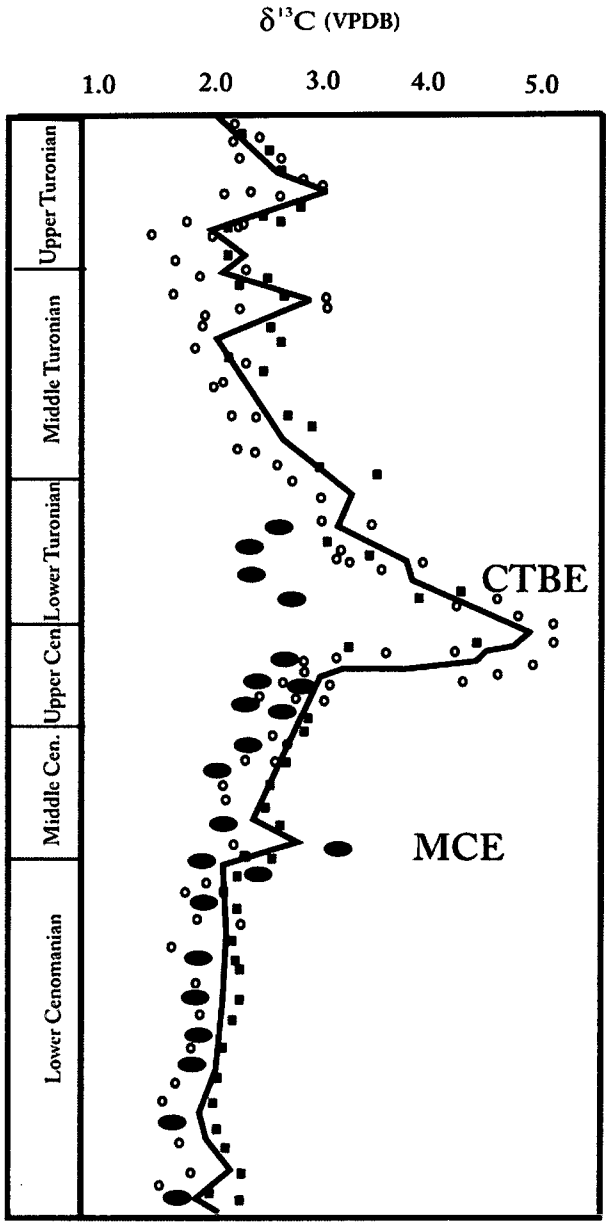

Figure 3.9 Carbon isotope data obtained from Bangestan section superimposed on Cenomanian-Turonian Carbon-isotope reference curve in Western and Central Europe (after Voigt et al. 2000). Symbols: Solid ellipsoids are data from Bangestan section, circles and squares are from Europe cited by Voigt et al. (2000).

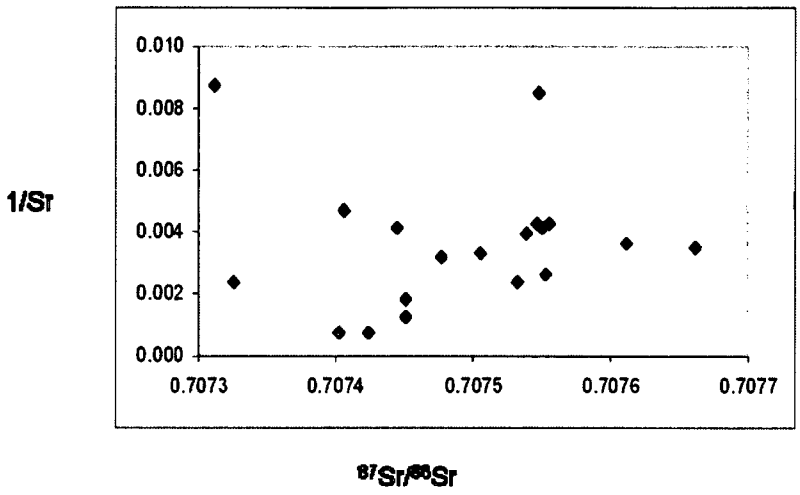

Figure 3.10a 1/Sr vs. $^{87}Sr/^{86}Sr$ plot for carbonate matrix samples from Bangestan section.

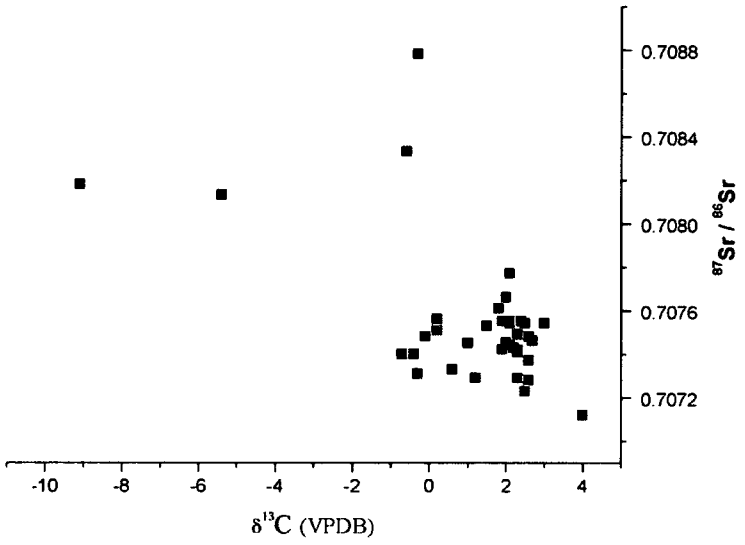

Figure 3.10b Plot of $^{87}Sr/^{86}Sr$ ratios vs. $\delta^{13}C$ of matrix shows the relationship between higher ratios of $^{87}Sr/^{86}Sr$ and lower $\delta^{13}C$ values which could be considered as an indicator of major unconformities.

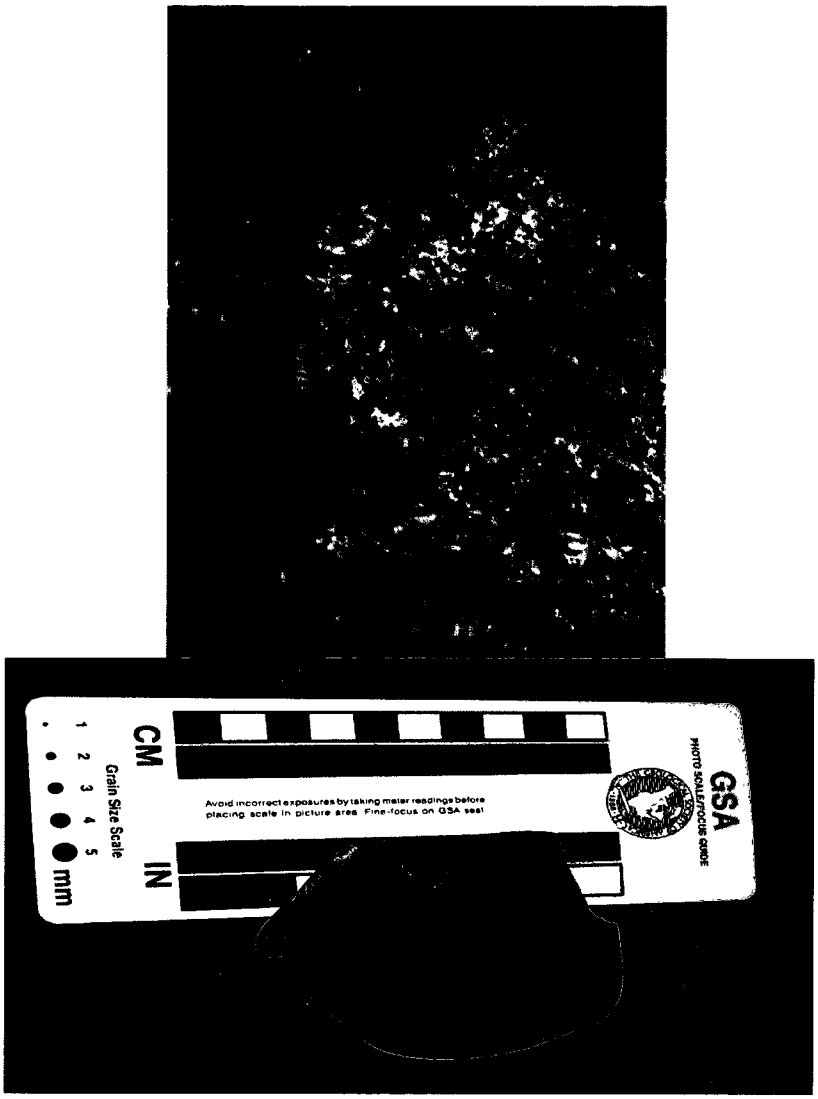

Figure 3.11 Field photograph of Fe-Mn nodules/concretion on top of the Sarvak Formation, Shahneshin Mountain.

Table 3.1 Carbon, Oxygen and Sr isotopic values and elemental concentrations of calcite matrix and palaeosol from surface sections

Sample No.	$\delta^{13}C$(VPDB)	$\delta^{18}O$(VPDB)	$^{87}Sr/^{86}Sr$	Sr (ppm)	Mn (ppm)
167-M	-0.3	-4.5	0.70878	154	13
166-M	-0.3	-3.4	0.70731	114	15
165-M	0.2	-2.1	0.70756	234	12
164-M	1.5	-2.3	0.70753		
163-M	0.6	-3.4	0.70733	422	17
162-M	1.7	-3.9			
161-M	2.3	-2.3		196	5
159-M	1.7	-2.7		298	6
157-M	1.5	-3.0			
155-M	0.2	-2.8	0.70751	303	9
151-M	-0.1	-3.1	0.70748	315	12
150-M	2.0	-1.1		306	5
143-M	2.1	-0.9	0.70755	235	4
140-M	2.4	-1.7		356	10
139-M	2.4	-1.6		280	20
134-M	2.0	-3.7	0.70766	288	9
132-M	2.6	-1.0			
129-M	2.4	-3.6	0.70755	252	7
128-M	2.6	-3.9		244	8
120-M	2.4	-1.2		117	2
114-M	2.5	-3.4	0.70754	254	3
111-M	2.3	-3.6	0.70741	213	5
110-M	2.3	-3.1			
109-M	2.2	-2.5			
108-M	1.2	-5.9			
106-M	2.2	-2.9			
105-M	2.2	-2.0			
102-M	2.6	-1.7	0.70728	236	4
97-M	1.9	-4.0	0.70755	377	4
95-M	2.3	-3.7		293	5
94-M	1.9	-3.6		327	11
88-M	0.5	-5.6		215	8
87-M	0.5	-4.5		159	3
83-M	1.8	-3.7	0.70761	276	3
80-M	3.3	-5.2		363	4
74-M	0.8	-5.4		260	3
71-M	1.5	-4.2	0.70745	242	2
69-M	1.8	-4.4		340	6
62-M	1.8	-4.4	0.70784		
58-M	2.2	-4.0			
54-M	0.3	-6.5		552	4
51-M	1.7	-4.6			

Table 3.1(Continued)

Sample No.	$\delta^{13}C$(VPDB)	$\delta^{18}O$(VPDB)	$^{87}Sr/^{86}Sr$	Sr (ppm)	Mn (ppm)
49-M	1.0	-5.8	0.70745		
36-M	-0.7	-9.4	0.70740	1298	16
27-M	1.2	-4.3			
21-M	0.9	-8.6	0.70743	1336	16
16-M	1.7	-4.4	0.70745	800	21
EH-2-M	2.6	-4.4			
EH-3-M	2.4	-5.2			
EH-4-M	2.1	-5.6			
EH-5-M	1.6	-4.3			
EH-6-M	1.5	-4.2			
EH-7-M	2.2	-5.3			
EH-9-M	2.5	-4.5		169	23
EH-10-M	-3.0	-4.2			
EH-11-M	0.8	-6.3			
EH-12-M	1.5	-4.2			
EH-13-M	2.5	-4.7			
SE-21-M	-5.8	-4.6		127	170
SE-22-M	-1.6	-4.5			
SE-23-M	0.6	-5.6			
SE-28-M	2.7	-5.1			
SE-29-M	2.4	-6.2			
BH-0-M	2.6	-4.4		144	18
BH-2-M	2.4	-4.8			
BH-3-M	1.6	-5.3			
BH-6-M	1.5	-4.2		164	35
BH-12-M	2.5	-4.7			
BH-107-M	0.8	-6.3			
BH-106-M	2.9	-5.4			
BH-104-M	2.3	-5.2	0.70749		
SK1-M	-3.4	-6.2			
SK2-M	-3.0	-5.8			
SK3-M	3.1	-5.2			
BH-5-P	-3.0	-4.2			
SS-1-P	-5.4	-3.7	0.70813		
SS-2-P	-1.6	-4.1			
SS-3-P	-7.3	-4.7			
SS-5-P	-9.1	-5.2			
SS-6-P			0.70818		

M: Calcite matrix, P: Palaeosol

Table 3.2 Carbon, Oxygen and Sr isotopic values and elemental concentrations of rudist shells and matrix from core samples

Sample No.	$\delta^{13}C$ (VPDB)	$\delta^{18}O$ (VPDB)	$^{87}Sr/^{86}Sr$	Sr (ppm)	Mn (ppm)
Bibi Hakimeh					
1-M	2.0	-4.0	0.707454	463	13
2-M	1.9	-3.8	0.707422		
3-M	2.2	-4.2			
4-M	2.1	-4.0	0.70777		
5-M	2.5	-4.2			
6-M	2.6	-4.6	0.70748		
7-M	2.3	-5.7	0.70742		
8-M	2.6	-4.7	0.70737		
9-M	3.6	-4.6		517	7
10-M	3.3	-4.1			
11-M	1.8	-6.9			
12-M	2.8	-5.0			
13-M	1.5	-6.5			
14-M	1.5	-6.5			
15-M	3.5	-4.4			
16-M	3.4	-3.8	0.70728	479	21
Sirri-D					
1-M	1.8	-5.1	0.70753	169	35
2-M	1.7	-5.1	0.70747		
3-M	1.8	-5.3	0.70788		
4-M	2.0	-5.1			
5-M	2.1	-5.3	0.70744		
6-M	2.1	-5.0	0.70754		
7-M	1.7	-5.2			
8-M	2.6	-5.0			
Rag-e Sefid A					
1-M	-4.8	-6.1	0.70732	197	28
2-M	-6.4	-6.1			
3-M	-0.6	-5.8	0.70833		
4-M	1.9	-2.7			
5-M	1.7	-3.2			
6-M	-1.0	-6.7		264	14
7-M	1.5	-3.1			
8-M	-0.6	-5.2			
9-M	-0.4	-3.8	0.70740	314	38
10-M	1.9	-3.7			
11-M	1.3	-3.7		254	21
12-M	1.2	-4.2	0.70729		
13-M	1.0	-3.8			
14-M	1.4	-3.6			
15-M	3.9	-3.8		327	2
16-M	1.4	-4.0		309	12
17-M	2.3	-3.8		263	8

Table3.2 (Continued)

Sample No.	$\delta^{13}C$ (VPDB)	$\delta^{18}O$ (VPDB)	$^{87}Sr/^{86}Sr$	Sr (ppm)	Mn (ppm)
18-M	1.9	-3.7			
19-M	1.9	-5.1			
20-M	2.1	-3.8		218	20
21-M	2.2	-3.3			
22-M	2.2	-4.5	0.70743		
23-M	4.1	-3.8		338	3
24-M	4.0	-4.0	0.70712	407	3
25-M	3.7	-4.0			
26-M	3.8	-3.7		229	3
27-M	2.5	-3.9	0.70723		
Rag-e Sefid B					
1-M	2.7	-3.8			
2-M	2.7	-4.4	0.70746		
3-M	2.8	-4.1			
4-M	3.0	-3.2	0.70754		
5-M	2.4	-5.3			
6-M	2.6	-4.2			
7-M	2.3	-3.7	0.70729		
8-M	2.4	-2.8			
9-M	2.2	-4.0			
10-M	2.9	-3.5			
11-M	2.6	-3.9			
Rudist Shell					
91-Sh	2.0	-3.7		340	10
92-Sh	1.9	-3.3	0.70740	349	2
98-Sh	1.8	-3.0	0.70736	319	4
8154-Sh	1.3	-5.2	0.70748	197	14
8217-Sh	2.4	-4.9	0.70717		
8173-Sh	1.7	-5.2	0.70714		
2514-Sh	2.7	-5.0	0.70750		
7404-Sh	2.6	-4.6			
8952-Sh	2.1	-3.6			
9438-Sh	1.8	-5.6			
9791-Sh	1.6	-5.3			
10102-Sh	2.4	-5.0			
10120-Sh	2.5	-5.2			
RV-1-Sh	2.0	-4.4	0.70750		
RV-2-Sh	2.1	-4.3			
RV-3-Sh	2.0	-4.5			
R-H-1-Sh	1.9	-4.9		354	37
R-H-2-Sh	1.8	-5.3			
R-H-3-Sh	1.5	-5.3			
BH-104-Sh			0.70749		

Sh: rudist shell M: Calcite Matrix

Chapter 4

The Diagenetic History and Reservoir Potential of the Mid-Cretaceous Sarvak Formation in Southern Iran

4.1. Introduction

The Mid-Cretaceous Sarvak Formation in southern Iran represents a carbonate ramp/shelf that developed at the northeastern edge of the Arabian Plate. Various types of porosities observed in these carbonates were created through extensive porosity and permeability enhancement by karstification.The upper part of the formation is marked by the presence of the Turonian unconformity that prepared the ground for widespread meteoric diagenesis (Hajikazemi et al., 2010).

The regional Turonian unconformity greatly influenced the diagenesis including the development of porosity, and hence the reservoir characteristics (Hajikazemi et al., 2010). In spite of previous studies on the Sarvak Formation, the diagenetic history and evolution of these heterogeneous carbonate rocks is not well understood and warrant further investigation.

The carbonate platform was periodically subaerially exposed, particularly during the Cenomanian-Turonian, resulting in the formation of economically significant secondary porosity (Hajikazemi et al., 2010). In Chapter 2 of this thesis we emphasised on the role of palaeoexposure surfaces and unconformities on reservoir development and modification and how the special climate conditions (i.e. Greenhouse conditions) dominated the Mid-Cretaceous affected Sarvak carbonates. In this study we carried out a detailed diagenetic study of the Sarvak Formation in basinal context using cement petrography and geochemistry including trace element content and stable isotopic composition at selected localities in southern Iran, where the effects of the unconformities were documented. This investigation is focused on the diagenesis of the Sarvak succession including carbonate cement precipitated in the vugs, moulds and fracture system in order to gain insight into the origin of cement and other diagenetic processes and their effect on reservoir characteristics and also to determine the nature of the fluids involved. A combination of

petrographic and isotope data is utilized in this study to help unravel the diagenetic history of the Cenomanian-Turonian carbonate in southern Iran. Precipitation of carbonate cements also provides a record of environmental conditions via the preserved fabrics and the stable isotope geochemistry (James and Choquette, 1987; Allan and Matthew, 1982; Moore, 1989).

4.2. Regional Geological Setting

The Sarvak Formation was deposited during Cenomanian- early Turonian time, on an extensive platform within intrashelf basins on the passive margin of the Arabian Plate (Setudehnia, 1978; Ziegler, 2001 See Fig. 4.1a for lithofacies map). One of the remarkable features of the Cretaceous carbonate platforms including the study area was the development of facies complexes dominated by rudist-foraminifera bioherms (Motiei, 1993; Hajikazemi et al., 2010).

Sea level changes, local tectonics and salt diapirism affected the formation thickness and facies variations (Burchette, 1993; Farzadi and Hesthmer, 2007). Sedimentation rates varied considerably, from low to high, as determined from isopach maps of Mid-Cretaceous strata (Koop and Stonely, 1982; Ghazban, 2007). This suggests periods of instability, characterized in some areas by active salt tectonism and extensive erosion. Paleo-highs in the basement structures also influenced basin configuration and topography and modified facies distribution (Taghavi et al., 2006).

The late Cenomanian was marked by the initiation of tectonic activity and major continental collision in the region. Periodic emergence and substantial erosion occurred after the regional exposure of the Sarvak carbonates removing the upper part of the succession in many areas with erosion of older paleoexposure surfaces. The presence of two unconformities has been recognized including a regional Turonian unconformity marked by a palaeosol and a local Cenomanian-Turonian boundary break (Beiranvand et al., 2007; Taghavi et al., 2006; Motiei, 1993; Hajikazemi et al., in press). The two unconformity surfaces show a cross-cutting relationship and display clear evidence of deep erosion and significant truncation (Hajikazemi et al., 2010). Similar horizons and evidence of the presence of this unconformity have also been described from other areas in the Persian Gulf region (Harris et al., 1984).

4.3. Sarvak Stratigraphy and Depositional Environment

The Sarvak Formation consists of different carbonate units with a thickness of 821 m at the type section locality in Bangestan Mountain (Motiei, 1993). The formation conformably overlies the Kazhdumi Formation with a transitional contact whereas the upper contact in the type locality is unconformably overlain by marls of the Gurpi Formation of Maestrichtian age.

The lower part of the formation has a thickness of about 255 m and is composed of argillaceous micritic limestones with lenticular bedding and thin-layered marl interbeds. The middle part (525 m thick) consists of massive chalky limestones with iron-rich siliceous nodules and rudist fragments. The top 42 m includes massive limestone with the topmost strata consisting of a weathered brecciated ferruginous limestone. An unconformity occurs at the top of the Sarvak Formation marking the boundary between the Sarvak Formation and the overlying strata. This unconformity is associated with pedogenesis, brecciation, karstification, fluvial features and hematite and Fe-Mn nodule development.

The formation was deposited in a shallow marine ramp setting, and records four main depositional environments: inner-ramp, mid-ramp, outer-ramp and open marine or basinal environment (Taghavi et al., 2006; Hajikazemi et al., 2010). Each environment is characterized by several microfacies. The benthic foraminiferal wackestone and packstones of the inner-ramp environment are the dominant microfacies. Rudist biostromes and sedimentary features such as burrowing and geopetal fabric are abundant in this environment.

Mid-ramp facies are mainly restricted to the Upper Sarvak Formation whereas outer-ramp facies are more dominant in the Lower Sarvak Formation but also occur in the lower part of the Upper Sarvak Formation. The basinal environment is represented mostly by Oligostegina wackestone/packstone in the lower Sarvak Formation.

4.4. Methods

Over 380 thin sections were examined using transmitted light and cathodoluminescence (CL) microscopy. The studied samples were collected from the type section located in Bangestan Mountain as well as additional surface sections with good exposure at Shahneshin Mountain and various subsurface localities in southwestern Iran (Rag-e Sefid and Bibi Hakimeh oil fields) and Sirri D oil field in northeastern Persian Gulf (Fig. 4.1b).

The carbonate units at the type section locality and cores from the four wells were logged and sampled based on facies and/or diagenetic variations. Cathodoluminescence microscopy of over 100 representative samples was performed using a Technosyn 8200 MKII model cold cathodoluminescence stage with a 12-15 kv beam and a current intensity of 420-430 μA on the unstained halves of the uncovered thin sections.

Core samples were impregnated with an epoxy mixed with blue dye for porosity identification. Microscopic observations of thin-sections were carried out to reconstruct the paragenetic sequence, focusing on cementation.

Calcite cements and dolomites were micro-sampled using a microscope-mounted dental drill assembly. Only cements with large enough dimensions that were sufficiently abundant were sampled from the bulk rock for analysis. Powdered samples were reacted with 100% pure phosphoric acid at 25°C for calcite and 50°C for dolomite for 4 hours (Al-Aasm et al., 1990) and the evolved CO_2 gas was analyzed for stable oxygen and carbon isotopes using a Finnigan Mat Delta Plus mass spectrometer. Replicate analyses using these procedures and comparisons with laboratory standards are within 0.05‰ for both $\delta^{18}O$ and $\delta^{13}C$ values. All analyses for oxygen and carbon isotopes are reported in per mil (‰) notation relative to the Vienna Pee Dee Belemnite (VPDB) standard. Precision for both isotopes was better than 0.05‰.

Major and trace elements data were obtained using an ICP-MS at Great lake Environmental Research Institute, University of Windsor. Each sample was weighed, reacted with 2gr of 5% HNO_3 and diluted with 3 mL of twice-distilled water. Calibration of the ICP-MS was achieved using well characterized rock reference materials and a procedural blank, selected to cover the range of elemental concentrations expected in samples. Data are reported as weight percent.

4.5. Major Diagenetic Processes

Based on field and petrographic investigation, a variety of diagenetic features and minerals, most notably multiple generations of calcite cement and dolomite has been recognized in this study. Calcite is the most abundant pore-filling mineral, and its distribution has an important influence on reservoir quality. Other diagenetic constituents include dolomite and minor pyrite. Pore and fracture-filling cements, stylolites, and crosscutting relationships were carefully documented in order to reconstruct the syn-to post-depositional evolution of the Sarvak carbonates.

The paragenetic sequence of Sarvak carbonates is based on standard petrography, cathodoluminescence and geochemical considerations and is summarized in Figure 4.2. The timing of diagenetic events is subjective and is based primarily on textural relationships. The most important diagenetic events which have influenced the reservoir characteristics of these strata could be summarized as follows: dissolution, compaction, recrystallization, fracturing, dolomitization, pyrite formation and calcite cementation.

4.5.1. Dissolution and Porosity Development

Dissolution is a common diagenetic feature of the Sarvak carbonates in surface and subsurface sections. It is the most important diagenetic process creating porosity which varies from 0.5% to more than 20% (obtained from petrography of the surface section samples and core analysis). Porosity is mainly secondary, dominated by vuggy, mouldic, and intercrystalline types. Vugs are sub-spherical or irregular in shape reaching up to a few centimetres in size. Cavernous porosity is present below the unconformity surface (Fig. 4.3a). Dissolution also enhanced the matrix porosity with moulds and vugs which may be totally or partially filled with calcite cement or bitumen (Fig. 4.3b). The main cavity of the rudists and chambers of some foraminifera form the most important interaparticle porosity (Fig. 4.3c).

4.5.2. Mechanical and Chemical Compaction

Evidence of mechanical and chemical compaction is observed in the Sarvak Formation. Mechanical compaction causes porosity reduction by fusing or breakage of the grains and reducing the interparticle porosity in some packstones. Dissolution seams and stylolites are the most common chemical compaction features especially in mud-supported rock units of the Upper Sarvak Formation. Our core studies show the role of these stylolites in enhancing the porosity and permeability and acting as conduits for hydrocarbon migration (Fig. 4.3d).

4.5.3. Carbonate Matrix Recystallization

Recrystallization is rare. However, partial recrystallization of micrite matrix, which enhanced the crystal size of the matrix, has been observed in some intervals especially immediately below the unconformity surface and sometimes adjacent to stylolites. This could indicate the dual origin (meteoric and burial) of this diagenetic process. Recrystallization is locally important in reducing the primary matrix porosity by enhancing the size of the micrite to larger calcite crystals with no porosity between the crystals.

4.5.4. Fracturing

Fractures are one of the most important types of secondary porosity in the Upper Sarvak Formation. Fractures are distributed in different directions and vary from vertical to sub vertical and horizontal. Widths range from hairline up to few centimetres wide. The first dominant set (fracture I) includes vertical to sub-vertical fractures which have a wider opening (more than 2 mm in some core samples and few centimetres in surface sections) compared to the second set (fracture II) which are usually horizontal. The first set is partially or completely filled with calcite cement. The latter cross-cuts the earlier set. Apertures do not exceed few micrometers and are devoid of cement. This second set also postdates the formation of stylolites and dissolution seams (Fig. 4.3e).

4.5.6. Dolomitization

Dolomitization is not a common processes in the Sarvak Formation in the studied sections, however three types of dolomite are recognized; (a) fine crystalline dolomite cement (up to 20 μm in size) filling the interparticle porosity in brecciated intervals underlying the unconformity; (b) subhedral-euhedral fine to medium-crystalline (40-60 μm) clear dolomite replacing carbonate matrix in association of dissolution seams, and (C) euhedral medium-crystalline cloudy center, clear rim dolomite with crystal size reaching 70 μm or greater. Dolomite which replaces the calcite matrix in argillaceous carbonate interbeds is mainly associated with stylolites. This latest generation of dolomite is common in subsurface sections and causes the enhancement of intercrystalline secondary porosity and usually hydrocarbon fills the porosity between the dolomite crystals (Fig. 4.3f). Only the latest dolomites were sampled for carbon and oxygen stable isotope analysis due to its abundance.

4.5.7. Pyrite Formation

Two types of pyrite were recognized in the Upper Sarvak Formation, microcrystalline framboidal pyrite which is more common below the unconformity surfaces and coarse crystalline pyrite which replaces either the matrix or calcite cement in subsurface sections. Both types of the pyrites are not very widespread. Framboidal pyrite consists of numerous spheroidal clusters of small, equant individual microcrysts (Fig. 4.4a). Coarse crystalline pyrite occurs as euhedral crystals which partially replace the calcite matrix or the fracture-filling calcite cement in some intervals suggesting their formation during the later stages of diagenesis and affects the reservoir characteristics by reducing the porosity (Fig. 4.4b).

4.5.8. Calcite Cementation

Calcite cements in the Sarvak Formation display different petrographic characteristics. Five types of calcite cements are recognized: (1) fine crystalline isopachous rim cement , which are not very common, surrounding skeletal grains in grainstones; (2) fine to medium crystalline equant calcite cement, filling the interaparticle pores of the skeletal grains in packstones or some interparticle pore spaces in grainstones; (3) syntaxial overgrowth calcite which is rare , surrounding some of echinoid fragments in grainstones; (4) drusy mosaic calcite, filling most of the fractures, some vugs and moulds; and (5) coarse blocky sparry calcite cement (Fig.s 4.4c-f).

The fine crystalline isopachous rim cement is non-luminescent under the CL. Equant calcite cements consist of dark to non-luminescent crystals with thin bright luminescent rims surrounding them projecting toward the center of the pores. Syntaxial overgrowth calcite commonly appears to be non-luminescent.

The drusy mosaic calcite cement composed of alternating of dull to non-luminescent and bright orange to yellow highly luminescent bands. Based on CL characteristics the drusy mosaic calcite cements are zoned indicating precipitation from fluids with slightly different chemistry (i.e., concentrations of Mn and Fe ions, Veizer et al., 1999) or changes in the environmental conditions (Machel et al., 1991).

Coarse crystalline blocky sparry calcite cement is the latest cement that partially fills remaining voids within the earlier set of fractures and some rudist body cavities. This cement phase also partially or completely fills some vugs which reduces the porosity and affect the reservoir quality. This calcite cement is commonly ferroan and characterized by dull to non-luminescent crystals. In core samples this type of cement is observed along stylolites. Two phase fluid inclusions are visible in some of the larger crystals, indicating a minimum temperature of 50°C for their formation.

Whereas some of the cements which occurred adjacent to stylolites are assumed to be formed in the burial history, two-phase fluid inclusions and cross-cutting relationships confirm that they must be a component of later precipitation of cement under higher ambient temperatures compared to earlier cements (Fig.4.5).

Precipitation of drusy mosaic and blocky calcite cements was volumetrically the most important diagenetic process in these rocks. These cements were selected for geochemical

analyses due to their size and abundance, which allowed relatively straightforward sampling without contamination by surrounding matrix. Obtaining samples from earlier cement types was not possible due to their less abundance and small crystal sizes.

4.6. Geochemistry

Modification of stable carbon and oxygen isotopes and trace element chemistry during diagenesis serves as an important clue to the diagenetic processes. The concentration of Ca, Mg, Mn and Sr, $\delta^{13}C$ and $\delta^{18}O$ values and $^{87}Sr/^{86}Sr$ ratios were determined in rudist shells, matrix as well as cement in order to recognize the diagenetic environments and their significance. Thus, by determining the isotopic values of original marine carbonates and different type of calcite cements, it is possible to elucidate the diagenetic history of the carbonates. Based on the CL characteristics, the rudist shells and matrix carbonates have not been affected by later alteration. However, the calcitic matrix immediately below the unconformity surfaces and adjacent to them are luminescent, while the majority of the matrix have not been affected and appear to be predominantly non-luminescent, which also provides further evidence of pristine marine calcite phases (Machel, 1991).

The $\delta^{13}C$ and $\delta^{18}O$ values for all the samples analyzed are summarized in Tables 4.1, 3.1 and 3.2 and shown in Figures 4.6 to 4.8.

4.6.1. Depositional Components

The data presented here expands upon previously reported data in Chapters 2 and 3with the $\delta^{13}C$ and $\delta^{18}O$ values of the calcite matrix range from -6.4‰ to +4.1‰ and -9.4 to -0.9‰, respectively. Compared to the postulated $\delta^{13}C$ and $\delta^{18}O$ values of Mid-Cretaceous marine carbonates (Veizer et al., 1999), the $\delta^{13}C$ values of matrix carbonates of the Sarvak Formation fall well within the range of marine carbonates (0 to +4‰ PDB for Mid-Cretaceous), whereas the $\delta^{18}O$ values reflect a 1‰ to 2‰ depletion. Figure 4.6 reveals that there is significant isotopic compositional overlap between various carbonate phases.

Nineteen samples of rudist shells from different intervals in the wells and surface sections were micro-sampled for $\delta^{13}C$ and $\delta^{18}O$ and $^{87}Sr/^{86}Sr$ and elemental analysis. The results (Table 3.2) have been used as a proxy for marine carbonate value to compare different type of cements (see the discussion on $\delta^{18}O$ values). This is based on the assumption that rudist shells have potential for stable isotope preservation because their outer shell layer originally consisted

of diagenetically stable low-Mg calcite (Al-Aasm and Veizer, 1986b). The $\delta^{13}C$ and $\delta^{18}O$ values of the rudist shells range from 1.3‰ to 2.7‰ and -5.6‰ to -3.0‰ PDB, respectively. The range of isotopic compositions of the rudist shells is similar to the range of marine carbonates of Mid-Cretaceous age presented by Veizer et al. (1999).

4.6.2. Calcite cements

Sampling for stable isotope data was focused only on drusy mosaic and blocky calcite cements. Drusy mosaic calcite cements display $\delta^{13}C$ and $\delta^{18}O$ values ranging from -5.8 ‰ to 3.6‰ and -9.3‰ to -0.6‰ PDB, respectively (Fig. 4.7). The $\delta^{13}C$ and $\delta^{18}O$ values for the blocky calcite cement range from -2.4‰ to +3.6‰ and from -12.3‰ to -2.8‰, respectively (Fig. 4.7). Calcite cements display a wider range in $\delta^{13}C$ and $\delta^{18}O$ values compared to the calcite matrix. Some of the blocky calcite cements display pronounced negative $\delta^{18}O$ values compared to matrix and drusy mosaic cements and $\delta^{13}C$ values show a significant overlap with other carbonate components.

The plot of $\delta^{13}C$ vs $\delta^{18}O$ of the blocky calcite cements from the vugs and fractures illustrate three distinct fields of values (Fig. 4.8). Group 1 includes four samples of the blocky calcite cement and shows the most negative values for $\delta^{13}C$ and $\delta^{18}O$ among all blocky cements. Group 2, consists of 5 samples and exhibits the most positive $\delta^{13}C$ and $\delta^{18}O$ values which are compatible with Mid-Cretaceous carbonates. Group 3 of the blocky calcite cement contains the largest number (17) of samples and the range of values is not very wide, with $\delta^{13}C$ and $\delta^{18}O$ exhibiting a relatively narrow range of values. The stable isotope analyses could be used to investigate the differences between various blocky calcites cements and their precipitational conditions or environments.

4.6.3. Dolomite

Nine samples of dolomite (III), which are the most abundant dolomite in the Upper Sarvak Formation in the studied sections, were analyzed for stable carbon and oxygen isotopes. The $\delta^{13}C$ ranges from +1.5 to +5.0‰ PDB and $\delta^{18}O$ ranges from -7.3 to -3.4‰ VPDB (Table 4.1 and Fig. 4.9).

4.6.4. Palaeosol

Five samples of Palaeosol (in the form of bauxite, laterite and carbonate soil)from below the unconformity surface in the Shahneshin surface section were analyzed and yielded $\delta^{13}C$ and $\delta^{18}O$ values of -5.7 to -2.9 ‰ VPDB and -6.1 to -4.2‰ VPDB, respectively (Table 4.1).

4.7. Interpretation of Isotope Geochemistry

The diagenesis of the Sarvak Formation is noteworthy because of its role in reservoir characteristics of this formation. We interpret the diagenesis of the Sarvak Formation based on the geochemical results obtained from the depositional components (i. e., rudist and carbonate matrix) and also the diagenetic components including calcite cements and dolomites.

Based on an integration of CL petrographic observations and the diagenetic tracers ($\delta^{18}O$, $\delta^{13}C$, $^{87}Sr/^{86}Sr$ ratios and trace elements), we have interpreted cement precipitation and the fluid evolution history of the Sarvak Formation.

4.7.1. Diagenesis of depositional components

Diagenetic processes in carbonates generally produce phases with more negative $\delta^{18}O$ and $\delta^{13}C$ comparing to original marine carbonate. Therefore, it has become an indication to many workers (e.g., Veizer et al., 1999) that samples of marine carbonate with the most positive $\delta^{18}O$ and $\delta^{13}C$ are the least altered. High $\delta^{13}C$ values from the Upper Sarvak are typical of Cenomanina-Turonian carbon isotopic compositions (Arthur et al., 1990; Scholle and Arthur, 1980). The Mid-Cretaceous carbonates are characterized by warm-water depositional conditions and are therefore expected to have formed from seawater typical of lower latitudes, resulting in depositional $\delta^{18}O$ values in the range -4 to -1‰ (Veizer et al., 1999). The lack of negative $\delta^{13}C$ values in most of the matrix samples (other than the ones taken at or close to palaeoexposure surfaces) does not support diagenesis in meteoric environment, because this would have involved a substantial decrease in $\delta^{13}C$ (e.g. Allan and Matthews, 1982; Al-Aasm and Veizer, 1986b).

In carbonates, the isotopic composition of waters involved in precipitation is the most important control meaning that the $CaCO_3$ precipitated in marine waters is often enriched in ^{13}C and ^{18}O relative to fresh and brackish water precipitates.

The least negative $\delta^{18}O$ values obtained here could indicate original (marine) carbonate precipitation. In addition, the most positive $\delta^{18}O$ and $\delta^{13}C$ values, found in the non-luminescent

rudist shells, considered the most pristine samples. The variations in $\delta^{13}C$ values observed here are most likely a reflection of original differences in terms of the amount of microbial activity and organic matter incorporated into the marine carbonate at the early stages of diagenesis. Petrographic examination of the samples also suggests that the matrix samples have not been altered by diagenesis except those sampled immediately below the unconformity surfaces (Hajikazemi et al., in press).

The $\delta^{18}O$ signature of the majority of the samples obtained from calcite matrix is mainly interpreted as original signature (Hajikazemi et al., in press). Most of the matrix data presented in Figure 4.10 show no definite correlation between $\delta^{18}O$ values and Mn concentrations also implying that these analyses represent a sample suite of marine carbonates that have not been significantly altered, and shows the original signature of marine carbonates. Mn is additionally assumed to be a main activator of orange-red cathodoluminescence distinctive of diagenetically altered calcites (Savard et al., 1995). Since oxygenated seawater is low in Mn, marine carbonates are non-luminescent, however Mn concentrations are higher in meteoric waters and thus meteoric calcites are luminescent. Diagenetic alteration can cause an increase in Mn concentrations in low-Mg calcite because this element becomes soluble under reducing conditions (Marshall, 1992). Further support is provided by the data obtained from the rudists shell material showing no alteration.

Manganese contents are very low in the investigated samples (2-40 ppm in majority of measured samples). The low Mn values obtained from calcite matrix and the cements are consistent with little diagenetic alteration. Because Mn incorporates into calcite only in its reduced state, its presence indicates precipitation under reducing conditions. Generally, Mn occurs in much low concentrations in modern calcite (i.e. < 200 ppm) while the elevated levels of Mn within biogenic calcite have been linked with diagenetic alteration (Brand and Veizer, 1980; Morrison and Brand, 1986). The Upper Sarvak carbonates are Mn-poor, consistent with no alteration in an oxidized environment.

Changes in organic carbon reservoir size can lead to global $\delta^{13}C$ shifts (e.g., Kump, 1991). Abnormally high rates of oceanic crust production and the formation of large igneous plateau led to high and rising levels of atmospheric CO_2 and increased hydrothermal fluxes to the oceans. The Mid-Cretaceous is a time of extensive volcanic activity with fluctuations in the organic deposition.

During high global sea level, the exposed continent area was smallest and oxidized organic carbon in the exposed continent decreased, but the corresponding burial proportion relatively increased, and ^{12}C incorporated into buried organic carbon increased, increasing the $\delta^{13}C$ of carbonate sediments. When the eustatic sea level fluctuated, the $\delta^{13}C$ also fluctuated in the same manner. Thus, it is clear that $\delta^{13}C$ values and associated variations and changes can be indicators of eustatic sea-level changes.

4.7.2. Diagenesis of Calcite Cement and Dolomite

Detailed analysis of cements using petrographic and geochemical data makes it possible to determine changes in chemistry of the fluid(s) responsible for their precipitation and diagenetic history (Given and Lohmann, 1985).

A distinction between meteoric and marine diagenesis could be made by analysis of stable oxygen and carbon isotopes, as meteoric diagenesis is characterized by lower values of carbon and oxygen isotopes (James and Choquette, 1990). Meteoric influence can be accounted for by the presence of petrographic, geochemical and sedimentological criteria for subaerial exposure (Given and Lohmann, 1985).

Early diagenesis will not modify the $\delta^{18}O$ value if it occurs at similar temperatures to sea surface temperatures and in equilibrium with the original pore fluids in the carbonates. However, precipitation or recrystallization at higher temperatures during burial in the presence of later fluids moving through the rock can significantly modify the original $\delta^{18}O$. Likewise, diagenesis in the presence of later meteoric waters can also lead to a decrease in the $\delta^{18}O$ in regions that have experienced surface uplift since primary carbonate deposition. Thus, subaerial exposure and accompanied diagenesis could be the main reason for the changes in stable isotope and trace element geochemistry of the Sarvak marine carbonates (cf. Veizer, 1983a).

An interesting aspect of the calcite cements obtained from the Sarvak Formation is the more positive carbon values of some of the drusy mosaic calcite (Fig. 4.7) and blocky calcite cements (i.e., Group 1 in Figure 4.8 and Table 4.1) compared to the other cements.

Results of the $\delta^{13}C$ analysis of the above mentioned cements indicate clearly the marine origin for the fluids involved in precipitation of most of the cements. This conclusion is evident considering the $\delta^{13}C$ of the Mid-Cretaceous marine carbonates ranging between 0 and + 4‰ PDB (Arthur et al., 1988; Voigt, 2000). Further, this highly positive $\delta^{13}C$ values (i.e. 3.6‰ PDB) may

be related to the Cenomanian-Turonian positive carbon isotope event (OAE). The analyzed carbonate matrix and adjacent cements show isotopically different characteristics in some cases.The matrix commonly shows values similar to those of normal sea water while the cement in some cases shows heavier $\delta^{13}C$ values (Table 4.1, 3.1 and 3.2) similar $\delta^{13}C$ diagnostic of carbon excursion known for Mid-Cretaceous (Scholle and Arthur, 1980 and many others after).

The $\delta^{13}C$ of cements suggest that the bicarbonate supply was mainly from the dissolution of primary carbonates with 'marine' isotopic composition. Original $\delta^{13}C$ will remain essentially unchanged by diagenesis in sediments with low organic carbon content (Barrera and Keller, 1990). The narrow range of $\delta^{13}C$ values for majority of cacite matrix, the rudist shells, and some drusy mosaic and blocky calcite cements are similar to marine values. The marine cements do not appear to have been significantly modified by meteoric (depleted $\delta^{18}O$ and $\delta^{13}C$) water throughout their diagenetic history. These cements may have precipitated and /or reequilibrated with relatively low temperature, $\delta^{18}O$ depleted waters that could have entered the reservoir during and after Cenomanian-Turonian and Turonian unconformities. A highly positive carbon in some cement could be the effect of the global carbon excursion in Cenomanian- Turonian boundary (Scholle and Arthur, 1980; Jenkyns et al., 1994).

Diagenesis appears to have affected geochemical characteristics of these rocks without homogenizing the $\delta^{13}C$ values within the cements. Since carbon is a major component of carbonate rocks and a minor component of sedimentary fluids, the $\delta^{13}C$ signature of carbonates is much less susceptible to alteration due to water-rock interaction than $^{87}Sr/^{86}Sr$ or $\delta^{18}O$. Consequently, carbonate successions that undergo diagenetic stabilization with a low water-rock ratio are unlikely to have $\delta^{13}C$ completely reset or homogenized. Magaritz (1983) found that $\delta^{13}C$ was not appreciably decreased until the water-rock ratio was raised to 1000 or more. This characteristic of carbon isotopes could explain the formation of most of the drusy mosaic calcite and Group 2 of blocky calcite cement with $\delta^{13}C$ values same as marine calcite but more depleted $\delta^{18}O$ values which could indicate the precipitation of these cement in mixed marine-meteoric environment.

A likely mechanism that could cause $\delta^{13}C$ depletion in Group 1 of blocky and some drusy mosaic cements is meteoric diagenesis associated with oscillations in sea level that episodically exposed the shallow-water carbonates. The presence of paleoexposure surfaces in the Upper Sarvak is confirmed by formation of pedogenic-fluvial features and negative $\delta^{13}C$ values that are linked to the unconformity (Hajikazemi et al., in press). The isotopic composition of pedogenic

carbonate cement is controlled by the primary $\delta^{13}C$ of the atmospheric CO_2-derived bicarbonate in the meteoric water. The $\delta^{13}C$ values of carbonate cements often decrease due to an influx of atmospheric-derived CO_2 with its distinctive low $\delta^{13}C$ values. Therefore, this could explain the negative values of carbon isotopes in some blocky and drusy mosaic calcite and their precipitation from meteoric fluids corroborating the conclusion drawn from the CL results and trace elements (i.e. lower concentrations of Sr, see Table 4.1 for values).

The narrow range of $\delta^{13}C$ observed from each blocky calcite cement generation (Group 1-3) indicates the precipitation of carbonate cements from fluids with small isotopic variations. Minor changes and less negative values in $\delta^{13}C$ of the most of calcite cement rules out any organic carbon being utilized as a major source for carbonate carbon.

A plot of Sr/Ca ratio vs. Mn concentration for the Sarvak carbonates presented in Figure 4.10 shows no particular trend in Sr/Ca ratio vs. Mn concentration. Veizer (1983a) used such a plot to illustrate alteration of marine carbonates by meteoric water showing a diagenetic trend of a decrease in Sr/Ca ratio associated with an increase in Mn concentration. Likewise, if Mn concentration was a proxy for alteration by fresh water, a plot of $\delta^{18}O$ vs. Mn concentrations would show a negative correlation. Lack of such correlation suggests the precipitation of most of the cements from marine or marine-like (mixed marine-meteoric) fluids.

The $\delta^{18}O$ values may provide important information pertaining to the temperature and origin of fluids from which calcite cements are precipitated. The $\delta^{18}O$ values of carbonate cements often decrease with increasing temperature because as the environment get warmer, minerals acquire lower $\delta^{18}O$ values due to temperature-sensitive isotope fractionation between formation water and carbonate minerals. Correspondingly, if the temperatures of precipitation are known, the $\delta^{18}O$ of precipitating water can be determined.

The $\delta^{18}O$ thermometry suggests that mean sea surface temperatures (SSTs) were highest during the Cretaceous thermal maximum, mostly in Turonian time (Huber et al., 2002; Wilson et al., 2002). The climate during the Mid-Cretaceous was unusually warm by today's standards, while the global average surface temperatures were more than 10°C higher than today (Barron, 1987; Bice and Norris, 2002). Global climate changes at this time have been linked to changes of oceanic water temperature and to changes in atmospheric CO_2 (Arthur et al., 1988; Bice and Norris, 2002). Thus, warm oceanic temperatures that characterize the Mid-Cretaceous greenhouse

conditions appear to have been existed during initial precipitation and diagenesis of the Upper Sarvak Formation.

Since the $\delta^{18}O$ of calcite is dependent on the temperature of the water from which it is precipitated.Based on the $\delta^{18}O$ values obtained from rudist shells, we calculated a temperature range of 25 to 36°C for mean SSTs during Sarvak sedimentation which happened in the global greenhouse period.These temperatures are in accordance with the data from other workers in theTethyan region (e.g., Steuber, 1996; Wilson and Norris, 2002; Immenhauser et al., 2005; Forster et al.). The setting is in a shallow marine environment and naturally represents a very warm environment compared to the deep oceans. The $\delta^{18}O$ of the calcite precipitated at these palaeotemperatures have been determined using the equation provided by O'Neil et al. (1969) and compared with the analyzed values. This expresses the $\delta^{18}O$ values of the water ($\delta^{18}O_{water}$), directly relative to the SMOW standard:

$$1000 \ln \alpha = (\delta^{18}O_{Calcite} - \delta^{18}O_{water}) = 2.78 (10^6 T^{-2}) - 2.87$$

The marine calcite cements precipitated at the above temperatures, assuming seawater compositions for the Mid-Cretaceous (no ice build-up) of -1.2 ‰ SMOW (White et al., 2001) and normal sea water (i.e., $\delta^{18}O = 0$) give a $\delta^{18}O$ range from -1.0 to -5.7‰PDB. It is important to note that the $\delta^{18}O$ values of rudist shells also fall within this range ($\delta^{18}O$ = -3‰ to -5.6‰VPDB) and the $\delta^{18}O$ range for calcite cements represents precipitation from marine waters. The majority of the cements shows $\delta^{18}O$ ratios between -1.2‰ and -5.5‰ PDB (see Figure 4-11), indicating their precipitation from fluids with approximate seawater signature. $^{87}Sr/^{86}Sr$ ratios measured in the carbonate cements vary little and fall well within the Cenomanian-Turonian portion of the secular seawater curve of Veizer et al. (1999) (see Table 4.1).

Based on the graphical presentation in Figure 4-12, more negative $\delta^{18}O$ values obtained from the cements could be explained either by precipitation from a fluid with lighter $\delta^{18}O$ than coeval seawater or higher temperature. One possible source of diagenetic fluids with lighter $\delta^{18}O$ values is meteoric water that could conceivably have infiltrated Sarvak strata as a consequence of subaerial exposure due to sea level fall combined with regional uplift. The $^{87}Sr/^{86}Sr$ ratios of some of the cements ($^{87}Sr/^{86}Sr > 0.7084$) are considerably more radiogenic than known from Mid-Cretaceous sea water values defined in this study and also by the other workers (e.g.,Derry et al., 1989; Veizer et al., 1999; McArthur et al., 2000). These cements are closely associated with

paleoexposure surfaces and show negative or more depleted $\delta^{13}C$ values. Thus, the $\delta^{18}O$ of some of the calcite cements might indicate local meteoric water influence.

Estimation of the ancient meteoric water composition depends on palaeolatitude and palaeotopography at the time of recharge, as well as the degree of water-rock interaction in the infiltration zone. During the Mid-Cretaceous, the study area was at an equatorial region, with warm climate. Thus, the $\delta^{18}O$ of meteoric water existed at this time could not have been less than -6‰ (White et al., 2001), while the global average temperature could have been from 12 to 20.8°C (Frakes et al., 1992; Donnadieu et al., 2006) and the palaeotemperature obtained from palaeosol in the area is between 22 and 29°C. Considering all these temperature data, it can be deduced that the calcite cements precipitated in equilibrium with meteoric waters could have $\delta^{18}O$ values ranging from -5 to -9 (Fig. 4.12). The $\delta^{18}O$ of pedogenic carbonate ($\delta^{18}O$ of palaeosol; -9.1 to -3.7‰) which certainly indicates meteoric water influence almost agree with such an interpretation. The $^{87}Sr/^{86}Sr$ ratios of pedogenic carbonates ($^{87}Sr/^{86}Sr > 0.70812$ and 0.70817) are also more radiogenic than the Mid-Cretaceous marine values. It has been shown that the $\delta^{18}O$ values of pedogenic carbonates are more susceptible to alteration than $\delta^{13}C$ values during diagenesis in the oxygenated zone (Morad et al., 1990). However, there is a possibility that the $\delta^{18}O$ of some of the cements represent the mixed marine- meteoric environment.

After extensive uplift and paleoexposure, the isotopically heavy water could have been flushed out of the system, replaced by lighter fluids responsible for precipitation of ^{18}O depleted calcite cements. Deposition of Laffan shales and Ilam carbonates on top of the Sarvak Formation indicate that following subaerial exposure, the Sarvak formation was flooded by marine water and additionally the platform may have been subjected to shallow burial diagenesis. Precipitation of calcite cements with $\delta^{18}O$ as light as -12‰, could be explained by an increase in temperature. Meteoric diagenesis of marine carbonates typically results in a shift towards more negative values of both $\delta^{18}O$ and $\delta^{13}C$ (Anderson and Arthur, 1983), whereas burial diagenesis produces appreciably larger shifts in $\delta^{18}O$ values than meteoric diagenesis, but $\delta^{13}C$ values do not change appreciably (e.g. Choquette and James, 1987). Elevated temperatures would imply precipitation during burial. To precipitate such isotopically depleted cements from pore fluids, the temperatures might have reached ~ 50°C. Therefore 50°C can probably be taken as the lower limit for cement precipitation. However, if there was a change in the isotopic composition of the fluids then higher temperature for cement precipitation is required.The maximum possible temperature during precipitation of these dolomites is near 85°C, assuming precipitation from aA

marine fluid. This is also in accordance with the presence of two-phase fluid inclusions in some of the cements indicating their formation under higher ambient temperatures compared to earlier cements.

In reality, the pore water at this time was probably an isotopically evolved mixture of marine and meteoric-derived waters, with a greater component of meteoric derived water toward the Mid-Cretaceous unconformities and greater component of depositional marine-derived pore water down section. Thus, we assume that the minimum temperatures for the calcite precipitation would be at least 50°C corresponding to about 1 km depth of burial.

Stable isotope analyses are important in interpreting the nature of the fluids responsible for precipitation of the Sarvak dolomite cements. This diagenetic event appears to be directly tied to fluid events related calcite cementation.

A possible carbon source for dolomite includes dissolved bicarbonate in the marine depositional water and bicarbonate production related to the modification of organic matter. The $\delta^{13}C$ values of the dolomite cements are relatively constant and generally fall into the upper range of values obtained from associated limestones. Thus, $\delta^{13}C$ values of the dolomites are indicative of marine source for their carbon. The dolomites have positive $\delta^{13}C$ values, probably as a result of their precipitation in equilibrium with subsurface fluids, with the source of carbonates being the primary marine carbonates.

The $\delta^{18}O$ values of dolomites are lighter than values of typical marine $\delta^{18}O$ value (0‰); including Mid-Cretaceous marine carbonates (see Table 4.1). Such light values are not expected for dolomite compared to calcite theoretically co-precipitated from the same parent fluids (Land, 1985). Calcite co-exisitng with dolomite often has "lighter" values than associated dolomite and in such a case dolomite should be enriched in $\delta^{18}O$ by at least 4‰ relative to calcite (Hoefs, 1987). Extrapolation from high temperature experiments and observations on sedimentary dolomite-calcite pairs predict an ^{18}O-enrichment of 5-7‰ per mil in the dolomite compared to calcium carbonate deposited in the same environment.

According to Zhou and Zheng (2006) almost constant fractionation values of ~ 2.73‰ occur at temperature range between 0 to 100°C between dolomite and calcite, indicating the fractionation between these carbonate phases are insensitive to temperature, with the nearly constant ^{18}O enrichment in dolomite relative to calcite at equilibrium. This indicates that the

isotopic composition of the Sarvak dolomite cement was determined by an isotopic equilibrium different from the extrapolated dolomite-water equilibrium. It is proposed that secondary dolomites precipitated as protodolomites and that their oxygen isotopic composition was controlled by the protodolomite-water fractionation. Experimental data demonstrate that the isotopic difference between protodolomite and $CaCO_3$ is considerably smaller than that between dolomite (extrapolated) and water; this could explain the observed small differences of the oxygen isotope composition between secondary dolomites and associated limestones (see Fritz and Smith, 1970; Moore, 1990, p.81).The $\delta^{18}O$ value of low temperature, hydrothermal dolomite (Hall and Friedman, 1963) and Holocene dolomites (Epstein et al., 1964) were invariably equal to, or slightly greater than, the ratios of the co-exiting calcites.

Dolomites could have precipitated either in equilibrium with subsurface fluids depleted in $\delta^{18}O$ or with fluids of a similar composition to the present brines but at higher temperature. Thus, the light $\delta^{18}O$ values might be explained by a later precipitation of the dolomite during burial.The dolomite is interpreted to have formed by replacement of calcite matrix. The $\delta^{18}O$ range of these dolomites probably reflects varying compositions or temperatures of the waters involved. Due to the variable precipitation temperature of dolomite there have been variable degrees of diagenetic resetting of dolomite $\delta^{18}O$ values during diagenesis. As Land (1980, 1983) has pointed out, dolomite normally originates as a metastable phase (protodolomite) which is susceptible to recrytalization and isotopic re-equilibration during burial and diagenesis. Due to the original metastability, the isotopic composition of dolomite might reflect the nature of recrystallizing fluids, rather that the composition of the original dolomitizing fluids.

Using the paleotemperature equation for dolomite (Land, 1983), we can employ measured $\delta^{18}O$ values (ranging from -7.3‰ to -3.4‰) to estimate water's $\delta^{18}O$. We discount isotopic influence from solely meteoric water because of the inability of such waters to form dolomite. Thus, it is likely that the parent fluid for dolomite precipitation was of initially marine origin as this would require that marine water temperatures over 80°C. We tentatively conclude that dolomite was precipitated from fluids with $\delta^{18}O$ ranging from 0‰ to 6‰ at elevated temperatures typical of waters involved in burial diagenesis (Morad et al., 2003). Two phase fluid inclusions could be used to asses the temperature of cement or dolomite precipitation and composition of dolomitizing fluids, and provide a tie to a specific diagenetic environment.

Burial to a depth of approximately 1 km would be required to give a temperature of 50°C, assuming a geothermal gradient of 30°C/km. The alternative explanation for the negative $\delta^{18}O$ is

that dolomite formed during burial and could be interpreted as being of burial in origin, based on their geochemistry and their occurrence with stylolites. The $\delta^{18}O$ and $\delta^{13}C$ field of stylolite-associated dolomite overlaps with the matrix and calcite cement.

4.8. Conclusions

Petrographic and geochemical study of shallow water carbonates of the Mid-Cretaceous revealed that they have been subjected to diagenesis in different diagenetic environments. Carbonate cements precipitated within the Sarvak Formation record a diagenetic history starting with marine cementation, exposure to meteoric diagenesis and finishing with burial. The chemical and isotopic compositions of diagenetic the carbonate phases show variations in pore water composition during diagenesis.

The $\delta^{18}O$ shift observed in carbonate cement may record changes in the $\delta^{18}O$ of sea water, and the temperature changes in regional climate. These changes may have been promoted by sea level fluctuations, variation in climate, or burial. Stable carbon and oxygen and strontium isotopic compositions of the cements indicates that diagenetic fluids responsible for their precipitation ranged from marine, meteoric to mixed waters while some of the calcite cements formed from heated (burial) fluids.

The series of events that led to initial lithification, cement precipitation and creation and destruction of porosity can be summarized as follows:

(1) Deposition of shallow marine carbonates of the Upper Sarvak Formation during the Cenomanian-Turonian.

(2) Tectonic uplift and salt diapirism at the Ceomanian-Turonian boundary causing subaerial exposure of the Sarvak Formation, that allowed the influx of meteoric water into the carbonates. Due to the subaerial exposure, the carbonates were subjected to meteoric diagenesis, causing vast dissolution and precipitation of calcite cements.

(3) Marine transgression and relative sea-level rise during the early Turonain and precipitation of marine cement in pores and fractures.

(4) Sea-level fall and regional Turonian unconformity. Deep erosion and removal of the carbonates and their dissolution (i.e., porosity creation), later meteoric and mixed meteoric-

marine cement precipitation. The extensive Turonian unconformity and the paleoexposure surfaces are responsible for creation, enhancement and development of the favorable reservoir characteristics.

(5) Burial of the platform drawn with circulating sea-water providing a site for the precipitation of the last generation of blocky calcite cement in remaining pore spaces. During burial the temperature increased and pore waters became additionally depleted in ^{18}O.

(6) Dissolution and calcite cementation recognized in this study are the most abundant diagenetic processes and its distribution has the most important influence on reservoir quality.

4.9. Acknowledgments

We express our deep gratitude to the NIOC and NISOC for their kind assistance and making the field work possible and also access to the core lab. Funding for this project was provided by StatoilHydro. Additional funding was provided by Natural Science and Engineering Research Council of Canada (NSERC) to I. Al-Aasm and M. Coniglio.

4.10. References

Al-Aasm, I. S. and Veizer, J., 1986b. Diagenetic stabilization of aragonite and low-Mg calcite, II. Stable isotopes in rudists. Journal of Sedimentary Petrology, **56**, 763-770.

Al-Aasm, I. S, Tylor, B. E. and South, B., 1990. Stable isotope analysis of multiple carbonate samples using selective acid extraction. Chemical Geology, **80**, 119-125.

Allan, J.R. and Matthews, R.K., 1982. Isotope signature associated with early meteoric diagenesis. Sedimentology, **29**, 797-897.

Anderson T. F. and Arthur, A., 1983. Stable isotopes of oxygen and carbon and their application to sedimentologic and paleoenvironmental problems. In Stable Isotopes in Sedimentary Geology. Society of Economic Paleontologists and Mineralogists, Short Course No. 10. 111-151.

Arthur, M.A., Dean, W.E. and Pratt, L.M., 1988. Geochemical and climatic effects of increased marine organic carbon burial at the Cenomanian-Turonian boundary. Nature, 335, 714–717.

Banner, J. L., and Hanson, G. N., 1990. Calculation of simultaneous isotopic and trace-element variations during water-rock interaction with, applications to carbonate diagenesis. Geochimica et Cosmochimica Acta , **54**, 3123-3137

Barron, E.J., 1987. Cretaceous plate tectonic reconstructions. Palaeogeography, Palaeoclimatology, Palaeoecology, **59**, 3–29.

Barrera, E., and G. Keller, 1990. Stable Isotope Evidence for Gradual Environmental Changes and Species Survivorship across the Cretaceous/Tertiary Boundary, Paleoceanography, **5**(6), 867–890.

Beiranvand, B., Ahmadi, A. and Sharafodin, M., 2007. Mapping and classifying flow units in the upper part of the Middle Cretaceous Sarvak formation (western Dezful embayment, SW Iran) based on a determination of the reservoir types. Journal of Petroleum Geology, **30**, 4, 357-373.

Bice, K.L. and Norris, R.D., 2002. Possible atmospheric CO_2 extremes of the Middle Cretaceous (late Albian-Turonian). Palaeoceanography, **17**(4), 1070.

Brand, U., Veizer, J., 1980. Chemical diagenesis of a multicomponent carbonate system: 1. Trace elements. Journal of Sedimentary Petrology, **50**, 1219–1236.

Burchette, T.P., 1993. Mishrif Formation (Cenomanian-Turonian), southern Arabian Gulf: carbonate platform growth along a cratonic margin basin. In: Simo, J.A.T., Scott, R.W., and Masse, J. P. (editors): Cretaceous carbonates platforms. American Association of Petroleum Geologists, Memoir **56**, 185-199.

Choquette, P. W. and James, N. P., 1987. Limestones 3. The deep burial environment., Geoscience Canada, **14**, 3-35.

Derry, L.A., Brasier, M.D., Corfield, R.M., Rozanov, A. YU. and Zhuravlev, A. U. 1994. Sr and C isotopes in Lower Cambrian carbonates from the Siberian craton: A paleoenvironmental record during the'Cambrian explosion' Earth and Planetary Science Letters, **128**, 671-681.

Donnadieu, Y, Pierrehumbert, R., Jacob, R., and Fluteau, F., 2006. Modelling the primary control of paleogeography on Cretaceous climate. Earth and Planetary Science Letters, **248**, 426-437.

Epstein, S., Graf, D. T. and Degens, E.T., 1964. Oxygen isotope studies on the origin of dolomite, in: H. Craig et al., (editors). Isotopic and cosmic chemistry. North Holland Publ. Company. Amsterdam, 169-l80.

Farzadi, P. and Hesthmer, J., 2007. Diagnosis of the Upper Cretaceous palaeokarst and turbidite systems from the Iranian Persian Gulf using volume-based multiple seismic attribute analysis and pattern recognition. Petroleum Geoscience, **13**, 227-240

Forster, A., Schouten, S., Bass, M. and Damste, J.S.S., 2007. Mid-Cretaceous (Albian-Santonian) sea surface temperature record of the tropical Atlantic ocean, Geology, **35**(10), 919-922.

Frakes, L.A., Francis, J.E. and Syktus, J.I., 1992. Climate modes of the phanerozoic, Cambridge University Press, 274p.

Fritz, P. and Smith, D.G.W., 1970. The isotopic composition of Composition of secondary dolomites. Geochim. et. Cosmochim. Acta, **34**. 1161-1173.

Ghazban, F., 2007. Petroleum geology of the Persian Gulf. Joint publication, The University of Tehran Press and National Iranian Oil Company, 706p.

Given, R.K. and Lohmann, K.C., 1985. Derivation of the original isotopic composition of Permian Marine cements. Journal of Sedimentary Petrology, **55**, 430-439.

Hajikazemi, E., Al-Aasm, S.I., and Coniglio, M., in press. Chemostratigraphy of Mid-Cretaceous Carbonates in the Tethyan Region: an example from the Sarvak Formation in southern Iran. Journal of Petroleum Geology.

Hajikazemi, E., Al-Aasm, S.I., and Coniglio, M., 2010. Subaerial Exposure and Meteoric Diagenesis of the Cenomanian-Turonian upper Sarvak Formation, southwestern Iran. In "Tectonic and Stratigraphic Evolution of Zagros and Makran during the Mesozoic-Cenozoic" Geological Society of London, Special publication, **330**, 253-272.

Harris, P. M. and Frost, S. H. 1984. Middle Cretaceous Carbonate Reservoirs Fahud Field and Northwestern Oman. American Association of Petroleum Geologists, Bulletin, **68**, 649-658

Hoefs, J., 1987. Stable isotope geochemistry. Third edition, Heidelberg and New York, Springer-Verlag, 24lp.

Huber, B.T., Norris, R. D., and MacLeod, K.G., 2002. Deep-sea paleotemperature record of extreme warmth during the Cretaceous, Geology, **30**, 123–126.

Immenhauser, A., Nagler, T. F., Steuber, T. and Hippler, D., 2005. A critical assessment of mollusk $^{18}O/^{16}O$, Mg/Ca, and $^{44}Ca/^{40}Ca$ ratios as proxies for Cretaceous seawater temperature seasonality. Palaeogeography, Palaeoclimatology, Palaeoecology, **215**, 221–237.

Jacobsen, S.B. and Kaufman, A.J., 1999. The Sr, C and O isotopic evolution of Neoproterozoic Sea water. Chemical Geology, **161**, 37-57.

James, N.P., and Choquette, P.W., 1990. Limestone diagenesis, the meteoric environment. In: Sediment diagenesis. Edited by I. McIlreath and Morrow. D., Geological Association Canada, Reprint Series **4**, 36–74.

Jenkyns, H. C., Gale, A. S. and Corfield, R. M., 1994. Carbon and oxygen isotope stratigraphy of the English Chalk and Italian Scaglia and its palaeoclimatic significance. Geological Magazine, **131**, 1–34.

Koop, W, and Stoneley, R., 1982. Subsidence history of the Middle East Zagros Basin, Permian to Recent. Phil. Trans. Roy. Soc. Lond., **305**, 149–168.

Kump, L. R., 1991. Interpreting carbon-isotope excursions. Strangelove oceans: Geology, **19**, 299–302.

Land, L.S., 1985. The origin of massive dolomite. Journal of Geological Education, **33**, 112-125.

Land, L. S., 1980. The isotopic and trace element geochemistry of dolomite: the state of the art. In: Concepts and Models of Dolomitization, Zenger, D.H., Dunham, J.B and Ethington, R.A. (editors). Society of Economic Paleontologists and Mineralogists Spec. Publ., **28**, 87-110.

Land, L.S., 1983. The application of stable isotopes to studies of the origin of dolomite and to problems of diagenesis of clastic sediments. In: Stable isotopes in sedimentary geology, Soc. Econ. Paleo. Mineral, Short Course, **10**, 4.1- 4.22.

Machel, H. G., Mason, R. A., Mariano, A.N. and Mucci, A., 1991. Causes and emission of luminescence in calcite and dolomite. In: C.E. Barker and O.C. Kopp (Editors), Luminescence Microscopy and Spectroscopy: Qualitative and Quantitative Applications. SEPM Short Course, **25**, 9-25.

Magaritz, M., 1983. Carbon and oxygen isotope composition of recent and ancient coated grains, in Peryt, T.M., editor, Coated Grains: Berlin, Springer-Verlag, 27-37.

Marshall, J. D., 1992. Climatic and oceanographic signals from the carbonate rock record and their preservation: Geological Magazine, **129**, 143–160.

Moore, C.H., 1989. Carbonate reservoirs, porosity evolution and diagenesis in a sequence stratigraphic framework, Elsevier, 444p.

Morad, S., Al-Aasm, I.S., Ramseyer, K., Marfil, R., Aldahan, A. A., 1990. Diagenesis of carbonate cements in Permo-Triassic sandstones from the Iberian Range, Spain: evidence from chemical composition and stable isotopes. Sedimentary Geology, **67**, 281-295.

Morad, S., Worden, R.H., Ketzer, J.M., 2003. Oxygen and hydrogen isotope composition of diagenetic clay minerals in sandstones: a review of the data and controlling parameters.

In: Worden, R.H., Morad, S. (Editors.), Clay mineral cement in sandstones. Special Publication of the International Association of Sedimentologists, **34**. , 63–91.

Motiei, H., 1993. Geology of Iran. The stratigraphy of Zagros. Geological survey of Iran (in Farsi).

O'Neil J. R., Clayton R. N., and Mayeda T. K. 1969. Oxygen isotope fractionation in divalent metal carbonates. J. Chem. Phys., **51**, 5547–5558

Savard, M. M., Veizer, J., and Hinton, R., 1995. Cathodoluminescence at low Fe and Mn concentrations: A SIMS study of zones in natural calcites: Journal of Sedimentary Research, ser. A, **65**, 208–213.

Scholle, P. A. and Arthur, M. A., 1980. Carbon isotope fluctuations in cretaceous pelagic limestones: Potential stratigraphic and petroleum exploration tool. American Association of Petroleum Geologists Bulletin, **64**, 67-87.

Setudehnia, A., 1978. The Mesozoic succession in S.W, Iran and adjacent areas. Journal of Petroleum Geology, **1**, 3-42.

Steuber, T., 1996. Stable isotope sclerochronology of rudist bivalves: growth rates and Late Cretaceous seasonality. Geology, **24**, 315–318.

Taghavi, A.A., Mork, A, and Emadi, M.A, 2006. Sequence stratigraphically controlled diagenesis governs reservoir quality in the carbonate Dehluran Field, southwest Iran, Petroleum Geoscience, **12**(2), 115-126.

Veizer, J., 1983a. Chemical diagenesis of carbonates: Theory and application of trace element technique, in Stable isotopes in sedimentary geology: Society of Economic Paleontologists and Mineralogists Short Course, 10, 3.1– 3.100.

Veizer, J., Ala, D., Azmy, K, Bruckschen, P., Buhl, D., Bruhn, F., Carden, G.A.F., Diener, A., Ebneth, S., Godderis, Y., Jasper, T., Korte, C., Pawellek, F., Podlaha, O.G. and Strauss, H. 1999. $^{87}Sr/^{86}$ Sr, $\delta^{13}C$ and $\delta^{18}O$ evolution of Phanerozoic sea water. Chemical Geology, **161**, 59–88.

Voigt, S., 2000. Cenomanian–Turonian composite $\delta^{13}C$ curve for Western and Central Europe: the role of organic and inorganic carbon fluxes. Palaeogeography, Palaeoclimatology, Palaeoecology, **160**, 91–104.

White, T., Gonzales, L., Ludvigson, G. and Poulson, C. 2001. Middle Cretaceous greenhouse hydrologic cycle of North America. Journal of Geology, **29**, 363-366.

Wilson, P.A., Norris, R.D. and Cooper, M.J.2002. Testing the Cretaceous greenhouse hypothesis using glassy foraminiferal calcite from the core of the Turonian tropics on the Demerara Rise. Geology, **30**, 607–610.

Zeigler, M.A., 2001. Late Permian to Holocene paleofacies evolution of the Arabian Plate and its hydrocarbon occurrence, GeoArabia, **6**, 445–504.

Zhou, G.T and Zheng, Y.F., 2006. On the Direction and Magnitude of Oxygen Isotope Fractionation Between Calcite and Aragonite at Thermodynamic Equilibrium. Aquatic Geochemistry, **12**, 239–268.

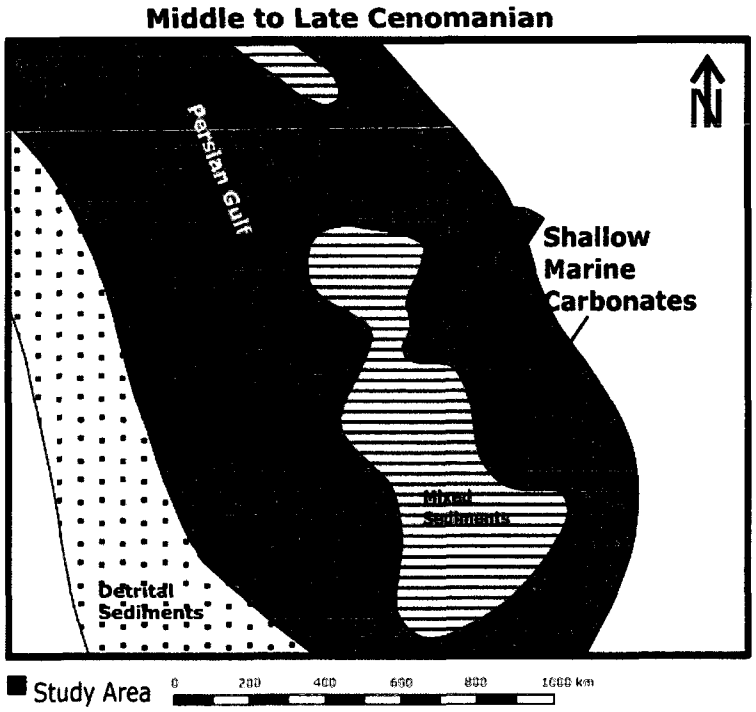

Figure 4.1a Lithofacies map of the region during mid-late Cenomanian.Squars show the sampling locations of this study.

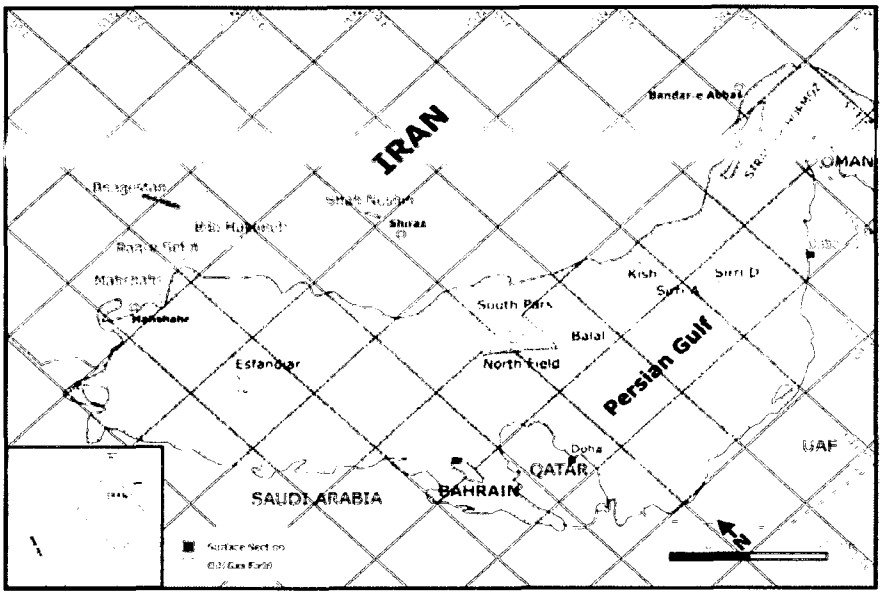

Figure 4.1b Location map of the study area

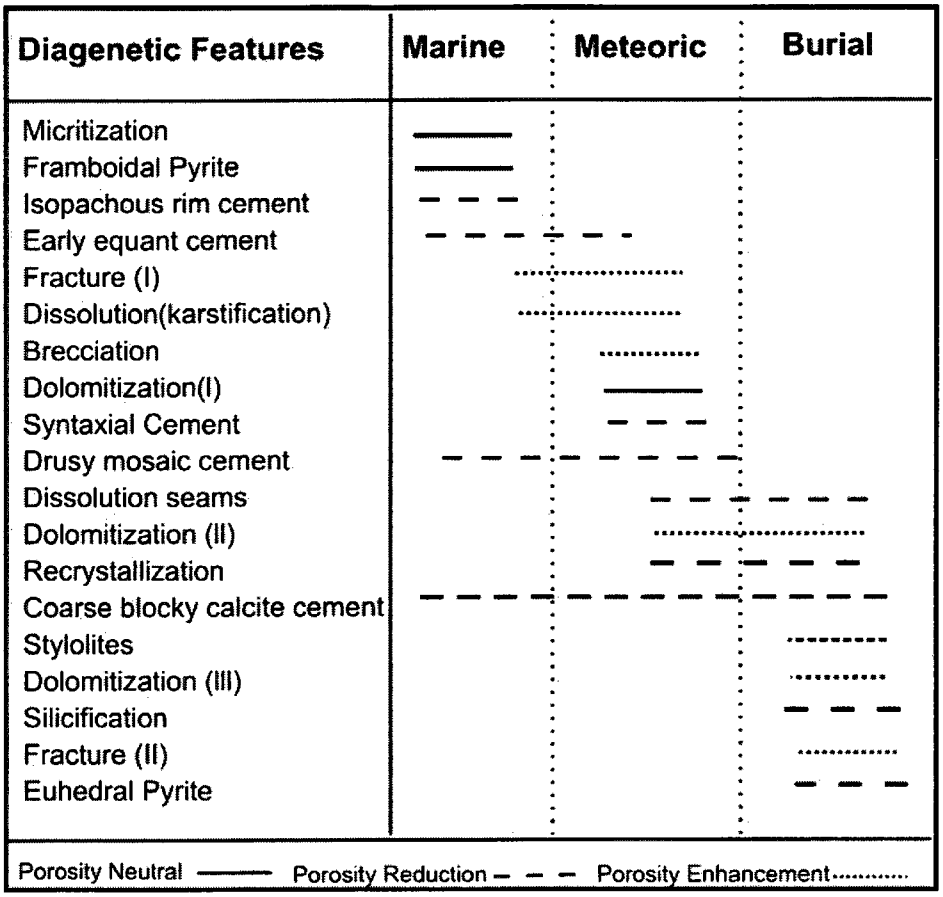

Figure 4.2 Paragenetic sequence of the most important diagenetic features and processes of the Sarvak Formation

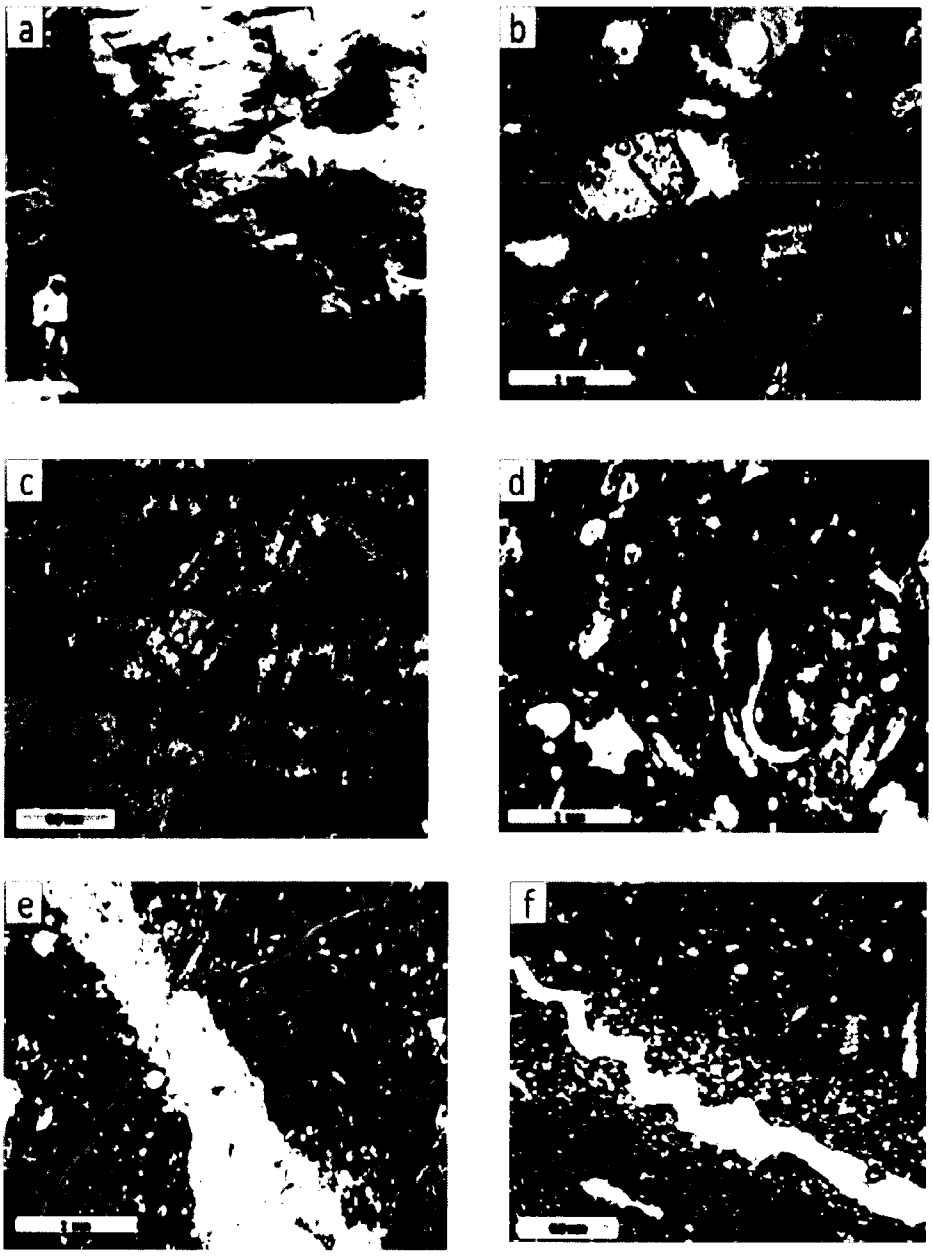

Figure 4.3. Photomicrograph of a) Cavernous porosity below the unconformity surface in Shahneshin Mountain, b) Mouldic porosity partially filled with calcite cement, c) Primary porosity of the rudist shell partially filled with calcite cement, d) Foraminifera packstone with stylolite which acted as a conduit for oil in subsurface sections, e) Two sets of fractures in Upper Sarvak Fm. The wider set is completely filled with calcite cement and the second set is deprived of any cement and filled with blue dye, f) Fine crystalline clear dolomite replacing the calcite matrix.

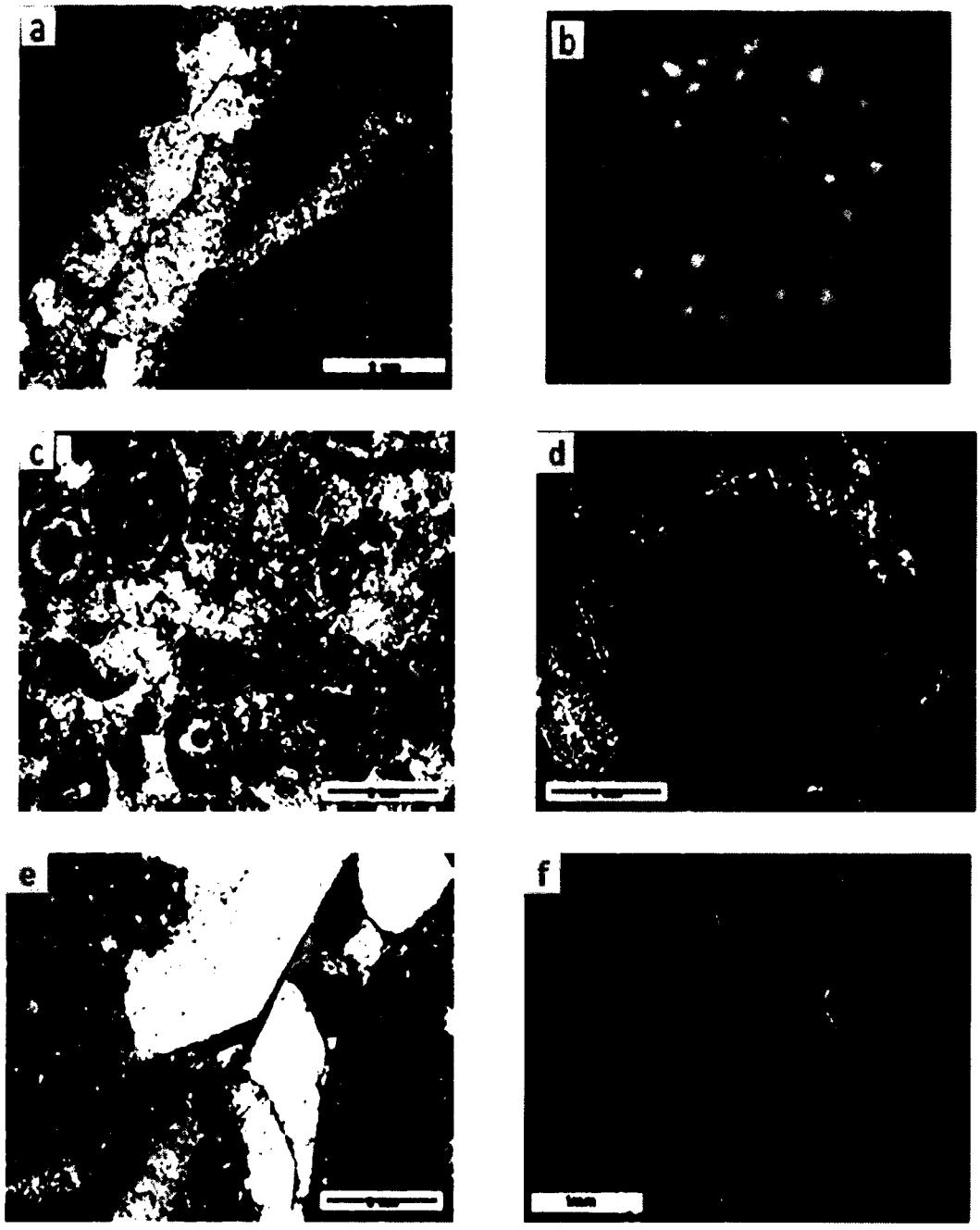

Figure 4.4 a) Photomicrograph of pyrite crystals formed adjacent to blocky calcite cement in a vein, b) SEM photomicrograph of framboidal pyrite, c) Photomicrograph of equant calcite cement in a grainstone, d) Syntaxial overgrowth calcite cement surrounding an Echinoderm in a grainstone, e) Blocky calcite cement and intercrstalline porosity filled with blue dye, f) Cathodoluminescence photomicrograph of banded drusy mosaic calcite cement in a vein.

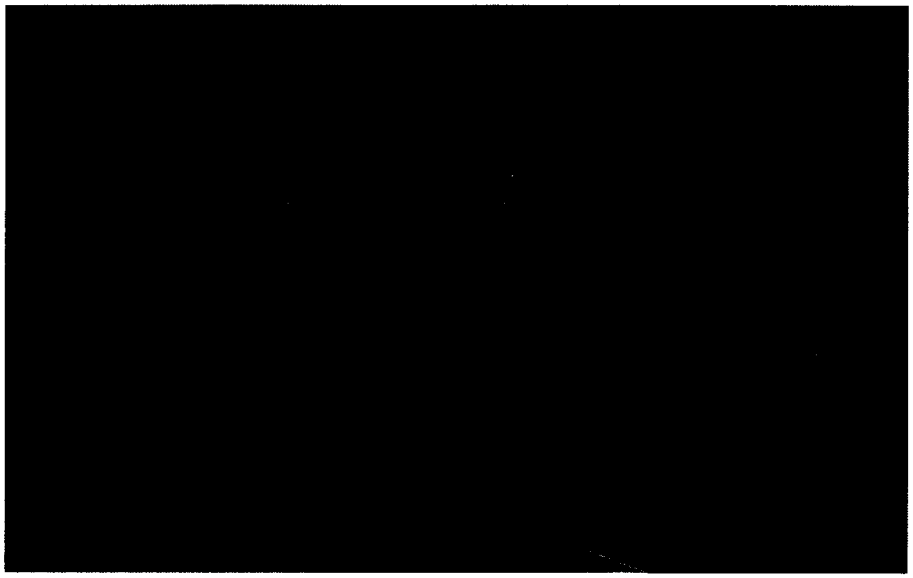

Figure 4.5. Two-phase fluid inclusion in blocky calcite cement (magnification x100).

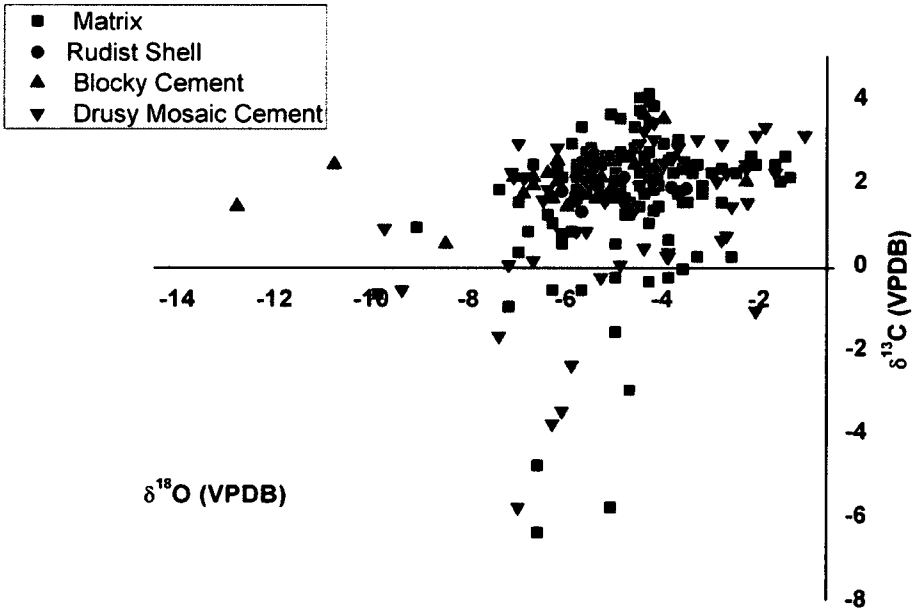

Figure 4.6. Plot of carbon and oxygen isotope data of all carbonate components of the Sarvak Formation.

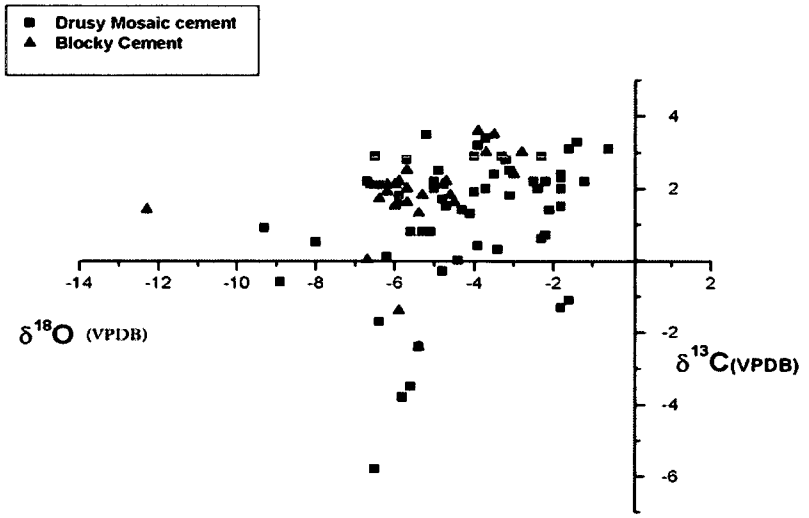

Figure 4.7 Carbon and oxygen isotopic composition of drusy mosaic and blocky calcite cements of the Sarvak Formation in the study area showing some overlap of isotopic values.

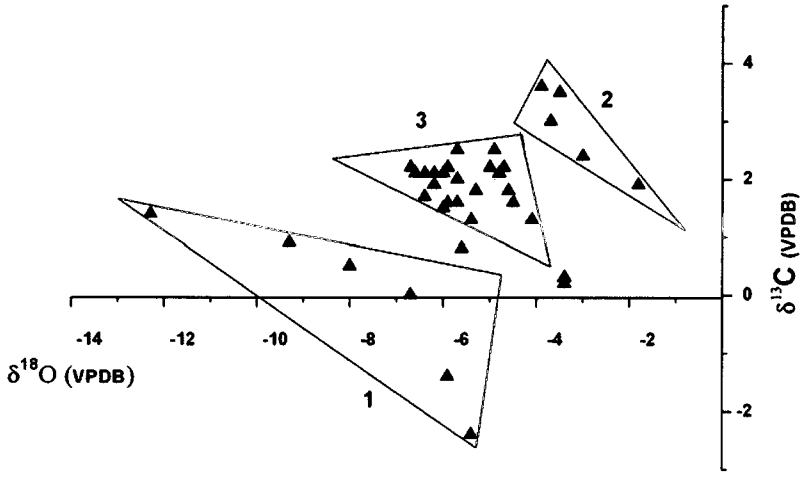

Figure 4.8 Carbon and oxygen isotopic composition of blocky calcite cement of the Sarvak Formation showing three distinct groups.

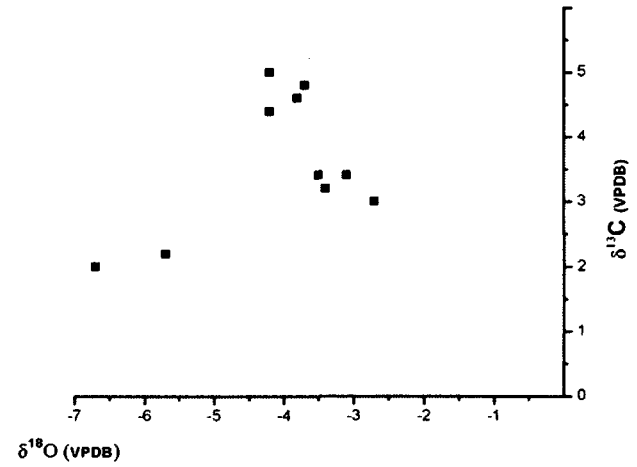

Figure 4.9 Carbon and oxygen isotope data of the dolomite (III).

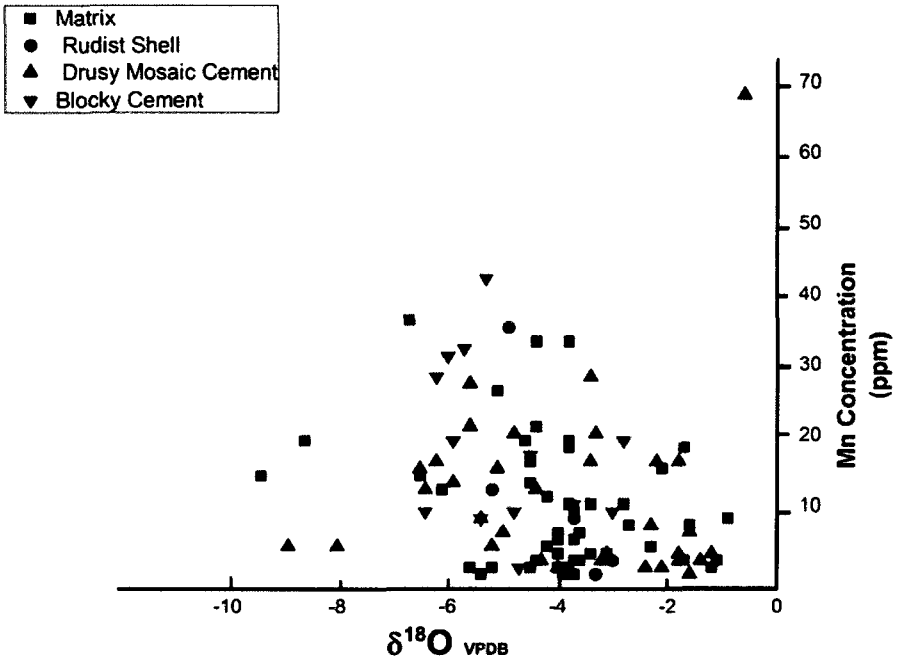

Figure 4.10 Plot of stable oxygen isotope values vs. manganese of the all carbonate component of the Sarvak Formation.

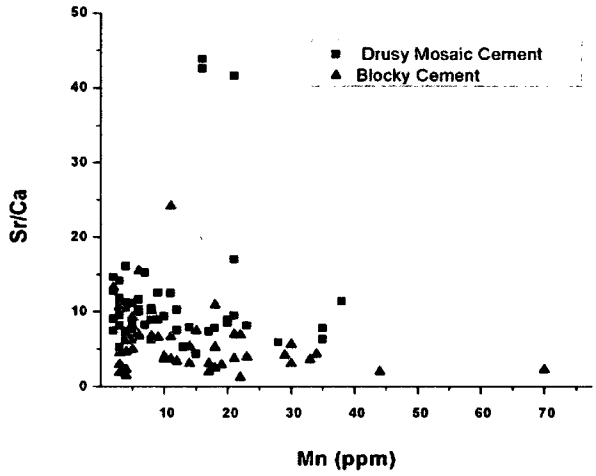

Figure 4.11 Variation of Sr/Ca vs Mn concentration of the drusy mosaic and blocky calcite.

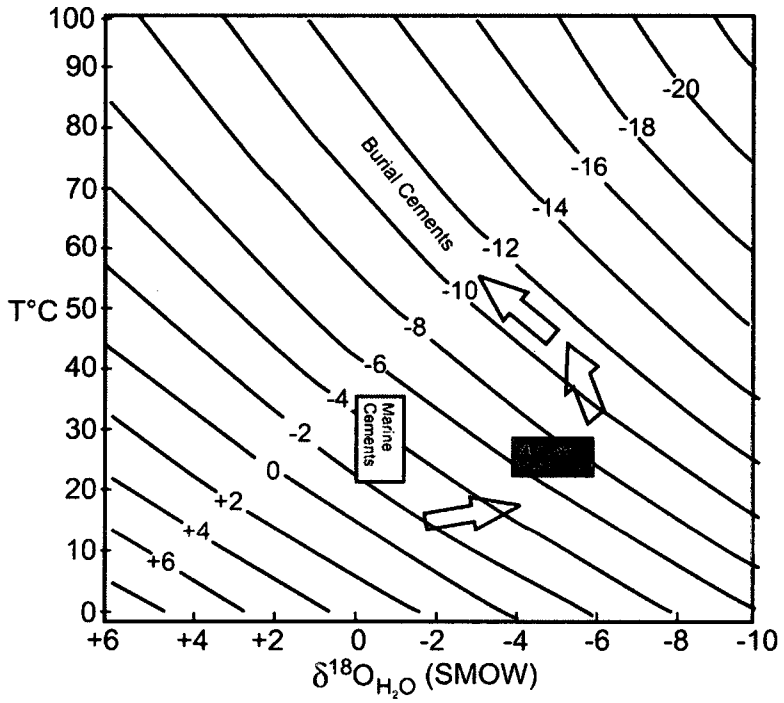

4.12. History of calcite cementation. The earliest cement precipitated from marine water with $\delta^{18}O$ ranging from -1.2 to 0. The shift in $\delta^{18}O$ indicated by the arrow is interpreted as an effect of changes in isotopic composition of the pore water from marine to dominantly meteoric water ($\delta^{18}O$ = -6 to -9‰) causing precipitatoin of some of the ^{18}O-depleted calcite cement (dark grey box). The most ^{18}O-depleted cement precipitated from heated mixed meteoric-marine waters.

Table 4.1 Stable isotope values and elemental concentration of drusy mosaic (C), blocky calcite (B) cement and dolomite (dol) of the Sarvak Formation in the study area.

Sample No.	^{43}Ca (ppm)	^{55}Mn (ppm)	^{86}Sr (ppm)	$^{87}Sr/^{86}Sr$	$\delta^{13}C$ (VPDB)	$\delta^{18}O$ (VPDB)
8700-C	363739	14	112		-1.6	-5.9
9211-C					2.2	-2.2
9447-C					2.1	-6.4
9441- C	270744	15	202	0.70745	1.8	-5.9
8955-C	281240	22	34		-0.3	-4.8
8446-C	297866	17	59		-5.8	-6.5
8447-C	283751	23	112		-3.5	-5.6
8447-C					-3.8	-5.8
8700-C	274763	10	102	0.70717	-2.4	-5.4
9428-C	252884	8	169		2.0	-5.0
9438-C	311404	70	70		3.1	-0.6
8943-C					0.4	-3.9
8961-C					2.2	-5.0
8185-C	279219	17	86	0.70747	0.8	-5.1
2517-C					2.1	-3.8
7354-C					2.9	-2.3
7423-C					2.9	-6.5
7464-C					2.8	-5.7
2520-C					1.7	-4.8
167-C	254058	18	277		0.1	-6.2
165-C	311181	14	166	0.70731	0.0	-4.4
161-C	321049	18	169	0.70745	-1.1	-1.9
160-C	278844	8	281		-1.0	-1.6
159-C	287371	5	266		1.5	-1.8
158-C					3.4	-3.7
157-C					3.4	-3.7
155-C	325269	9	213	0.70729	0.6	-2.3
153-C	281752	18	146	0.70846	0.7	-2.2
147-C				0.70746	1.8	-3.1
143-C	223250	4	51	0.70771	2.8	-3.2
140-C	600350	21	225	0.70766	3.0	-2.8
129-C	290026	6	195	0.70732	3.5	-5.2
128-C	292198	3	55		2.9	-4.0

Table 4.1 (Continued)

120-C	278000	5	222	0.70731	2.5	-3.0
139-C					2.4	-1.8
134-C					2.4	-3.5
132-C	312811	22	214	0.70762	2.9	-3.3
109-C	203820	4	30	0.71015	1.4	-3.4
108-C	317418	4	147	0.71016	1.4	-4.3
102-C	287798	3	306	0.70728	2.0	-2.4
99-C	347276	4	212	0.70746	2.3	-1.8
97-C				0.70718	2.2	-2.5
95-C	306083	3	136	0.70714	1.4	-2.1
94-C	88971	2	118		3.1	-1.6
88-C				0.70772	1.5	-4.7
89-C				0.70756	0.8	-5.3
71-C					1.9	-4.0
57-C					3.2	-3.9
RU-B	281592	33	101		2.1	-6.0
BH-104-B	281028	44	56	0.70731	1.8	-5.3
BH-104-B					0.8	-5.6
BH-104-B					1.6	-5.9
BH104-CB					2.0	-5.7
BH105-CB					1.5	-6.0
BH-4-B	252204	29	105	0.70752	1.9	-6.2
BH106-B					0.9	-9.3
BH-2-B					2.5	-4.9
BH-12-B					2.1	-6.4
BH101-B					1.3	-4.1
BH-0-B					2.2	-6.7
BH-4-B	281839	33	101		2.1	-6.6
106-B					1.8	-4.6
140-B					2.2	-5.9
BH106-B					1.4	-12.3
9211.5-B					1.9	-1.8

Table 4.1 (Continued)

8700-B	293239	10	117	0.70745	-2.4	-5.4
7351-B					3.5	-3.5
8943-B	292706	30	89		0.2	-3.4
163-B	313373	6	484	0.70745	0.5	-8.0
9442-B	393586	11	260	0.70745	1.7	-6.4
8173-B	281557	11	680	0.70717	2.1	-4.8
8951-B	298215	34	129		2.2	-5.0
28-B	245837	30	138		2.1	-6.2
8952-B					1.3	-5.4
165-B					0.5	-8.0
7465-B					3.6	-3.9
BH-2-B					2.5	-5.7
8955-B	240743	21	168		-1.4	-5.9
7348-dol					3.4	-3.5
7468-dol					2.0	-6.7
7465-dol					3.2	-3.4
7253-dol					2.2	-5.7
9809-dol					4.4	-4.2
9791-dol					4.8	-3.7
9799-dol					4.6	-3.8
9815-dol					5.0	-4.2
9441-dol					3.4	-3.1
9425-dol					3.0	-2.7
BH-5-P					-3.0	-4.2
SS-1-P				0.70813	-5.4	-3.7
SS-2-P					-1.6	-4.1
SS-3-P					-7.3	-4.7
SS-5-P					-9.1	-5.2
SS-6-P				0.70718		

C: Drusy mosaic calcite cement; B: Blocky calcite cement; dol: Dolomite; P: Palaeosol

Chapter 5

Conclusions of Research

5.1. Implication of the Research

The Cenomanian-Turonian Sarvak Formation forms one of the main reservoir rocks in many oil fields in southern Iran and the Persian Gulf region. This thick succession of carbonate rocks was deposited in a shallow marine ramp-setting environment within the Zagros Basin.

The Sarvak carbonates are of particular interest because they represent an important part of the depositional history of the northeastern Margin of the Arabian Plate. Their formation recorded the geologic history of the region including parts of Tethys Ocean during a critical time in Earth history: the greenhouse of the Mid-Cretaceous.

Although Sarvak succession is of primary importance for the carbonate petroleum reservoirs in the region, few studies were conducted on these carbonates, and those concerned were biostratigraphic in nature. There are still many uncertainties regarding these carbonates, such as what environmental conditions promoted their deposition, and how these carbonates changed or modified during their diagenesis. The Sarvak carbonates provided an opportunity to answer some of these fundamental questions, with a unique perspective from diagenetic and geochemical records.

The present study has made the following pioneer and significant contributions;

- Detailed diagenetic history including; paragenetic sequence, major processes, nature of the diagenetic fluids, and porosity evolution of these heterogeneous carbonates was determined.
- Providing the first comprehensive chemostratigraphic work identifying major and local unconformities and sedimentologic breaks important in lithostratigraphic correlation. The stable O and C and Sr isotope ratios along different profiles from wells and surface sections, allow stratigraphic correlation.
- Recognition of the occurrence of the Cenomanina-Turonian global Anoxic Oceanic Event (AOE) in the Sarvak carbonates. This event marked by a positive $\delta^{13}C$ excursion is observed in various parts of the world and used as a stratigraphic tool for high resolution correlation.
- Construction of the $\delta^{13}C$ curve for Sarvak Formation type section, suggests that the Sarvak carbon isotope signal have a regional as well as global significance.

- Identification of local Cenomanina-Turonian unconformity essential for establishing the proper stratigraphic and diagenetic framework was made possible by geochemical signatures where no subaerial exposure surface or other field or visual effects were available.
- Recognition of warm oceanic temperatures and climate that characterize the Mid-Cretaceous greenhouse in Upper Sarvak Formation, intensifying karstification and reservoir development.

5.2. Conclusions

At the time of Sarvak deposition, large basins existed in the region rimmed by carbonate platforms. These basins including Zagros Basin developed onto self-contained hydrocarbon systems sealed regionally beneath shales. The sedimentary succession of the Sarvak was dominated by widespread carbonate accumulation on an extensive development of carbonate platforms.

Four main depositional environments were identified in the ramp setting including the inner-ramp, mid-ramp, outer-ramp and open marine or basinal environments. Each environment is characterized by several microfacies. The distribution of the lithofacies was controlled mainly by regional tectonics and local salt movements.Salt diapirs and basement structures modified basinal configuration forming different highs and lows, causing changes of facies and their distribution by localizing high energy grainstones and rudist reefs and generating local intraformational unconformities.

Among the microfacies, bioclastic grainstones have the most significant pertrophysical characteristics to form reservoir rocks with primary intraparticle and secondary moldic and vuggy porosity identifiable both in surface outcrops and subsurface cores from drilled wells. A wide range of reservoir characteristics displayed by these carbonates resulted from extensive lateral and vertical facies variations as well as effects of the subaerial exposure associated mainly with the regional Turonian and also local Cenomanian-Turonian unconformities.

Following the deposition of the Upper Sarvak Formation a major sea level fall in the mid Turonian exposed large areas covered by these carbonates resulting in regional Turonian unconformity. The top part of the formation was subjected to major erosional processes resulting in removal of large volumes of carbonates forming the regional Turonian unconformity. Profound changes due to karstification, development of palaeosol and extensive bauxite deposits occurred that were limited to the upper few meters of the top of the formation. The above changes

combined with stable isotope evidence confirm that these carbonates were subjected to warm and humid climatic conditions during Mid-Cretaceous.

The extensive regional unconformity was responsible for the creation, enhancement and development of the favorable reservoir characteristics. Thus, the presence of other sedimentary gaps or subaerial surfaces could make other horizons a prime target for reservoir development. Thus, it was of vital importance to identify the presence of sedimentary sedimentary gap within the succession and this warranted a detailed investigation of the succession.

Chemostratigraphic analysis carried out in continuous surface sections and subsurface core samples on the Sarvak Formation confirms the presence of the regional Turonian and local Cenomanian-Turonian unconformities. This was a major contribution finding a powerful geochemical tool for recognition of unconformities. Both of these unconformity surfaces were identified by their geochemical characteristics including negative $\delta^{13}C$ values coupled with high $^{87}Sr/^{86}Sr$ ratios and low Sr concentrations. The durations of these paleoexposures were different. Based on the $^{87}Sr/^{86}Sr$ ratios the Turonian unconformity lasted longer whereas the Cenomanian-Turonian exposure was of shorter duration characterized by the lack of pronounced radiogenic $^{87}Sr/^{86}Sr$. Negative $\delta^{13}C$ and $\delta^{18}O$ values obtained from the stratigraphic profiles revealed the presence of previously unrecognized paleoexposure surfaces or sequence boundaries within the Sarvak Formation and could be attributed to the sea-level changes.

The Sarvak carbonates at or near the sequence boundaries or palaeoexposure surfaces commonly exhibit different degrees of diagenetic modification where more extensive alteration is associated with longer periods of exposure. Most of the geochemical evidence obtained in this study is in agreement with records through the Cenomanian-Turonian in Tethyan realm. The results also demonstrate the potential of the combined $\delta^{13}C$ and $^{87}Sr/^{86}Sr$ reference curve as an effective tool for surface and subsurface correlation.

The high-resolution $\delta^{13}C$ record of Cenomanian-Turonian carbonates curve allowed the direct comparison of certain stratigraphic intervals. Superimposing our data obtained from stratigraphic sections on the global sea-water $\delta^{13}C$ curve showed that there is very good comparison and correlation with the Cenomanian portion of the curve up to the Cenomanian-Turonian boundary.

The positive $\delta^{13}C$ of the matrix carbonates, rudist shells and some of the calcite cements are within the range of marine Cretaceous carbonates and reflect values of sea water coeval with Oceanic Anoxic Event (OAE). The highest positive $\delta^{13}C$ values determined along the stable isotope profiles represented Mid-Cenomanian Event (MCE), which has been identified and correlated both on the surface and subsurface sections and could be correlated with such event

globally. The well-documented Cenomanian-Turonian boundary with $\delta^{13}C$ excursion has not been correlated within the Sarvak Formation due to Cenomanian-Turonian unconformity and the subsequent extensive erosion.

Negative $\delta^{13}C$ values measured within the successions which are an indication of subaerial exposure and invasion of the system by meteoric waters, are usually associated with porosity enhancement. Furthermore, the most depleted $\delta^{13}C$ values in carbonate soils formed due to subaerial exposure resulted from interaction of marine carbonates with aggressive meteoric waters charged with atmospheric CO_2. This caused pronounced karstification and development of favorable reservoir characteristics including effective porosity and permeability.

Sea-level fall and associated unconformities and paleoexposure surface had dual effects on reservoir quality a constructive effect, which refers to enhancing the porosity by extensive dissolution and karstification and a destructive effect which includes occlusion of some of the porosities by meteoric cement precipitation within the system. Petrographic evidence indicated that early and late diagenetic cementations are the predominant contributor to the porosity loss in reservoirs.

Meteoric waters entered the Sarvak Formation during the emergence of the Sarvak Formation in Cenomanian-Turonian and Turonian time and initiation of the unconformities. Therefore, meteoric waters were responsible for precipitation of most of the calcite cement observed in the upper most part of the strata. The range of $\delta^{13}C$ values obtained suggest that the ultimate source of carbon in calcite cements was primarily from a marine source with mixture of isotopically more negative atmospheric CO_2.

Recognition of the Cenomanian-Turonian and Turonian unconformities is a key factor in locating high porosity and permeability zones in the succession and is based on the presence of (a) sediment filling scoured surface; (b) preserved palaeosols and bauxite rich horizons; (c) iron oxide staining of underlying horizons; and (d) solution-collapse breccia. These features and processes are compatible with warm tropical and greenhouse conditions dominating the region during Mid-Cretaceous.

By combining detailed field and core examination with petrographic and geochemical investigations, several conclusions were made regarding the diagenesis and evolution of reservoir porosity of the Sarvak Formation. Petrographic and geochemical study of the shallow water carbonates of the Sarvak Formation revealed that they underwent different diagenetic modifications in variable diagenetic environments.

The main diagenetic features which affected the carbonates of the Sarvak and subsequently the reservoir characteristics resulted from dissolution and cement precipitation.

Most of the profound diagenesis subsequent to marine diagenetic realm took place in the meteoric, mixed and shallow burial realm. Dissolution affected the entire upper part of the Sarvak Formation. The majority of the carbonate cements were precipitated as drusy mosaic calcite cement and some blocky calcite cement.

A series of diagenetic events that led to cement precipitation and creation or destruction of the effective porosity were summarized in the form of a brief diagenetic history. (1) Deposition and shallow burial of the sediments still in contact with circulating sea-water provided a site for the precipitation of marine calcite cements, (2) The exposure of the carbonates and introduction of meteoric water to the system occurred during sea-level fall, (3) Burial of the carbonates which caused the temperature increased and pore waters became additionally depleted in $\delta^{18}O$.

Three diagenetic trends are apparent in the calcite cements on the basis of isotopic data. The first trend occurs in some of the blocky and drusy mosaic calcite cements characterized by heavy $\delta^{13}C$ and relatively heavy $\delta^{18}O$ values. This has been interpreted to be precipitated in a marine diagenetic environment.

The second trend is characterized by covariants of positive $\delta^{13}C$ and negative $\delta^{18}O$ values and is interpreted to result from the interaction in a meteoric-marine mixed environment. The third trend is characterized by light $\delta^{18}O$ and $\delta^{13}C$ which can be interpreted as a result of precipitation in a meteoric environment with high ambient temperature or shallow burial. Based on cement petrography the burial diagenesis for some of the blocky calcite cements formed adjacent to the stylolites is confirmed.

The $\delta^{18}O$ and $\delta^{13}C$ values obtained from calcitic matrix, various generations of calcite cements and rudist shells in the Upper Sarvak overlap to a large extent indicating their equilibration with fluids of similar isotopic composition. The difference in cement isotopic composition suggests that most of these carbonates experienced diagenesis by interaction with meteoric water or formed under higher temperatures. Partial dolomitization in some mud supported intervals is another significant factor in enhancement of the intercrystalline porosity filled with hydrocarbon. Most of the dolomites which are ^{18}O-depeleted formed adjacent to stylolites and indicating their occurrence during burial diagenesis.

Carbonate cements of the Sarvak Formation record a diagenetic history starting with early marine cementation and finishing with burial. The chemical and isotopic compositions of diagenetic carbonates show some variations, implying similar variations in pore water composition during diagenesis. Isotopic analyses of cements in the Sarvak carbonate suggest that pore waters with variable isotopic composition and (or) elevated temperature controlled the nature and extent of carbonate cement precipitation during diagenesis.

5.3. Recommendations for Future Work

Investigation of diagenetic processes in a sequence stratigraphic framework has recently gained significant interest. This has also been predominantly applied to carbonate successions. The relationship between diagenetic processes and sequence boundaries are not adequately investigated in the Sarvak Formation. Chemostratigraphic work on a regional scale will significantly improve the sequence stratigraphic investigations of the Sarvak Formation and similar carbonate successions in the oil fields (subsurface sections) where cuttings and well logs are the only available data.

Identification of sequence boundaries is usually difficult when working with sparse seismic data and core samples. In seismic sections, these boundaries are characterized by irregular reflectors overlying depositionally horizontal reflectors. Geochemical analyses will be a great help in identifying and confirming such sedimentologically important surfaces.

Vita Auctoris

Elham Hajikazemi was born in 1968 in Tehran, Iran. She studied Geology at the University of Tarbiat Moallem in Tehran, where she obtained her B.Sc. degree in geology in 1990. She started working for National Iranian Oil Company (NIOC) from 1990 where she was awarded a graduate scholarship and successfully completed her M.Sc. in sedimentology in 1994. She continued working for NIOC and IOOC till 2005. In January 2006 she attended the University of Windsor in Canada, where she started her Ph.D degree.